GENERALIZED SENSOR-BASED TOOL FAILURE DETECTION AND PREVENTION SYSTEM FOR INTERMITTENT CUTTING OPERATIONS

Mahmoud Hassan

Department of Mechanical Engineering
McGill University

Montreal, Quebec
August 2018

A thesis submitted to McGill University in partial fulfillment of the requirements of the degree of Doctor of Philosophy

ABSTRACT

Unmanned manufacturing systems have recently gained great interest due to the ever-increasing requirements of optimized machining for the realization of the fourth industrial revolution in manufacturing, 'Industry 4.0'. A survey conducted by a major tool manufacturer has demonstrated that only 40% of tools are used to their full tool-life in order to avoid late replacement of defective tools. Therefore, tool condition monitoring (TCM) systems are essential to achieve the desired competitive advantage in terms of reducing cost, increasing productivity, improving quality, and preventing damage to the machined part. Tool condition cannot be predicted analytically due to the high dynamics of the process in an industrial environment. Hence, research work has focused on indirect TCM systems, where feedback signals are analyzed to define the tool condition. Critical review of the literature has indicated the inability of available TCM systems: (a) to predict sudden tool failure, (b) to work in an adaptive control environment, where the cutting feed is changing continuously during the cutting process, and (c) to extract generalized key features of the tool condition. Additionally, these systems need high learning effort and long processing time to identify the tool condition in a highly dynamic process. Hence, it is essential to develop a generalized non-intrusive TCM system that can isolate the tool failure features in real-time and take corrective action with a high level of accuracy and decision certainty.

To overcome the limitations of the existing TCM systems, experimental investigation has been carried out to characterize and discriminate tool prefailure, failure and post-failure phases, using various sensors and processing techniques. A new intelligent TCM system has been developed for accurate detection of tool wear failure as well as prediction of sudden tool chipping/breakage before damaging the machined part. The system analyzes process-born features gathered from multi-sensor feedback signals using advanced signal processing and machine learning methods to detect the tool condition during cutting processes.

For tool wear detection, robust, real-time signal processing and decision-making algorithms were developed using feedback signals from the spindle drive motor. The system extracts descriptive generalized features in the time and frequency domains,

determines the tool condition, and then, communicates a decision to the machine controller in the adaptive control environment. The proposed approach accentuates the tool condition effect on the extracted features while masking the effects of the cutting parameters, namely, cutting speed, feed and depth of cut, tool path, and cutting tool geometry. Such capability has never been achieved before. Extracted features were filtered and ranked based on their sensitivity to the tool condition using analysis of variance (ANOVA) tests. Furthermore, top-ranked features were optimized using a Sequential Feature Selection method, and then, employed to enhance the tool condition detection approach using a Linear Discrimination Analysis (LDA) model. The selection of the LDA model was based on benchmarking of the pattern recognition methods to optimize the learning effort, classification accuracy and calculation time. The results indicated the capability of the processing technique to minimize system learning effort by at least 75% and to detect tool wear above the threshold level with an accuracy above 95% with a confidence level above 90%.

For sudden failure prediction, a novel signal processing approach for online prediction and prevention of tool chipping/breakage during intermittent machining was developed. The approach analyzes the Acoustic Emission (AE) waves associated with the generation of new surfaces during unstable crack propagation, which precede tool fracture, in the time-frequency domain using the Hilbert-Huang transformation method. The features of the prefailure phase were identified using the Teager-Kaiser Energy Operator and the Bartlett window function, which can discriminate high energy events in the prefailure phase while depressing any other low energy signal variation. Extensive experimental results, supported by high-speed imaging of the cutting operation and tool failure, demonstrated the accuracy of the developed system to consistently predict tool failure by four to six tool/workpiece engagements before tool fracture. The system output has also been shown to be independent of the cutting parameters and workpiece material. A correlation between the chipping size and the prefailure features was developed for decision making. An ultra-high-speed processor was integrated into the TCM system for real-time decision making within a noticeably short time span (in the order of 10 ms) for high speed machining processes. Communication between the developed system and a CNC machine controller has been

implemented. The time required for signal processing, decision making and communication with the machine controller allows stopping the operation before part damage. Experimental results confirmed the accuracy and robustness of the proposed TCM system. No such system previously existed.

RÉSUMÉ

Les systèmes de fabrication sans pilote ont récemment gagné beaucoup d'intérêt en raison des exigences croissantes d'usinage optimisé pour la réalisation de la quatrième révolution industrielle dans la fabrication de « Industrie 4.0 ». Un sondage réalisé par un fabricant d'outil majeur a démontré que seulement 40 % des outils sont utilisés à leur capacité maximale de leur durée de vie, pour éviter le remplacement tardif d'outils défectueux. Par conséquent, les systèmes de surveillance de l'état d'outil (TCM) sont essentiels pour réaliser l'avantage concurrentiel industriel souhaité, en termes de réduction des coûts, augmentation de la productivité, amélioration de la qualité et éviter d'endommager la pièce usinée. La condition de l'outil ne peut être prédite analytiquement en raison de la nature dynamique du processus dans un environnement industriel. Par conséquent, cette recherche a mis l'accent sur les systèmes indirects de TCM, où les signaux du processus sont analysés pour définir l'état de l'outil. Un examen critique de la littérature a indiqué l'incapacité des systèmes TCM disponibles à : (a) prévoir la défaillance soudaine de l'outil, (b) travailler dans un environnement a contrôle adaptative AC, où la vitesse d'avance de coupe change continuellement pendant le processus, et (c) extraire les caractéristiques principales de l'état de l'outil. De plus, ces systèmes nécessitent un effort d'apprentissage important et un long temps de traitement pour identifier l'état de l'outil dans un processus hautement dynamique. Il est donc essentiel de développer un système TCM non intrusif généralisé capable d'isoler les caractéristiques de défaillance de l'outil en temps réel et de prendre des mesures correctives avec un niveau élevé de précision et de certitude de décision.

Pour surmonter les limites des systèmes de TCM existants, des études expérimentales ont été menées pour caractériser et discriminer les phases de pré-défaillance, défaillance et de post-défaillance des outils, en utilisant divers capteurs et techniques de traitement. Un nouveau système TCM intelligent a été mis au point pour détecter avec précision les défaillances d'usure des outils, ainsi que la prédiction de brisure d'outils soudains avant d'endommager la pièce usinée. Le système analyse les caractéristiques du processus recueillies à partir de signaux des multi-capteurs en

utilisant des méthodes avancées de traitement du signal et d'apprentissage automatique pour détecter l'état de l'outil dans les processus de coupe intermittents.

Pour la détection de l'usure des outils, des algorithmes de traitement du signal et de prise de décision robustes et en temps réel ont été développés à l'aide de signaux de retour provenant du moteur d'entraînement de la broche. Le système extrait des caractéristiques générales descriptives, dans les domaines temporel et fréquentiel, détermine la condition de l'outil, puis communique une décision au contrôleur de la machine en présence de système de contrôle adaptif. L'approche proposée souligne l'effet de l'état de l'outil sur les caractéristiques extraites, tout en masquant les effets des paramètres de coupe tels que la vitesse de coupe, la vitesse d'avance, la profondeur de coupe, et la trajectoire et la géométrie de l'outil. Une telle capacité n'a jamais été atteinte auparavant. Les caractéristiques extraites ont été filtrées et classées en fonction de leur sensibilité à l'état de l'outil en utilisant l'analyse des tests de variance ANOVA. En outre, les caractéristiques du classement le plus élevé ont été optimisées à l'aide de la méthode de sélection des caractéristiques séquentielles, puis utilisées pour améliorer l'approche de détection des conditions des outils à l'aide du modèle d'Analyse de Discrimination Linéaire LDA. La sélection du modèle LDA était basée sur l'analyse comparative des méthodes de reconnaissance des formes afin d'optimiser l'effort d'apprentissage, la précision de la classification et le temps de calcul. Les résultats ont indiqué la capacité de la technique de traitement à minimiser l'effort d'apprentissage du système d'au moins 75% et à détecter l'usure des outils au-dessus du seuil avec une précision supérieure à 95% et un niveau de confiance supérieur à 90%.

Pour la prévision de défaillance soudaine, une nouvelle approche de traitement du signal a été développée pour la prédiction en ligne et la prévention de la brisure des outils lors de l'usinage intermittent. L'approche analyse les ondes d'émission acoustique associées à la génération de nouvelles surfaces lors de la propagation instable des fissures, qui précèdent la fracture de l'outil, dans le domaine temps-fréquence en utilisant la méthode de transformation de Hilbert-Huang. Les caractéristiques de la phase de pré-défaillance ont été identifiées à l'aide de la fonction de Teager-Kaiser Opérateur Énergétique et de la fonction de fenêtre Bartlett, qui distinguent les événements à haute énergie de la phase de pré-défaillance tout en

abaissant toute autre variation de signal à basse énergie. Des résultats expérimentaux étendus, appuyés par une imagerie à grande vitesse des opérations de coupe et des brisures d'outils, ont démontré la précision du système développé pour prédire de manière cohérente la défaillance de l'outil de quatre à six engagements d'outils / pièces avant la brisure de l'outil. La sortie du système s'est également avérée indépendante des paramètres de coupe et du matériau de la pièce. Une corrélation entre la grandeur de fissure et les caractéristiques de pré-défaillance a été développée pour la prise de décision. Un processeur ultrarapide a été intégré au système TCM pour une prise de décision en temps réel dans un laps de temps très court (de l'ordre de 10 ms) pour les processus d'usinage à grande vitesse. Une communication du système développé avec le contrôleur de machine CNC a été mise en place. Le temps nécessaire au traitement du signal, à la prise de décision et à la communication avec le contrôleur de la machine permet d'arrêter le processus avant d'endommager une partie. Les résultats expérimentaux de la validation ont confirmé l'exactitude et la robustesse du système de MTC proposé. Aucun système similaire n'existe.

CLAIMS OF ORIGINALITY

1. A novel, generalized, real-time tool prefailure detection and sudden failure prevention system for intermittent cutting operations has been developed and optimized. The system predicts tool chipping and/or breakage in real-time and controls the machine tool with corrective actions to safeguard the machined part. The developed system is insensitive to the cutting conditions, workpiece material, tool diameter and tool path. The system can accurately capture small chipping sizes down to 0.25 mm^2. Such a system did not previously exist.
2. A new, real-time sensor-fusion tool wear detection system was developed for milling applications in adaptive control environment. The system is based on a linear discriminant analysis model that fused generalized features extracted from the spindle power, current and voltage. The system is insensitive to the cutting speed, feed rate, axial and radial depth of cut, as well as the tool diameter, number of flutes and corner radius. The system also accounts for the dynamic tool-workpiece interaction during milling. The developed system reduced the learning effort by 75% compared to available systems and could capture a predefined tool wear level with an accuracy ranging from 91% to 100%.
3. A unique method was devised to induce cracks on the tool cutting edge and monitor the cutting forces, vibrations, acoustic emission and power generated during the unstable crack propagation phase. This allowed performing an experimental characterization of the effect of the tool prefailure phase, the onset of fracture and the post-failure phase on the indirect means of sensing that was not investigated before. The features of each phase were identified. This study led to discover the capability of AE sensors to capture tool prefailure.
4. A novel time-frequency signal processing approach has been developed to accentuate the features of the tool prefailure phase. The approach deals with the nonlinear and non-stationary nature of the acoustic emission signals, which are developed during unstable crack propagation that precedes sudden tool failure as

well as signal contamination due to the high dynamics of the intermittent cutting processes.

5. A quantitative relationship has been generated for the first time between the processed AE signals and the chipped/broken area. Such a relationship provides a thresholding measure that defines acceptable chipping sizes, which is useful for industrial applications where chipping can be tolerated to a certain limit.
6. A novel signal processing approach has been developed to mask the effect of cutting conditions on acquired spindle feedback signals for tool wear detection applications. The approach masks the effect of the cutting conditions on the acquired signals. Such an approach accentuates the sensitivity of the extracted features to the tool condition.
7. A comparative study of widely-used pattern recognition methods was carried out based on a non-determined problem dataset. The study provided a clear benchmark of the feasibility of applying these methods in TCM systems with respect to their accuracy, conservation characteristics as well as calibration and computational effort.

ACKNOWLEDGMENT

I would like to thank my supervisors Prof. Helmi Attia, Prof. Vincent Thomson and Prof. Jozsef Kovecses for their continuous and invaluable support throughout my PhD research work. Special thanks and sincere gratitude to Prof. Helmi Attia for all the support, patience and guidance on the scientific, professional and personal levels over the years. Without his technical advice and management, this thesis would not have reached its full potential. I am really honored to be his student and to learn from him in various aspects of life. Without his input I would not have transitioned to a self-sufficient researcher, which made working with him a process of comprehensive development.

Joining the Advanced Metal Removal group at the Aerospace Manufacturing laboratory of the National Research Council (NRC) of Canada has been a truly transformative experience and without a doubt the most crucial step in my academic career. At NRC I have had the opportunity of using state-of-the-art equipment for my research and learning from a group of exceptionally talented professionals, especially Dr. Ahmad Sadek, Dr. Ahmad Damir, Dr. Mouhab Meshreki, Dr. Ben Shi, Dr. Zhongde Shi, Mr. Patrick Turnblom and Mr. Nicola de Palma. Their collaboration allowed me to improve every day during the past four wonderful years. More importantly, they made all the time and effort spent on this project worthwhile and helped me to enjoy it even in the most stressful moments. For this, I am and always will be thankful to every person involved in this group. Also, I would like to express my deep gratitude to Dr. Ahmad Sadek for all that I have learned from him, and I can confidently say that this research would not have been in such a good form without his great and sincere support.

Words cannot express my gratitude to my passed father, Refaat, who was the reason behind my success in life, my mother Aziza for all her invaluable support, and my wife Ayat for her great patience and sincere support and love. Finally, I would like to thank my daughters Mariam and Maya for their understanding and for having to reschedule many of their planned weekend entertainment activities for the sake of this research.

TABLE OF CONTENTS

LIST OF FIGURES

LIST OF TABLES

NOMENCLATURE

Symbols

A_c	Crack area
a_e	Radial depth of cut
$a_j(t)$	HHT instantaneous amplitude for each IMF
a_p	Axial depth of cut
BP	Band power
C	Pooled covariance matrix
D	Diameter
E	Area under the curve
F_r	Resultant force
f_{mean}	Mean frequency
f_{med}	Median frequency
ft_{mean}	Mean frequency of all signal peaks
f^+	Added feature in SFS
f_{ap}	Axial depth of cut *f*-value
f_f	Feed rate *f*-value
f_{TC}	Tool condition f-value
f_z	Feed per tooth (mm/tooth/rev)
h	Extracted component in signal sifting process
K	Kurtosis
m	Mean of upper and lower envelopes of the sifting process
min	Minimum
N	Number of tools
n	Spindle speed rev/min
P	Power
$P2rms$	Peak magnitude to rms ratio
Pp	Max peak value of the periodogram

Pw	Welch power spectral energy
p_i	p-value
q	Number of features extracted
R	Feature ranking score
r	Residue of sifting process
$\boldsymbol{r}\ (a, b)$	Pearson's Linear correlation coefficient
rms	Root mean square
S	Analytic signal
SD	Standard deviation
Ti	Training data subset
V_c	Cutting speed (m/min)
V_f	Vibrations in feed directions
Var	Variance
VB	Flank wear
W_{max}	Maximum number of windows to detect prefailure
W_{min}	Minimum number of windows to detect prefailure
$\bar{X}$	Mean of feature observations
$\mathbf{X}_{qn}$	Feature observation matrix
$y_i(t)$	Hilbert transform
Z	Number of flutes
α	ANOVA test significance level
β	Linear model coefficients
μ	Mean vector
$\theta_j(t)$	HHT phase function for each IMF
Ψ	TKEO
Ψ_B	Bartlett window of TKEO
Ψ_{BW}	Max of (Bartlett window of TKEO) per segment
$\omega j\ (t)$	Instantaneous frequency

Abbreviations

ACC	Adaptive control with constraints
AE	Acoustic emission
ANN	Artificial neural network
ANOVA	Analysis of variance
ASIC	Application specific integrated circuit
DB	Database
DT	Decision trees
FFT	Fast Fourier transform
FPGA	Field-programmable gate array
HHT	Hilbert Huang transform
HSC	High speed camera
HSM	High speed machining
IIOT	Industrial internet of things
IMF	Intrinsic mode functions
KNN	K-Nearest neighbor
LDA	Linear discriminant analysis
MCE	Misclassification error
MEMS	Microelectromechanical
MRR	Metal removal rate
NB	Naïve Bayes
PR	Pattern recognition
PWM	Pulse width modulation
SFS	Sequential feature selection
SVM	Support vector machine
TCM	Tool condition monitoring
TKEO	Teager–Kaiser energy operator

CHAPTER 1
RESEARCH MOTIVATION, OBJECTIVES AND OUTLINE

1.1. Introduction

Over recent decades, manufacturers have realized the benefits of advances in digital technologies along with the development of the Industrial Internet of Things (IIoT), where a multitude of devices connected by communication technologies monitors, analyzes, and delivers valuable new insights. The IIoT has expanded at a rapid rate due to the development of smart sensors and data storage capacities that has led to an 'Industry 4.0' revolution where advanced manufacturing techniques are combined with IIoT systems to drive further intelligent action back in the physical world, motiving unmanned manufacturing. This drives industrial competitive advantage in terms of reducing cost, increasing productivity, improving quality, and preventing damage to machined parts during processing. Advanced investigations using Tool Condition Monitoring (TCM) systems and adaptive control systems are required to achieve such automated machining systems. Therefore, there are tremendous efforts exerted towards developing new methods and implementing innovative technologies to improve the performance of TCM systems and to introduce novel approaches that can provide solutions to the challenges facing manufacturers.

1.2. Research Motivation

With more than 700 companies in the aerospace industrial field, Canada has been ranked third globally in terms of global civil aircraft production, especially for aerostructures, providing more than $25 billion of direct revenue annually [1]. Hence, it is clear that improvement and optimization of metal cutting processes are essential for continuous improvement in this sector. In high speed cutting processes, late replacement of defective tools may lead to machine breakdowns as well as severely affect product quality, which subsequently leads to scrapped parts and high process costs. To avoid such losses, manufacturers tend to replace cutting tools before they are

fully utilized. A recent survey conducted by a major tool manufacturer has demonstrated that only 40% of tools are used to their full tool-life. Therefore, accurate tool condition detection is essential to achieve a high level of competitiveness via increasing process productivity and standardizing the quality of produced parts. Therefore, TCM systems have been widely emphasized as an important way to achieve these industrial demands.

As shown later in the literature review in Chapter 2, several studies for tool condition monitoring systems have been carried out to capture tool failure using predictive and sensor-based models. However, these studies have failed to provide a generalized, robust and reliable TCM system, which can accurately detect the state of a tool under different cutting conditions and which can be easily integrated into adaptively controlled industrial processes. In addition, available TCM systems need high learning effort to be able to detect the state of a tool within a defined range of cutting conditions. Such a limitation would suppress the implementation of these systems in industrial facilities. Moreover, present systems do not have the ability to control a CNC machine and take corrective action to safeguard the machined part. An extensive investigation of the available literature shows that the extraction of key features that can describe the state of a tool under different cutting parameters in highly dynamic cutting processes is not available. Furthermore, a significant drawback with present TCM systems is that they focus on detecting the post-failure phase (i.e., after the onset of catastrophic failure). In addition, they suffer from a long processing time (up to 1 second), after which, in a high speed milling process, the workpiece surface integrity may be impaired. The fact that there is no available system that can predict sudden tool failure in real-time, regardless of the cutting conditions or the part material, represents a remarkable gap, which needs to be addressed.

1.3. Research Objectives

The terminal objective of this work is to develop a non-intrusive real-time sensor-based TCM model that can *detect* and *prevent* sudden and progressive tool failure to

safeguard the surface integrity of the machined part. The proposed system must incorporate the following features:

- Detects the prefailure phase of sudden tool failures, which is defined as the phase from damage evolution to failure occurrence, and accentuates tool failure features.
- Isolates and takes into account the effects of the cutting parameters, the high dynamics of the intermittent cutting processes (e.g., milling and intermittent turning), and the effect of adaptive control systems.
- Requires minimum effort in term of experimental calibration.
- Takes corrective action based on the identified tool condition and controls the machine tool to safeguard the machined part.
- Minimizes the detection and action time to be useful for high speed machining processes and real-time applications.
- Uses non-intrusive hardware to be applicable for all industrial applications.

Such aspects were not considered in the available literature. Hence, based on the aforementioned discussion as well as the review and gap analysis of the literature presented in Chapter 2, the specific objectives of this work to overcome the limitations of existing TCM systems are the following.

First, characterize the tool prefailure, failure and post-failure phases due to catastrophic wear, brittle fracture and/or breakage during intermittent cutting processes. This objective aims at selecting the appropriate means for sensing, monitoring and defining tool conditions under the main, independent cutting parameters (speed, feed rate, axial and radial depth of cuts, tool geometries and path, and tool and workpiece material). A method is devised to induce separate tool failure phenomena to study their effect on acquired feedback signals. Experimental tests and statistical analyses are carried out to find the appropriate key features that can be extracted from the feedback of different sensors to describe the tool condition regardless of the dynamics of the cutting process.

Second, develop a non-intrusive, sensor-based TCM system that can accurately detect tool wear failure as well as the prefailure phase of sudden tool

chipping/breakage in order to take corrective action before there is damage to the machined part. To achieve this objective, it is required to develop robust and real-time signal processing and decision-making approaches that can process the feedback signals from multiple sensors, accentuate and detect tool failure features as well as communicate a decision to the machine controller in an adaptive control environment with a high level of accuracy and decision certainty. Extracted features are generalized to be applicable for a wide range of cutting conditions requiring minimum learning effort. The outcome of these algorithms should be unaffected by the range of cutting parameters, namely, cutting speed, feed rate, radial and axial depth of cut, workpiece material and cutting tool diameter, corner radius and number of flutes.

1.4. Research Scope

In general, this work targets the development of a generalized TCM system for tool failure detection and prevention during intermittent cutting operations regardless of the cutting parameters or workpiece material. However, the main focus is the high speed milling process, which is categorized as one of the most complex processes among intermittent cutting operations for aerospace applications. This work concentrates on milling processes for large aerostructure parts (approx. 1 m^3) made of high strength aluminum alloys. The work targets commonly used uncoated carbide end mill *families* with the same geometrical parameters, but different diameters, number of flutes and corner radii. It considers *tool failure* due to wear and *prefailure* due to unstable crack propagation leading to chipping and/or breakage. The capabilities to be developed in this research should be insensitive to cutting parameters and adaptive control working environments, which adjust the feed rate continuously to maintain a fixed power level. According to ISO standards [2], tool flank wear (VB) is the phenomenon of tool life deterioration. It has maximum acceptable uniform and localized values of 0.3 and 0.5 mm, respectively. In this work, uniform tool wear is divided into two ranges, namely, fresh ($0 \leq VB < 0.07$) and worn tools ($0.25 \leq VB < 0.3$). Chipping is treated as *localized VB wear* with an acceptable range of up to 0.5 mm. Tool breakage is defined by the absence of a major tooth cutting edge such that there is no

tooth/workpiece engagement. Cutting conditions that induce chatter or a built-up edge are avoided.

1.5. Thesis Outline

The first three chapters are aimed at describing the research question and objectives, literature review and background as well as experimental setups. Afterwards, the thesis is divided into two equally important sections. The first section includes Chapters 4 and 5, which describes the TCM system generated for tool prefailure detection and prevention of sudden tool failure during intermittent cutting processes. The second section describes the developed tool wear detection system, represented in Chapters 6 and 7. Finally, Chapter 8 presents the research conclusion and future work. A detailed description of the contents of the thesis outline is as follows.

1. Chapter 1 presented an orientation on the relevance of the research question and the motivation behind this work. In addition, it provides a brief introduction of the scope and the outline of the proposed approach for dealing with the research problem.
2. Chapter 2 discusses the research work that has been reported in the available literature on real-time tool failure detection with a high focus on sensor-based TCM systems and their signal processing approaches. Furthermore, the chapter discusses the research work done in the literature on artificial intelligence based TCM systems and machine learning for sensor-fusing and TCM system accuracy. A background of the processing techniques is discussed as well. This discussion encompasses the full picture of the problem and leads to defining the missing links that need to be addressed in this research work.
3. Chapter 3 provides a description of experimental setups in terms of the selected machine tools as well as sensor selection and usage. It also describes the cutting tools and the workpiece materials employed in this research as well as the hardware used for real-time implementation of the developed TCM system.
4. Chapter 4 shows the potential of different sensors and the proposed signal processing approach to capture tool prefailure. This includes experimental

investigation and characterization of the tested sensors as well as testing the developed approach using artificial signals.

5. Chapter 5 discusses the experimental results of the prefailure detection system in milling and intermittent turning applications. It also presents the online implementation of the system and the real-time control of the CNC machine to protect the machined part.
6. Chapter 6 describes the development of a real-time tool wear detection system based on motor feedback signals. It presents the signal processing and decision-making algorithm to provide a generalized TCM system. This includes feature extraction, generalization and selection. It also includes benchmarking of the commonly used machine learning algorithms that can identify the tool condition with high accuracy.
7. Chapter 7 shows the experimental validation of the tool wear monitoring model in highly complex milling applications. It shows the system capability to capture the tool condition under different cutting parameters including the adaptive control environment. Then, the capability of the validated model being implemented in real-time applications is presented.
8. In Chapter 8, the main conclusions of the entire research are presented as well as the recommendations for future research work.

CHAPTER 2
BACKGROUND AND LITERATURE REVIEW

2.1. Introduction

Manufacturing of large aerostructures requires hours of complex metal removing processes. Evaluation of these processes through inspecting the resultant workpiece at the end of the manufacturing cycle is insufficient since any shortfall cannot be corrected and the product may be considered scrap. In addition, 7–20% of total tool machine downtime is caused by tool failure, and the cost of tools and tool changes accounts for 3–12% of the total processing cost [3]. Therefore, proper and reliable manufacturing of aerostructures requires accurate prediction of the condition of the cutting tool and continuous control of the variations of the cutting process. Advanced investigation of tool condition monitoring and adaptive control systems is required to achieve the industrial demand for automated machining systems. These demands include increasing process productivity, standardizing the quality of produced parts, and reducing process cost. This is achieved through minimizing in-process human decisions and interventions, which do not follow a defined standard. Over recent decades, the broad range of manufacturing processes and the rich physical variability associated with them have continued to drive the evolution of technologies for TCM and process adaptive control. Tremendous effort has been exerted towards developing TCM systems for discrete manufacturing to achieve a high level of competitiveness via increasing process productivity and standardizing the quality of produced parts. In the following sections of this chapter, the contributions and findings of research effort that is reported in the open literature, with focus on applications for intermittent cutting processes (e.g., milling), are discussed. In addition, research gaps are highlighted as well as the background of different signal processing and decision-making algorithms, which were employed in TCM systems, are analyzed.

2.2. Tool Deterioration and Adaptive Control Environment

Tool failure is a complex phenomenon that manifests itself in different and diverse ways. It is generally shaped by accumulation of tool damage over time and it is mainly caused by one or more of the following:

1. *Wear*: change in the shape of the cutting edge resulting from progressive loss of tool material [2],
2. *Brittle fracture (chipping)*: crack occurrence in the cutting portion of a tool followed by the loss of small fragments of tool material [2],
3. *Breakage*: loss of a major portion of the tool wedge, which terminates tool cutting ability [4].

Each of these tool failure causes has different mechanisms, types and consequences depending on the tool load and the process influence. For example, high mechanical or thermal tool loads can cause different mechanisms of tool wear such as adhesion, abrasion or plastic deformation. The development of these wear mechanisms is also affected by the cutting conditions and the tool and workpiece material. Sequentially, this leads to different tool wear profiles that can be quantified by geometry metrics, typically flank and crater wear. As a result, different consequences affect the process and machined part quality, such as high cutting forces and temperatures as well as deviation in the dimensional accuracy and surface roughness of the machined part. According to ISO standards [2], tool flank wear (VB) is the phenomenon of tool life deterioration. It has maximum acceptable uniform and localized values of 0.3 and 0.5 mm, respectively. Tool chipping is usually treated as *localized VB wear* with an acceptable range of up to 0.5 mm.

Tool wear is a progressive deterioration phenomenon. Depending on process influences, tool wear can take from seconds to hours to take place. On the other hand, tool chipping and breakage are defined as sudden tool failures because they are stochastic phenomena that occur in milliseconds. Tool prefailure can be defined as the phase from damage evolution to failure occurrence [5]. For tool wear, the prefailure phase can be established according to the application itself by defining the maximum allowable flank wear. Usually the manufacturer defines the acceptable tool wear level

and the prefailure threshold at which the tool should be changed. On the other hand, during the cutting process, sudden tool failures such as chipping are preceded by crack initiation and propagation. A process can continue with the existence of tool cracks without tool failure. However, at certain conditions (i.e., high cutting forces), these cracks start to propagate unstably causing tool failure. The unstable crack propagation stage is considered the prefailure phase for sudden tool failure.

An adaptive control system is a digital controller that adapts itself to the time varying parameters of cutting process dynamics at each control interval [6]. Different approaches have been implemented in adaptive control systems, including model-based, robust and AI approaches, to maintain a fixed cutting force at the tool edge. Available adaptive control systems can be categorized into three categories depending on the process control method:

1. Adaptive control with constraints (ACC), which maintains a certain variable (i.e., forces or power) at a predefined value. In this method, no physical understanding of the process is required, and sensor feedback is employed,
2. Adaptive control for optimization, which aims at minimizing or maximizing a performance index such as cutting time or effort,
3. Geometrical adaptive control, which seeks to maintain specified part quality despite structural deflections and tool wear to maximize the quality of the finishing operations.

Cutting forces can change significantly during the course of cutting operations. Consequently, the bulk of the available research work as well as commercial systems have concentrated on adaptive control with constraint type systems, which use real–time feedback to maintain a fixed force/power level. The cutting feed is typically selected as a regulation parameter due to its influential effect on process forces, as shown in the following equation [7].

$$F = K d^{\beta} V^{\gamma} f^{\alpha} \qquad 2.1$$

where F is the cutting force, K is the specific cutting force coefficient, d is the depth of cut, V is the cutting speed, f is the feed, and β, γ and α are coefficients describing the nonlinear relationships between the force and the process variables. Usually, the depth-

of-cut is constrained by the part geometry and material, and the force–speed relationship is weak (i.e., $\gamma \approx 0$); therefore, these variables are not actively adjusted for force control. However, changes in the feed rate vary the stress distributions at the tool cutting edge. In an adaptive control with constraints environment, if the feed rate is increased until the principal tensile stresses in the tool reach the fracture limit, cracks are initiated, leading to tool failure [4].

2.3. What is TCM?

Currently, most manufacturers use uniform time periods as a conventional tool replacement strategy depending on operator experience. However, such strategies usually result in either early replacement of workable tools or late replacement of worn tools. This either increases tool cost and downtime or results in defective machined parts. Therefore, TCM systems are used to deal with the uncertainty of tool life prediction by estimating the tool condition based on analytical or sensor-based models. The evolution of tool failure and the associated alteration of tool geometry are affected by many parameters due to the complexity of the machining process. Therefore, empirical models such as Taylor's tool life equation may not be accurate enough to predict tool life [8]. Further, due to the complexities involved and multiple microstructural wear mechanisms seen in machining, there is no unique solution for describing the complete milling process [9]. An effective real-time sensor-based TCM, therefore, can put a cutting tool under surveillance to safeguard the workpiece from damage by dealing with the uncertainty of analytical tool life prediction.

Sensor-based TCM systems can be divided into direct and indirect methods. Direct TCM methods rely on direct measurements, such as machine vision, to capture actual geometric changes due to tool wear. During the cutting process, the interfacial region where tool failure takes place is not readily accessible either physically or from a process monitoring standpoint due to the interaction between the tool and workpiece. Also, the harsh environment of machining processes affects the accuracy of vision sensing methods. Hence, direct TCM methods are very difficult to implement online [10]. On the other hand, indirect methods, which use the existing relationships between

process parameters to monitor the tool condition using indirect signals such as forces, vibrations, acoustic emission (AE) or power, can be measured online. However, they are less accurate and are very much dependent on the type of machining process and its process parameters [11]. Additionally, there is a need to develop a reliable model to predict how the acquired signals are related to tool deterioration. Thus, advanced signal processing approaches are required to extract key features from acquired signals to accurately describe the tool condition. Due to the difficulty of implementing direct methods in online TCM, more interest has been given to indirect methods [10, 11].

Sensor selection, multi-sensor fusion, signal processing, feature extraction and selection, and prediction models are the major research topics in indirect TCM systems. Despite the tremendous effort exerted on these topics, there is still no clear methodology for developing TCM systems to accurately detect the tool condition in real-time. Moreover, the literature has witnessed numerous, contradictory research studies. For example, Bassiuny and Li [12] mentioned that in interrupted cutting operations, where shock pulse loading occurs during the entry and exit of each individual tooth to the workpiece, the magnitude of these shock pulses might equal those generated during tooth fractures. This prevents detecting tool failure events and/or increases false alarms [13]. In contrast, Vallejo et al. [14] concluded that an AE sensor had higher reliability to detect the tool condition when compared to an accelerometer or dynamometer. Furthermore, the contradiction was even extended to the sensor mounting position and orientation. Vallejo et al. [14] concluded that there was higher reliability of the AE sensor when mounted on the tool holder rather than on the workpiece. In contrast, Haber et al. [15] indicated the inability of AE sensors, either mounted on the work piece or tool holder, to distinguish between the new and worn phase of the tool condition compared to accelerometer and dynamometer signals. These contradictions can be related to the dependency of indirect TCM systems on the type of machining process and its process parameters. The research conclusions are also affected by the acquired and analyzed datasets, which are gathered from determined-problem experimental results. Therefore, the performance, accuracy and efficiency of these TCM systems cannot be generalized or standardized.

Table 2-1 Comparison of different research efforts in cutting tool condition monitoring

Operation	Monitoring states	Ref.	Signals					Tool failure	
			Forces	AE	Vibrations	Spindle feedback	others	Predict	Detect
Turning	Tool wear	[16]					✓		✓
		[17]					✓	✓	
		[18]		✓					✓
		[19]	✓						✓
		[20]		✓					✓
	Surface finish	[21]		✓					✓
Milling	Tool wear	[22]	✓	✓	✓				✓
		[11]	✓	✓					✓
		[15]	✓	✓	✓				✓
		[10]				✓		✓	
		[23]	✓						✓
		[24]		✓	✓				✓
		[25]				✓		✓	
	Tool chipping/ breakage	[26]			✓				✓
		[27]				✓			✓
		[28]	✓						✓
		[12]				✓			✓
		[29]		✓					✓
		[30]			✓				✓
	Surface finish	[31]	✓	✓	✓			✓	
		[32]					✓		✓
Drilling	Tool prefailure	[33]	✓	✓		✓			✓

2.4. Application of TCM Systems

Several TCM models have been developed in the literature to detect and predict the tool condition as well as the machined part surface finish, using different indirect sensors in different machining processes such as turning and milling. In this section, the effort toward capturing the tool wear, fracture and prefailure is addressed and concluded. Table 2-1 summaries the main efforts done in recent literature in the TCM field, including the machining process, monitoring states and applied sensor signals. Table 2-1 also shows the capabilities of the developed TCM models to predict or detect the tool condition in real-time applications. As shown in this table, different means of sensing have been applied or fused to detect the tool condition and surface finish in the milling and turning processes. However, no work was able to predict the tool wear condition in real-time industrial applications, and tool breakage prediction was not

discussed. The significance of the measured signals to capture the tool condition and the efforts presented in this table are discussed in the following subsections.

2.4.1. Tool Wear Monitoring

The evolution of tool wear is affected by many parameters due to the complexity of the machining process [8]. Tool geometry changes as wear increases, represented by the flank wear level, and impacts the cutting forces. As a result, the spindle feedback signals (i.e., drive motor power, current and voltage) also increase by increasing the required cutting forces. Additionally, abrupt redistribution of internal stresses occurs and propagates stress waves through the tool/workpiece material [34]. These waves can be captured using AE sensors. Furthermore, tool wear can cause high vibrations which can be measured and calibrated to monitor the tool condition, especially for single point cutting processes. However, this approach is difficult to generalize towards milling processes due to the high dynamics of the process. All these indirect signals can be acquired in real-time and calibrated to the tool condition.

Cutting forces are known to be the best indicator to describe the cutting process and the tool edge [35]. Nouri et al. [23] have used cutting forces to detect the tool wear condition. Their TCM method was based on tracking a new coefficient which depends on four cutting force model coefficients during the cutting process. The behavior of these coefficients has been shown to be nearly independent from the cutting condition and has a high correlatation with the condition of the cutting tool. However, such systems cannot be applied in industrial applictions due to their dependendcy on force signal measurements.

Many attempts have been made to correlate the AE signals to tool wear. Chung and Geddam [11] studied the variation of the cutting forces, torque and the root mean square of the generated AE signals (AE_{rms}) during an endmilling operation. For the signal variation with cutting conditions, they showed that the AE_{rms} had increased when increasing speed while force and tourque decreased; whereas, the forces, torque and AE_{rms} increased by increasing the feed rate, radial and axial depth of cut as these parameters tend to increase the metal removal rate. They concluded that the frequency

peaks of the cutting torque and the AE_{rms} to flank wear were highly sensitive to predict tool wear. Haber et al. [15] investigated tool wear monitoring for milling in high speed machining (HSM) processes by assessing the deviation in representative variables in the time and frequency domains using force, vibration and AE signals. They concluded that the cutting forces and vibration signals were highly sensitive to indicate the tool wear condition in the time and frequency domain. They showed that the second harmonic of the tooth-path excitation frequency in the vibration signals is the best indicator for tool wear monitoring. On the other hand, they found that the AE signals did not indicate clearly the tool condition and that the AE effeciency depended on the transmission path. In contrast, Vallejo et al. [22] concluded that AE signals were sensitive to the tool condition during milling in HSM processes. They employed features that were extracted from the AE signals in different machine learning models and proved their high accuracy in detecting the tool wear condition. However, it was concluded that AE signals were not a suitable tool wear indicator [36].

Kalvoda and Hwang [26] studied the effect of tool wear on vibration signals in the frequency domain during end milling processes. They found that the indicator of cutter tool wear or tool fault was the increase in power together with a slight shift of the main peak to a lower frequency in the power density spectrum. The peak shift was more recognizable in a Hilbert Huang Tranform (HHT) than a Fast Fourier Transform (FFT). However, they concluded that an accelerometer was not a good indicator for high speed operations as the higher the speed, the lower the worn and fault peaks, and that peak shifting was lower.

Shao et al. [25] presented a mathmatical model relating the mean instantaneous cutting power to flank wear in face milling processes. The model first generated a simulated power depending on the measured one, and then, used it to define the tool condition. However, the model was not able to simulate the power in the transient stages (e.g., tool entrance and exit), which limited the developed system capability for application in complex machining processes. Additionally, high learning effort was needed to find the constants of the developed model for each tool and workpiece material combination. For tool life prediction due to tool wear, Zhang [10] provided a modified Taylor tool life prediction equation with time-variant parameters in which the

drive motor current was used to adaptively calculate these parameters. The model was based on the relevance vector machine technique, which is "a machine learning technique that uses Bayesian inference to obtain parsimonious solutions for regression and probabilistic classification" [37]. However, results depended on the accuracy of the relevance vector machine model, which could result in a local minimum during its optimization technique [38, 39]. Additionally, the difference between the predicted tool life with and without adaptation did not follow the actual tool life in the failure region.

Despite the efforts exerted in developing tool wear monitoring systems, present systems suffer from the lack of generalization to be able to cover a wide range of cutting conditions, and regardless of the sensor or processing technique, they suffer from requiring high learning effort to calibrate their models.

2.4.2. Tool Chipping/Breakage Monitoring

To detect tool chipping/breakage in milling processes, the extracted features from sensor feedback signals need to fulfill the following requirements: (a) must reflect tool breakage under variable cutting conditions and different workpiece and tool materials, and (b) must be uniquely distinguishable to avoid interference with other process irregularities (e.g., tool/workpiece interactions, material inclusions or complex geometry machining). An abrupt tool geometry change due to brittle fracture or breakage can alter the characterization of the acquired signals. It can usually be detected by a high sudden burst in the acquired forces, power or vibrations due to a sudden change in the cutting edge, and subsequently, the interaction between the tool and the workpiece. In addition, the generation of new surfaces associated with the separation of major fragments of the tool material at fracture releases high elastic waves. These waves can be observed in the AE signals as a high abnormal burst.

Liu et al. [35] studied the geometry features of the breakage section and the variation of cutting force for end mills after brittle breakage. They concluded that the forces were sensitive to tool chipping and/or breakage regardless of the chipping size. Hsueh and Yang [28] processed the cutting force signal and employed a pattern recognition technique named support vector machine (SVM) to diagnose tool breakage

during milling. In addition to using the force signals, the developed system needed to be calibrated by 70% of the collected data in order to be able to detect tool breakage under different cutting conditions.

Acoustic emission (AE) has been reported as a good indicator for tool breakage [36]. Many attempts have been made to automate a TCM system based on AE signals. Cao et al. [29] proposed a method which relies on feature extraction by AE signals that was unique to healthy tools and broken tools using a lifting scheme and Hilbert transform. Subsequently, they used Mahalanobis distance, which is a measure of the distance between a point and a distribution, as a criterion to estimate tool state (threshold). The TCM system was then simplified as an operation just comparing the current Mahalanobis distance value with pre-learned thresholds. A main drawback of this system is that it needs to collect a segment of data during three rotating periods of the spindle to indicate the cutting edge fracture by which time the machined part surface integrity is already defective. Moreover, a model reference datum needs to be regenerated for each combination of cutting conditions.

Wang et al. [30] have developed an on-line diagnosis method with the use of FFTs and an algorithm for short time signal variation analysis in order to analyze the vibration signals to detect tool breakage. A 2-way communication module was established between the CNC controller and the developed system to automatically extract the machining parameters and send control commands in real-time to stop the machine for cutter replacement. Although no complex computation was involved, the system was able to detect tool breakage after one second and stop the process within three seconds. However, such time spans are not acceptable in aerospace applications where HSM processes take place, and damage to machined parts can easily occur within such time spans. Additionally, as the developed system depends on accelerometers fixed on the machine vice, it would not be able to clearly detect the signals when processing large aerostructures.

Prickett and Grosvenor [27] developed a hybrid approach for tool monitoring based on the spindle load and speed. To detect the onset of tool breakage, they employed a sweeping filters technique to determine the frequency components of the acquired signals as well as a tooth rotation energy estimation technique. Consequently, the

outputs of the techniques were used to verify each other's results before making a final decision about the health of the tool. However, the developed system was only validated for low rotational speeds (i.e., 500 rpm) and a chipping of a minimum of 0.5 mm. Such chipping cannot be tolerated in aerospace machining applications. Bassiuny and Li [12] detected end mill flute breakage using the root mean square (rms) of feed-motor current signals based on the Hilbert-Huang Transformation (HHT). They extracted the critical characteristics from the measured signals, after removing the unnecessary signal components, and then, applied wavelet de-noising to the remaining signals. The developed algorithm was able to indicate successfully the variations of the current signal due to small edge fractures. However, the algorithm constants needed human inference and judgement to be calibrated using trial and error methods, depending on the cutting process parameters. Hence, they were not able to automate the detection algorithm for a real-time application.

Within the large body of research done to develop and automate a tool chipping and/or breakage system, none of them were able to predict sudden tool failure before it happens. Additionally, the systems were not sensitive to small chipping sizes, which might not be tolerated in the finishing operations of aerospace machining applications. In addition, the bulk of the research work focused on detecting the changes in acquired signals after tool breakage. A significant drawback with these TCM systems is that they detect tool breakage within the order of one second [30] by which time, in high speed milling processes, the workpiece surface integrity may be impaired. Hence, developing a TCM system that can predict sudden tool failure by detecting the tool prefailure phase is crucial to protect the machined part, which has not been done up to now.

2.4.3. Tool Prefailure Monitoring

For tool prefailure detection, the research work conducted by Kondo and Shimana [33] discussed tool prefailure from the tool wear perspective only, and did not consider other causes of tool failure. It concluded that spindle current and cutting forces were effective to detect the prefailure phase and reported the lack of efficacy of AE sensors. No assessment of vibration signals was reported. Satpute et al. investigated cracked

rotating cylindrical tools which were fixed at one end to introduce local flexibility [40] and concluded that the non-continuous nature of the milling operation can greatly mask the effect of tool flexibility on vibration signals and cause misunderstanding of the outcome signal. In general, detection of the prefailure phase was discussed from the tool wear perspective only, as it is a lengthy and gradual mechanism.

In contrast, prefailure due to abrupt causes, namely, chipping and breakage, has never been addressed during intermittent cutting. Hence, in-depth characterization of the capability of indirect signals to capture information during the prefailure phase is required. This is a building block in the development of a TCM system that can predict sudden tool failure, which has been done in this thesis.

2.5. Sensor Selection for TCM Systems

The cutting process can be characterized by a variety of physical quantities, which can be transformed into electrical signals using appropriate sensors. As mentioned earlier, the open literature for TCM systems has witnessed several contradictions in selecting the appropriate sensor to detect the tool condition. This section analyzes the usage of these sensors in TCM applications.

2.5.1. Acoustic Emission (AE) Sensors

Acoustic emissions derived from material deflection, chip breakdown and pulse shock loading are produced during milling operations. The cutting state can be reflected by both continuous and transient AE signals [29]. Continuous AE signals are made up of overlapping transient signals and are associated with shearing in the primary zone. Transient impacted AE signals are generated when a pulse shock loading occurs, such as chip breakage and entry/exit of each individual tooth to the workpiece. A transient AE wave is typically a nonlinear and non-stationary signal which exhibits a shape that reflects impacting and exponential decay properties.

AE sensors can capture abnormalities during the milling process, and have the flexibility to be mounted on the tool/workpiece without major disturbances to various machining activities [41]. In addition, the frequency level of the AE signals produced

from cutting processes has been found to be separable from audible noise [42]. In general, for TCM, an AE sensor mounted on a spindle showed higher reliability than when mounted on the workpiece [14, 15, 31]. However, the physical meaning and interpretation of many of the AE signal features are not fully understood. Therefore, data and conclusions reported in the open literature on TCM using AE sensors are contradictory. Additionally, most of the efforts in modeling acoustic emission in manufacturing processes are built on the same model [43, 44]. This model is based on the dependency of AE energy on material properties, such as flow stress, volume of material undergoing deformation and the strain rate. However, the influence of feed and depth of cut variations are not accurately predicted. Additionally, AE signals are sensitive to the sensor location with respect to the signal source and the transmission path. Therefore, available TCM systems described in the open literature based on AE signals need to be calibrated for each set of cutting conditions. Moreover, it was found, in practice, that AE signals were corrupted with white noise generated from sources like electron movements during signal transmission [29]. Hence, more attention is required towards conditioning AE signals.

2.5.2. Current and Power Sensors

Current and power transducers have high potential to be used in industrial applications. This is because they can give a practical indication of the tool condition as they are causally related to the cutting forces. In addition, the non-intrusive nature, low cost and high flexibility of these sensors give them an advantage over other sensors.

Early investigations of the performance of these sensors revealed their limited sensing bandwidth due to the inertia of the motor rotor, which acts as a low pass filter during TCM [45]. If the motor frequency is less than the passing frequency of the cutting tool, the acquired signal may lose some information. However, 400 Hz 2-pole induction motors are popular now in CNC machines, which extend the frequency limits up to 24,000 rpm.

2.5.3. Dynamometers

Cutting forces are considered to be the best variables to describe the cutting process due to the completeness of the cutting process information and the sensitivity of the cutting force to tool geometry changes [46]. The feed and radial forces were found to be more sensitive to tool wear than the cutting force [46]. According to reported findings in [11, 23, 28], piezoelectric dynamometers can provide accurate cutting force measurements that can be applied to detect tool wear and tool breakage. On the other hand, the limited workspace of multi-axis dynamometers in addition to their intrusive nature in production environments as well as their cost have limited their usage for TCM in industrial applications [15, 17, 27].

2.5.4. Accelerometers

Worn and broken tools can cause high vibrations during milling operations; these vibrations can be detected using accelerometers. The rms of a vibration signal is proportional to its energy (or power). Therefore, an increase in the cutting energy generated due to flank wear should generate a proportional increase in vibration magnitude [47]. Moreover, monitoring systems based on accelerometers have the advantages of simplicity and low cost. Such systems have demonstrated the ability of detecting serious tool faults, e.g., breakage and built up edges [30]. On the other hand, the non-continuous cutting nature of some machining processes, as in milling, and the dependency of the sensor signals on the tool path represent the main challenges for using accelerometers for TCM applications. Moreover, accelerometers have been shown to be less sensitive to tool conditions in HSM operations [26]. Additionally, vibration signals are highly affected by surrounding noise in the cutting processes such as noise coming from the coolant system, chip collection and disposal system, or nearby machines.

2.5.5. Other Sensors

Other sensors have been used to detect the tool condition in machining processes. However, these sensors did not show the feasibility to be applied in industrial

applications. For example, temperature sensors have been used to monitor the cutting zone as the temperature can be a good indicator of the tool condition. This is because the temperature varies as the tool wears due to changes in the tool geometry [45]. Different temperature sensors such as thermocouples, thermal resistant elements, semiconductors elements, thermopiles and other types of thermal elements can be used to monitor the tool/workpiece engagement zone temperature [45]. However, the accurate monitoring of cutting temperature is complicated because temperature is usually monitored as an average of the temperatures in the vicinity of the cutting tool [7]. Moreover**,** cutting temperature measurements are rarely utilized in industrial applications.

Ultrasonic sensors have been applied to provide a surface profile measurement which can be related to the tool condition [32, 48]. The calibrated surface roughness measured using an ultrasonic sensor showed a good agreement with stylus profilometer measurements in a narrow range (up to VB = 0.3) [32]. However, in addition to its sensitivity to a harsh machining environment, it has limitations when used for predicting tool wear in a wide range of tool wear situations.

2.6. Signal Processing Techniques for TCM Systems

The dynamic status of a system or a process can be monitored through analyzing its operation signals. Signals collected from operations can be divided into two categories: steady signals and transient, dynamic signals. Steady signals usually represent a stable operation, or an operation that has been running for an extended period. On the other hand, transient, dynamic signals reflect the variation of a system encountering changes in operating conditions, external impacts, or abnormalities. Since both types of signals display distinctive characteristics, they should be processed by using different, appropriate techniques.

The signal processing methods used in TCM cover the majority of conventional processing techniques, including time domain analysis [25, 49, 50], frequency domain analysis [11, 26, 30, 41], time–frequency analysis techniques [15, 29, 32, 48] and artificial intelligence techniques [14, 22, 31, 51]. The techniques that are applicable to

TCM can be mainly divided into two main types, namely, trend analysis and pattern recognition.

2.6.1. Trend Analysis Techniques

In these techniques, the main goal is to detect the abnormal events in the signal trend compared to the signal history, e.g., analysis of sensor signal changes in the time or frequency domain. Trend analysis techniques have been applied in time, frequency and time-frequency domains in TCM applications. A time domain analysis may include feature extraction such as peak value, root mean square and mean value. A simple example of these techniques in the time domain is the detection of tool breakage in the force signals, where a high burst can be clearly distinguished at the onset of breakage compared to the normal cutting signals. These time-domain, trend analysis techniques have shown to be inadequate for complex process monitoring due to the high dependency of the acquired signals on cutting parameters. Hence, the implementation of these methods results in high learning effort. Typically, such techniques need to be trained for each tool, workpiece material and G-code combination. The change of any of these parameters affects the developed model and relearning is required.

FFTs and wavelet analysis were widely used in order to represent cutter tool wear or tool fault in the frequency domain. FFTs have been used to detect tool faults in the frequency domain [26]. In addition, wavelet analysis has proven its efficiency to determine tool breakage during drilling [12]. However, these techniques have drawbacks [26]. The transient, dynamic stages during intermittent cutting processes generate nonlinear and non-stationary signals. The FFT is a powerful tool, but it cannot process signals with a nonlinear or a non-stationary nature. Although wavelet analysis can deal with signal nonlinearity, it cannot accurately process non-stationary signals. In contrast, the Hilbert–Huang transform (HHT) is a new empirical method for analyzing nonlinear and non-stationary signals in the time–frequency space [12]. The HHT method has many advantages over other methods, including wavelets and other extensions of Fourier analysis [12]. It provides a more precise definition of particular events in time–frequency space than wavelet analysis and offers a more physically

meaningful interpretation of the underlying dynamic processes. Hence, such a technique can provide explanations of the transient signals during the prefailure phase of machining.

2.6.2. Pattern Recognition Techniques

Pattern recognition (PR) can be defined as a branch of machine learning that employs a variety of statistical, probabilistic and optimization tools to *learn* from past examples, and then, to use that prior training to classify new data and identify new patterns [52]. Currently, PR methodologies have surpassed human ability to learn from data at an efficient speed [53]. Typically, to apply PR methodologies on industrial data, the acquired signal is divided into small segments to extract repetitive patterns. Features extracted from these segment patterns are compared to preprocessed ones extracted from a healthy tool through a supervised pattern recognition technique to define the tool condition. However, when machine data is targeted, selecting the appropriate PR methodology for industrial applications is crucial. For example, most of the modern applications of aerospace machining are dependent on high-speed machining technologies, and hence, they are time sensitive. Therefore, time sensitivity must be considered in the development of PR classifiers.

The general scheme for applying a pattern recognition technique consists of five steps, namely, signal conditioning, segmentation, features extraction, features selection and supervised classification training. In the first step, signals are treated for any continuous bias and then filtered. This is to reduce the noise in the acquired signals and to keep only the signal frequencies that best describe the cutting process and the monitored states. The conditioned signals are then segmented in the second step to provide a signal that represents the actual tool/work piece engagement. The segments should be for a repetitive pattern of the actual cutting process such as full tool rotation during milling applications. However, for continuous turning processes, fixed-time-based segments can also be applied. Moreover, it should be noted that the selection of the segment size and the relative time sampling used for collecting these segments affects the ability to process the resulting signals for feature extraction in the third step

[45]. For example, small segments with a limited number of sampling points cannot be analyzed in the frequency and/or time-frequency domains. This is because the available techniques cannot accurately represent frequency content composed of such small segments. Hence, features to be extracted from these small segments are limited to time domain analysis only, such as segment peak value, mean, variance or root mean square.

The output of step three is a considerable number of potential features that can be used to describe tool status. However, which subset of features should be used for the accurate detection of the tool condition is the main focus of step four. The usage of numerous features that can be extracted in the time and frequency domain to develop a PR classifier does not always assure success. The use of too many features, which is usually referred to as the 'curse of dimensionality', generates an overfitted PR classifier which delivers low prediction accuracy. Additionally, optimizing the number of features reduces the measurement and computational cost. Hence, in step four, only features with high sensitivity to the tool condition must be selected. This simplifies the classifier complexity and improves the classification accuracy. In TCM applications, numerous time and frequency domain features have been integrated into PR methods to detect the tool condition [18, 31, 45, 54]. However, the literature does not provide key features that can describe the tool condition under different cutting parameters, and selection of the best subset of features is not fully addressed.

There are several methods and criteria to select the optimum feature subset including exhaustive, heuristics and sequential feature selection methods. Sequential search-based approximation schemes have been widely proposed for supervised pattern recognition methods [55]. In particular, sequential feature selection (SFS) is one of the most widely used methods to optimize the feature selection process [56]. It selects a subset of features by sequentially adding (forward search) or removing (backward search) features until a termination criterion is met [57]. This criterion is usually the classification error rate within the training data, which makes the feature selection process not only dependent on the TCM application, but also on the selected PR method.

In this last step, supervised PR methods are trained using 'labeled' training data. Features extracted from each segment are assigned to one of the classes (e.g., healthy

or worn tool). Labeled data are generated from the extracted features, and then, fed to the PR classifier as training data. Several PR methods have been integrated in TCM applications to monitor the tool condition and to allow automated decision making. The main PR methods applied for TCM applications are Support Vector Machine (SVM) [58-61], Linear Discriminant Analysis (LDA) [62-65], k-Nearest Neighbor (kNN) [66 , 67, 68], Artificial Neural Network (ANN) [23, 69-71], Naïve Bayes (NB) [72-74] and Decision Trees (DT) [75-77]. Although these techniques have been shown to be effective approaches for TCM, their main drawback is due to their dependence on probabilistic and optimization techniques and not physically meaningful models. This may not guarantee their resulting performance [78]; however, high accuracy can be achieved if the PR method is built using a learning experiment that is properly designed and has high sensitive features for the tool condition, and if the results are robustly validated. Hence, it is essential to carry out a systematic study of the feasibility of the PR methods for industrial TCM applications based on a set of generalized features.

2.6.3. Multi-Signal Processing TCM Systems

Pattern recognition techniques have been combined with trend analysis routines to gather more information from collected signals [27, 41, 50] to increase the level of certainty and information. Such an action can increase the level of certainty and signal information, but it also increases the processing time. However, none of the available TCM systems in the literature, which use trend analysis, PR or a combination of both, were successful to mask the effect of cutting parameters on the acquired signals and accentuate the tool condition effect only. Hence, a novel signal processing approach is required to identify the tool condition (i.e., tool prefailure, wear, chipping and breakage) under different cutting parameters in highly dynamic cutting processes.

2.6.4. Descriptive Features

In general, this section discusses the features reported in the literature of TCM as well as condition monitoring and diagnosis of rotary machineries. In the time domain, the most indicative features are the root mean square, maximum peak value, standard

deviation, variance, average, harmonic and trimmed mean value, mean absolute deviation, skewness and kurtosis, and the ratios between these features. The mean and median frequency, band power and the statistical features of the wavelet, empirical mode decommission as well as Welch and Periodogram power spectra have also been reported as sensitive features to the tool condition in the frequency domain. These time-and-frequency-domain features were reported for the forces [15, 79-83], motor feedback signals [84-86], vibrations [30, 87-90] and AE signals [20, 24, 29, 60]. Additionally, these features showed sensitivity when extracted from each signal component (e.g., forces in x, y and z directions) or from the resultant signals.

Several physical and statistical features have been reported as sensitive features to the tool condition. However, the reported sensitivity of these features cannot be generalized as they were extracted from problem-dependent data. The level of sensitivity was much dependent on the machining process, cutting parameters, acquired signal, and signal conditioning and processing. Hence, it is crucial to carry out a systematic study to test and rank the sensitivity of these features after masking the effect of the cutting parameters on the acquired signals, which is done in this work.

2.7. Multi-Sensor TCM Systems

From the literature, it can be concluded that a reliable online TCM system must have the following features:

- Be sensitive to changes in tool conditions [7],
- Be insensitive to other process variations and dynamics [7],
- Provide signal information reflecting the tool condition type [30],
- Provide a high level of decision certainty, i.e., minimum error percentage [14],
- Perform signal processing and decision making in an adequate time span [30].

Many TCM systems for milling applications suffer from a lack of certainty, key feature extraction, standardization and generalization [14, 46]. This is mainly due to the absence of a stand-alone sensor capable of reflecting tool conditions under diverse cutting conditions, due to the high dynamics of the milling process, which limits extracting and generalizing a descriptive feature of the tool condition, and due to the

lack of a highly informative signal processing technique. In order to overcome these problems, recent systems have enhanced their performance by using multi-sensor fusion techniques to enrich system certainty and information. These systems depend on more than one sensor to achieve multiple tool condition detection capability. Many systems [14, 22, 31, 47, 49] employ artificial intelligence techniques to integrate information, extract features and make more reliable decisions. This can increase the system sensitivity and level of certainty. However, there is a need for more hardware (i.e., sensors, cables and separate signal conditioner/amplifiers) which can interfere with the available working space for machining. In addition, if AI processing is not correctly fused, it may increase the response time and may lead to unnecessary alarms.

2.8. Summary

From the above-mentioned literature review, the following conclusions can be drawn.

- Tool prefailure detection of chipping and breakage in milling operations has never been discussed before.
- Available real-time post-failure detection systems have a high response time.
- None of the available TCM systems have considered working in an adaptive control with constraints environment.
- Available TCM systems are not effective due to the lack of robust standalone sensors and processing techniques that meet the requirements of real-life applications.
- Vibrations are less correlated with tool monitoring in milling operations due to the non-continuous cutting nature of the process and low sensitivity to tool conditions in HSM processes
- The excessive cost of multi-axis dynamometers, their intrusive nature in production environments, their lack of overload protection in case of collision, and their limited frequency response make it exceedingly difficult to apply them in industry.

- Despite their challenges to be implemented for TCM, spindle feedback sensors associated with AE sensors are the best sensors to be applied in industrial applications.
- Spindle feedback sensors have a non-intrusive nature and are independent of sensor position, orientation or signal path.
- AE signals are sensitive to the generation of new surfaces during tool chipping and/or breakage. Additionally, the AE signals generated by the machining process are not contaminated by process noise. However, they are not fully understood.
- Acoustic emission sensors mounted on the spindle show higher reliability than when mounted on the workpiece.
- Time domain trend analysis techniques are not applicable for reliable TCM systems and need enormous learning effort.
- The HHT method has many advantages over other frequency or time-frequency domain methods.
- There are no key features available that can describe the tool condition under different cutting conditions in highly dynamic processes.
- No systematic study is available to benchmark the available pattern recognition techniques according to their accuracy and applicability in TCM applications.
- Developing a reliable TCM system requires combining multi-sensor fusion with multiple signal processing types, namely, trend analysis and pattern recognition. Multi-sensor fusion guarantees a high level of decision certainty, whereas using two signal-processing types for each signal helps gather an adequate amount of signal information. None of the available TCM systems combines both components to achieve a desirable performance.

CHAPTER 3
EXPERIMENTAL SETUP AND DESIGN OF EXPERIMENTS

3.1. Introduction

This chapter provides a description of the machine tool, cutters, workpiece materials and experimental setups used for all the tests conducted in this research work. In addition, selection of sensors and the position and orientation of each sensor are discussed in this chapter. In this research work, milling and intermittent turning experiments were conducted to develop and validate tool wear and tool prefailure detection systems. Different setups were prepared for each cutting process to agree with the system needs. For the tool prefailure detection system, intermittent turning operations were conducted to investigate the capabilities of different sensors to capture tool prefailure and to validate the proposed signal processing technique in order to capture tool prefailure and the onset of tool failure due to chipping. Afterwards, two setups were prepared for milling and intermittent cutting operations to test and validate the results. For the tool wear detection system, milling operations were conducted for developing and validating sensor-based models to detect tool conditions due to progressive failure. They were also employed to provide reference data for the sake of feature analysis and classification method comparison, as is shown later in Chapters 5 and 6. The following subsections illustrate the machine tools, cutters, tools, workpiece materials, sensor selection, experimental setups and cutting conditions with which all the research tests were performed. It also describes the hardware used for implementing the TCM systems in real-time.

3.2. Machine Tool

All the milling tests were performed on a 5-axis DMU-100P duoBlock machining center, shown in Figure 3-1 (a). This machining center is featured with 28 kW spindle power, three linear and two rotary axes, a maximum spindle speed of 18,000 rpm and a maximum feed rate of 60 m/min. The working envelope of this machining center is

1000 mm x 1000 mm x 1000 mm which can accommodate large workpieces for aerospace applications. Turning operations were carried out on a 6-axis Boehringer-NG200 CNC turning center, shown in Figure 3-1 (b). This machine tool has a maximum spindle power and rotational speed of 36 kW and 4,000 rpm, respectively. It has a maximum turning length, swing diameter over bed and turning diameter with external tools of 850 mm, 600 mm and 300 mm, respectively. Both CNC centers have a Siemens

Figure 3-1 (a) DMU-100P duoBlock CNC machining center used for milling tests

Figure 3-1 (b) Boehringer-NG200 CNC turning center used for turning tests

SINUMERIK 840D controller which accepts limited third-party communication and overwriting. This capability is utilized for process control to avoid tool fracture and safeguard the machined part as is shown later.

3.3. Cutting Tool

A wide range of tungsten carbide (WC) turning and endmill cutters with different geometries were used during the development and validation of this research work. The tool geometrical parameters are shown in the schematic drawing in Figure 3-2. Table 3-1 shows the geometrical and structural data of the used tools. Collet and shrink-fit tool holders were used interchangeably between endmills. These tool holders provided different configurations to provide a variety of cutting tool geometries using similar cutting inserts. On the other hand, for turning applications, a Sandvik PD JNL 2020K 11 tool holder was used with the different turning inserts as reported in Table 3-1. In total, 14 milling tools were used during the course of this work to develop and validate the TCM systems. Selected endmills consisted of 2, 3 and 4 flutes and diameters varying from 10 to 50 mm. They had flat and rounded cutting edges with corner radii varying from 0 to 4 mm. The turning inserts were diamond shaped with an angle of 55° and a cutting-edge length of 9.56 mm. However, they had different coatings and nose radii.

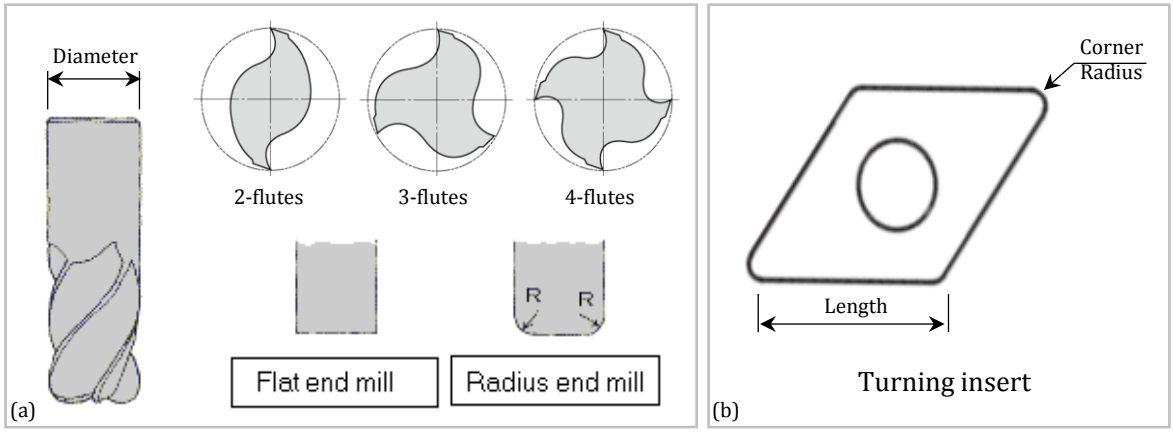

Figure 3-2 Schematic drawing of (a) an endmill (b) a turning insert

Table 3-1 Geometrical and structural data of the used tools

Tool	Application	Structural Type	Diameter (mm)	Number of flutes	Corner radius	Coating
T10F2R00	Milling	Solid	10	2	Flat	-
T12F2R00	Milling	Solid	12	2	Flat	-
T16F2R00	Milling	Solid	16	2	Flat	-
T16F2R04	Milling	Insert	16	2	04	-
T16F2R33	Milling	Insert	16	2	33	
T20F2R04	Milling	Insert	20	2	04	-
T20F2R33	Milling	Insert	20	2	33	-
T20F2R40	Milling	Insert	20	2	40	-
T25F2R04	Milling	Insert	25	2	04	
T25F2R40	Milling	Insert	25	2	40	-
T25F3R04	Milling	Insert	25	3	04	-
T25F3R33	Milling	Insert	25	3	33	-
T50F4R04	Milling	Insert	50	4	04	-
T50F4R40	Milling	Insert	50	4	40	-
DCMT11T304	Turning	Insert	-	-	0.4	CVD (TiCN / AI2O3 / TiN)
DCMT11T308	Turning	Insert	-	-	0.8	PVD (Ti, Al) N / TiN)

3.4. Workpiece Material

As this thesis focuses on the application of TCM for aerospace manufacturing applications, the high and low strength aluminum alloys, AL7075T6 and AL6061T6 respectively, were selected for testing and validating the tool wear detection method. However, to speed up the tool failure process, severe, controlled cutting conditions were applied. Hence, two grades of steel plates were used during the course of this research: a high-yield-strength quenched and tempered steel alloy ASTM A514-B and a hot-rolled low carbon steel AISI1018. Table 3-2 and Table 3-3 show the main

mechanical properties and chemical components respectively of the workpiece materials used in the cutting tests during this research.

Table 3-2 Mechanical properties of the used workpiece materials

Material	ASTMA514-B	AISI1018	AL6061-T6	AL7075-T6
Yield strength (@0.2%) MPA	690	370	276	503
Tensile strength MPA	760 to 895	440	310	527
Brinell hardness	293	126	95	150
Modulus of elasticity GPA	210	205	68.9	71.7

Table 3-3 Chemical components of the used workpiece materials

Element	Content (%)			
	AISIA514B	AISI 1018	AL 6061-T6	AL 7075-T6
Al			95.8 - 98.6	87.1 - 91.4
Iron, Fe	98	98.9	0.7	0.5
Manganese, Mn	0.85	0.6	0.15	0.3
Chromium, Cr	0.48		0.04-0.35	0.18 - 0.28
Silicon, Si	0.28		0.4 - 0.8	0.4
Molybdenum, Mo	0.2			
Titanium, Ti	0.02		0.15	0.2
Carbon, C	0.12 - 0.210	0.14		
Vanadium, V	0.05			
Boron, B	0.003			
Phosphorous, P		0.04		
Sulfur, S		0.05		
Cu			0.15 - 0.4	1.2 - 2
Mg			0.8 - 1.2	2.1 - 2.9
Zn			0.25	5.1 - 6.1

3.5. Sensor Selection

Sensors were used to measure the cutting forces, vibrations, acoustic emissions and drive motor power during the course of this work. For the milling applications, the three orthogonal components of the cutting forces were measured using a quartz 3-component KISTLER dynamometer type 9255B. This dynamometer has a measuring range of ±20kN in the x and y directions and from -10kN to 40kN in the z direction with a crosstalk of less than ±2%. The acquired force signals were amplified using a 5070A

KISTLER charge amplifier. For the turning applications, the cutting forces were measured using a three component KISTLER dynamometer type 9121 with a measurement error of ±3% and amplified using a KISTLER 5010 amplifier. These dynamometers cover the cutting force range generated during high speed processes with high accuracy. It should be noted that the measurement of the cutting forces is essential for the development phase only. Therefore, the dynamometer sizes and limitations on the machine workspace were not considered for optimization for industrial application.

The measurement of the vibration signals during cutting processes, especially for milling, requires accelerometers with high sensitivity, high resolution and high bandwidth. Additionally, minimum intervention with the machine workspace should be guaranteed for industrial applications. Although microelectromechanical (MEMS) accelerometers have the advantage of small size to be integrated into intelligent modules, they still suffer from high noise and low bandwidth [89]. Hence, a miniature triaxial PCB accelerometer type 356A71 was used to acquire the vibrations during the cutting processes. It has a sensitivity and a frequency range of 1.02 pC/(m/s^2) and 4 kHz, respectively. Acquired signals were conditioned and amplified using a PCB signal conditioner model 480C02.

A KISTLER Piezotron AE sensor type 8152B was used to capture the process AE generated signals. The machining AE generated signals typically fall into the range of 100-600 kHz, whereas the tool chipping or fracture causes high powered oscillations in the frequency range from 300 kHz to 1.0 MHz [42]. Hence, a KISTLER AE coupler model 5125C1 was used to filter out the high-frequency emission signals only and to capture the analogue root mean square of the AE signals. In this coupler, the analogue AE signals were filtered using a 50 kHz high-pass filter and a 1 MHz low-pass filter. This filtering range selection represents the typical range of AE signals generated from tool chipping and fracture while eliminating those coming from mechanical vibrations and audible noise. Subsequently, a root mean square converter with an integration time constant of 1.2 ms was used. This helps to reduce the required sampling rate and to minimize the data storage for the AE signals.

The spindle motor of the CNC machines used in this work is powered by a pulse width modulation (PWM) module which converts a 600 V DC input to a three-phase AC output of 400 V. The output rated, base load and maximum current of this module is 60 A, 51 A and 113 A, respectively. It has a rated pulse frequency of 4 kHz and an output frequency up to 650 Hz depending on the voltage/frequency controlling mode. Therefore, to measure the drive motor power on the Boehringer-NG200 CNC turning center, a POWERTEK universal power cell model UPC-LB was used. This power cell uses balanced Hall effect sensors, which provide high sensitivity and low noise when applied for variable-frequency power measurements. The cell has a capacity, frequency range and response time of 100 kW, 1kHz and 50 ms, respectively. This sensor was suitable for the turning machining center due to the low rotational speed and single point cutters used in this application.

As for the DMU-100P duoBlock CNC machining center used for milling tests, it has a maximum speed of 18,000 rpm. In addition, during the course of this work, two, three and four fluted endmills are tested. Therefore, a sensor with higher response time is required. This is because the passing frequency of a rotating endmill is equal to the rotational speed (rpm) divided by 60 and multiplied by the number of flutes. Hence, assuming a 4 fluted endmill rotating at 18,000 rpm, the passing frequency is equal to 1,200 Hz. Hence, according to the Nyquist rate, the sampling rate should be at least 2,400 Hz. This is equivalent to 0.4 ms. Such response time is not available for commercial power sensors. However, commercial voltage and current transducers can provide such a response time. Therefore, for the milling tests, the instantaneous voltage and current were measured, and the instantaneous power was calculated digitally by the dot product of the acquired signals. The spindle drive motor current and voltage signals were measured at each phase of the drive module using LEM transducers type LF 310-S and DVL 1000, respectively. These transducers can measure AC, DC and pulsed current signals with measuring range, reaction time and frequency bandwidth of ±500 A, 0.5 μs and 100 kHz, respectively, for the current transducers, and ±1500 A, 30 μs and 14 kHz, respectively, for the voltage transducers.

3.6. Assessment of the Cutting Tool Condition

Tool wear, which is a change in the shape of the cutting edge of a tool due to progressive loss of tool material during cutting, can be expressed in several terms. These terms, as shown in Figure 3-3, include flank wear (VB), which is a loss of material from the tool flank. The VB can be defined using three measures [14]:

1. *Uniform flank wear* (VB1): Wear land which is normally of constant width and extends over the tool flank of the active cutting edge,
2. *Non-uniform wear* (VB2): Wear land which has an irregular width and the original flank varies at each position of measurement,
3. *Localized flank wear* (VB3): Exaggerated and localized form of flank wear, which develops at a specific part of the flank.

Usually in practical industrial machining applications, tool life is ended when the tool is no longer providing the desired dimensions or surface integrity. However, as a general practice, uniform flank wear VB1 is used as a tool-life criterion. According to ISO standards, a predetermined value of 0.3 mm, averaged over all teeth, is used as an indicator for a worn tool [2]. In addition, localized flank wear VB3 is another deterioration phenomenon that must be respected per tooth. A predetermined VB3 value of 0.5 mm should not be exceeded on any individual tooth. In a normal cutting process, the tool must be changed after reaching these values of wear.

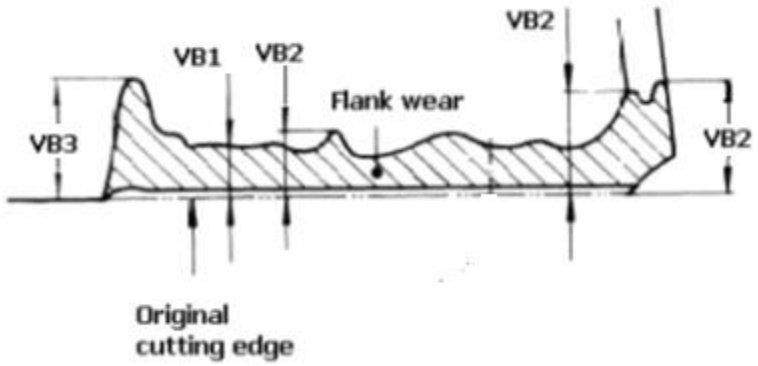

Figure 3-3 Tool wear land and different terms in the flank wear for an end mill cutter [2].

Tool chipping is another tool deterioration phenomenon which is monitored during the course of this work. It can be defined by the loss of small fragments of tool material due to crack occurrence in the cutting part of a tool [2]. Chipping occurs due to an overload of the tensile stresses on the cutting edge, which can be from numerous sources such as high feed or depth of cut, vibrations or hard inclusions in the workpiece material.

In multi-point cutting tool applications, such as milling, chipping may not totally prevent the cutting ability of the cutters. Usually the uncut part of the workpiece due the chipping of one cutting edge is removed by the subsequent cutting edges. However, such an action increases the cutting forces and stresses during the cutting operation. Depending on the cutting conditions and the chipping size, the chipping may affect the surface integrity of the machined part by inducing residual tensile stresses and altering the surface finishing and roughness. This cannot be tolerated in aerostructure machining processes. Additionally, undetected chipping may lead to tool breakage, and hence, must be prevented. On the other hand, for single point cutters, such as in turning tools, chipping cannot be tolerated because it directly affects the surface integrity of the machined part. The chipping usually occurs at the cutter nose, as shown in Figure 3-4.

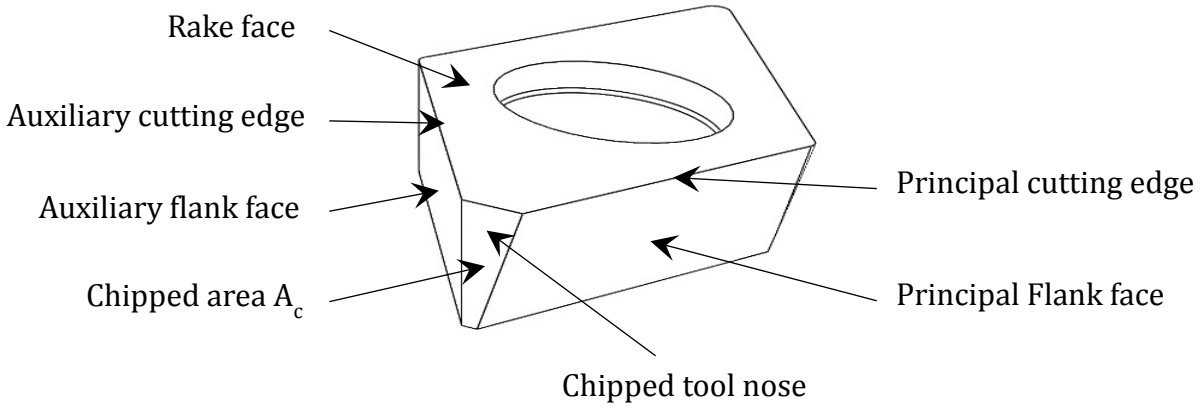

Figure 3-4 Single point cutting tool insert

According to ISO standards, for endmill cutters, chipping is usually assessed on the flank face and treated as localized tool wear, which should not exceed 0.5 mm. However, this value changes, depending on manufacturer standards and required surface finish.

In this work, tool chipping in endmill cutters is assessed following ISO standards, as shown in Figure 3-3, and different ranges of chipping are generated from 0.05 mm up to 2 mm on the flank face. For turning processes, the chipping area A_c is assessed by the new surface area occurring on the tool faces due to this event, as shown in the schematic drawing in Figure 3-4.

3.6.1. Offline Tool Condition Assessment

Flank wear and chipping were measured in this work in accordance with the ISO 3685-1993 method. Uniform and maximum flank wear, VB1 and VB3 respectively, were measured using a Winslow Engineering tool analyzer Model 560. It permits precise inspection of the tool geometry characteristics with 12X optical magnification and a resolution of 0.0001 mm. Tools were assessed after each predefined machining interval for both milling and turning applications to evaluate the wear and chipping geometries and features.

3.6.2. Real-Time Tool Condition Assessment

During the development of the tool prefailure detection system, real-time evaluation of the tool condition during the cutting process is required. Therefore, a FASTCAM high speed camera (HSC) type UX100-800K-M was used to record the chipping events in real-time during cutting. This HSC provides 1280 x 1024 pixels resolution with a selectable region of interest. It has a maximum frame sampling rate of 800 kfps and can be triggered to start recording using selectable +/- TTL 5V and switch closure with a response time of 0.1 μs. These characteristics provided the ability of evaluating the tool condition in synchronization with the acquired signals for analysis purposes. The synchronized imaging of this HSC was used to detect and measure the chipping events during the cutting processes and relate it to the acquired signals.

3.7. Experimental Setup

During the development of the tool prefailure detection system, the focus was placed on testing the ability of various signals to capture the unstable crack propagation

phase that precedes the chipping and/or breakage event as an indicator of tool prefailure. The research mainly focused on cracks due to mechanical loads only while avoiding the occurrence of tool wear and heat build-up. Therefore, a method was devised to induce a cyclic impact load on the cutting tool tip in an intermittent turning operation. This represented the loading conditions in milling as well. This type of test allowed characterizing the features of the signals collected by various sensors (forces, vibrations, AE and drive motor power) due to unstable crack propagation and tool edge chipping, while ensuring minimal tool wear. The workpiece fixture is shown in Figure 3-5. To induce a cyclic impact load on the tool tip, different steel workpieces, reported in Table 3-2 were used in the shape of plates. The plate thickness to width ratio was selected to reduce the cutting time and to allow air cooling during 85% of the cutting revolution. This minimized the thermal effect on the tool tip and provided failure due to mechanical loads only. The plate holding seats, shown in Figure 3-5, were designed to guarantee workpiece balance during the cutting operations. This test was designed to ensure tool failure due to unstable crack propagation while minimizing the occurrence of tool wear.

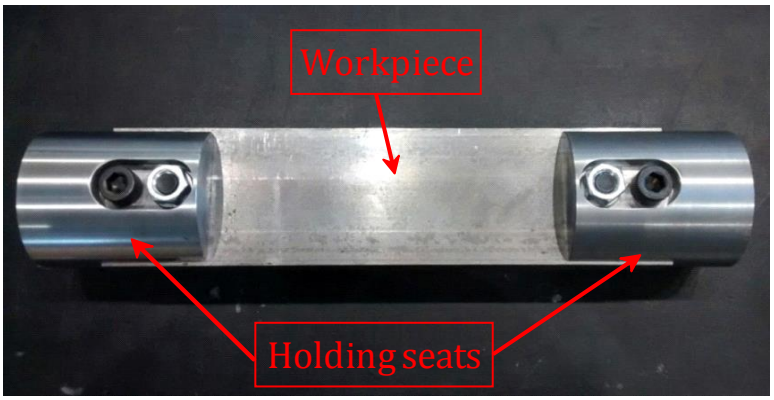

Figure 3-5 Workpiece fixture for intermittent cutting operations

Figure 3-6 shows the devised experimental setup to induce a cyclic load on the cutting tool tip. Dry turning operations were carried out using a Sandvik PD JNL 2020K 11 tool holder (1) and different carbide inserts, reported in Table 3-1, on the 6-axis Boehringer NG 200, CNC turning center. Workpieces were pre-shaped as seen in this figure to minimize the transient stage of tool entry. The cutting path was conducted as follows:

- The tool is first moved downward in air normal to the workpiece axis until it reaches the desired cutting depth of cut.
- A linear cutting operation is conducted parallel to the workpiece axis.
- The tool is vertically retracted at the end of the cutting process.

The HSC (4) was mounted on the machine turret (3) to avoid any relative motion between the point of focus and the tool tip. The tool holder was mounted on the dynamometer (5) to measure the cutting forces, which were amplified using a KISTLER 5010 amplifier. The KISTLER piezotron AE sensor (7) was mounted on the back of the tool shank to be as close as possible to the cutting zone while the tri-axial ICP accelerometer (6) was mounted on the side of the tool holder. The power sensor was mounted to measure the motor drive module output to the spindle motor over the three motor phases. The sensor position and orientation were selected to guarantee high signal resolution and not to interfere with the cutting workspace. Acquired forces, vibrations, AE and power signals were digitalized and stored on a personal computer using a National Instrument data acquisition system NI PCI-4474.

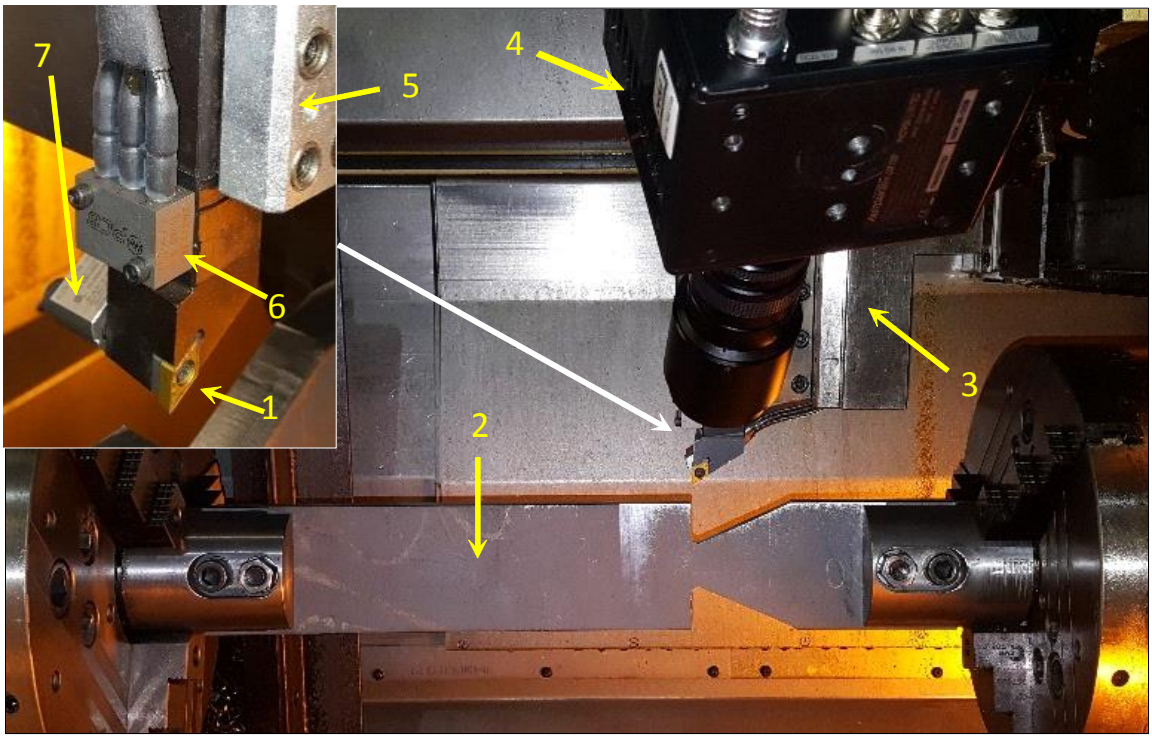

Figure 3-6 Experimental setup for intermittent turning (1) cutting insert, (2) workpiece, (3) turret, (4) HSC, (5) dynamometer, (6) accelerometer and (7) AE sensor

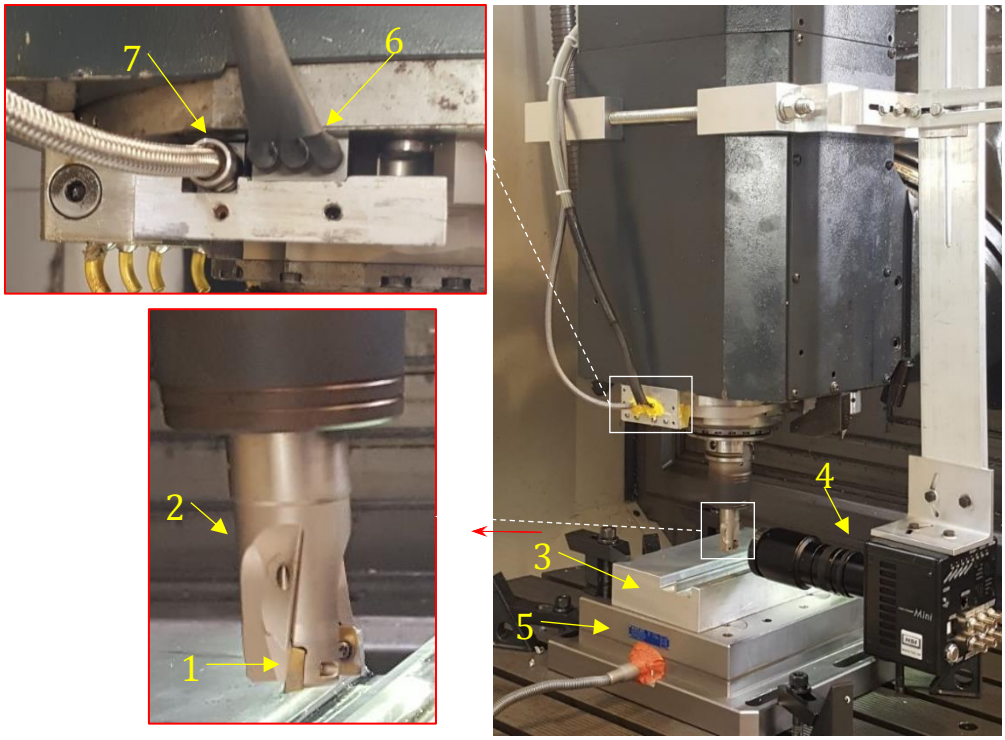

Figure 3-7 Experimental setup for milling (1) cutting insert, (2) tool holder, (3) workpiece, (4) HSC, (5) dynamometer, (6) accelerometer and (7) AE sensor

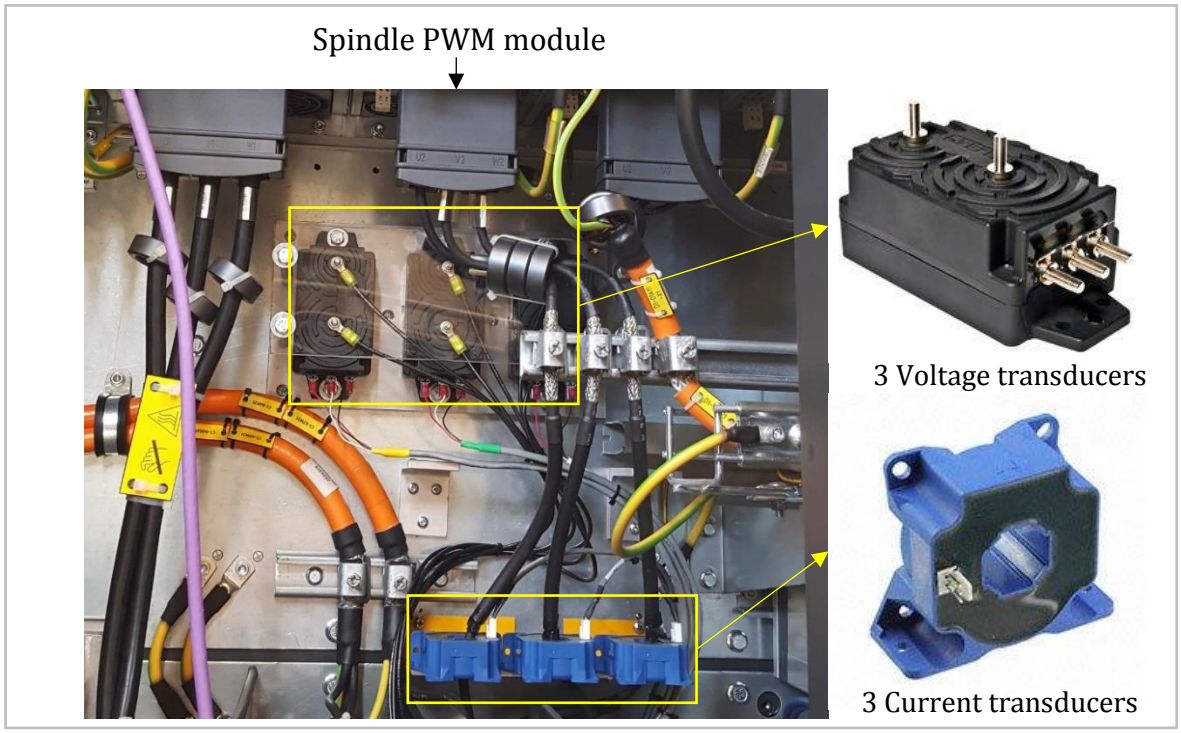

Figure 3-8 Voltage and current transducers

Figure 3-7 shows the experimental setup employed to develop and validate the prefailure and tool wear detection systems during milling operations. Milling experiments with different tool paths were carried out using endmill cutters, reported in Table 3-1, on the 5-axis DMU 100P duoBlock machining center. Aluminum and steel workpieces (3), reported in Table 3-2, were mounted on the dynamometer (5) to measure the three components of the cutting forces. A fixture was designed and built to mount the HSC (4) on the spindle head to follow the tool path. This fixture maintained rigid support for the HSC while providing 3 degrees of freedom consisting of sliding movement along its axial and two rotational movements. The accelerometer and AE sensor were mounted on the spindle around the tool holder and covered for protection against chip strikes. The current and voltage transducers were mounted to measure the drive motor output to the spindle motor over the three phases, as shown in Figure 3-8. The instantaneous spindle power was digitally calculated from the acquired voltage and current signals. A National Instrument data acquisition card type NI 4472 Series was used to digitalize and store the acquired signals. The cutting forces, vibrations and AE signals were acquired during the tests in synchronization with the HSC.

3.8. Real-Time Implementation of TCM Systems

Different hardware configurations are available for online data acquisition and monitoring systems. They are mainly dependent on Application Specific Integrated Circuits (ASICs) or a Field Programmable Gate Array (FPGA). The main advantages of an FPGA over an ASIC are its reconfigurable and reprogrammable ability. This provides more flexibility and scalability to implement and optimize new algorithms. Therefore, a National Instrument real-time embedded industrial compact controller chassis cRIO with a field-programmable gate array and a real-time processor was used as the TCM system hardware. It is a data acquisition and control system that can concurrently perform multiple data acquisition and signal processing tasks. In addition, it can simultaneously acquire signals from multiple channels at different sampling rates. Pairing the developed signal processing approaches for tool wear and prefailure

detection with the FPGA and real-time controller of the cRIO system enhanced the computational capability of the developed system.

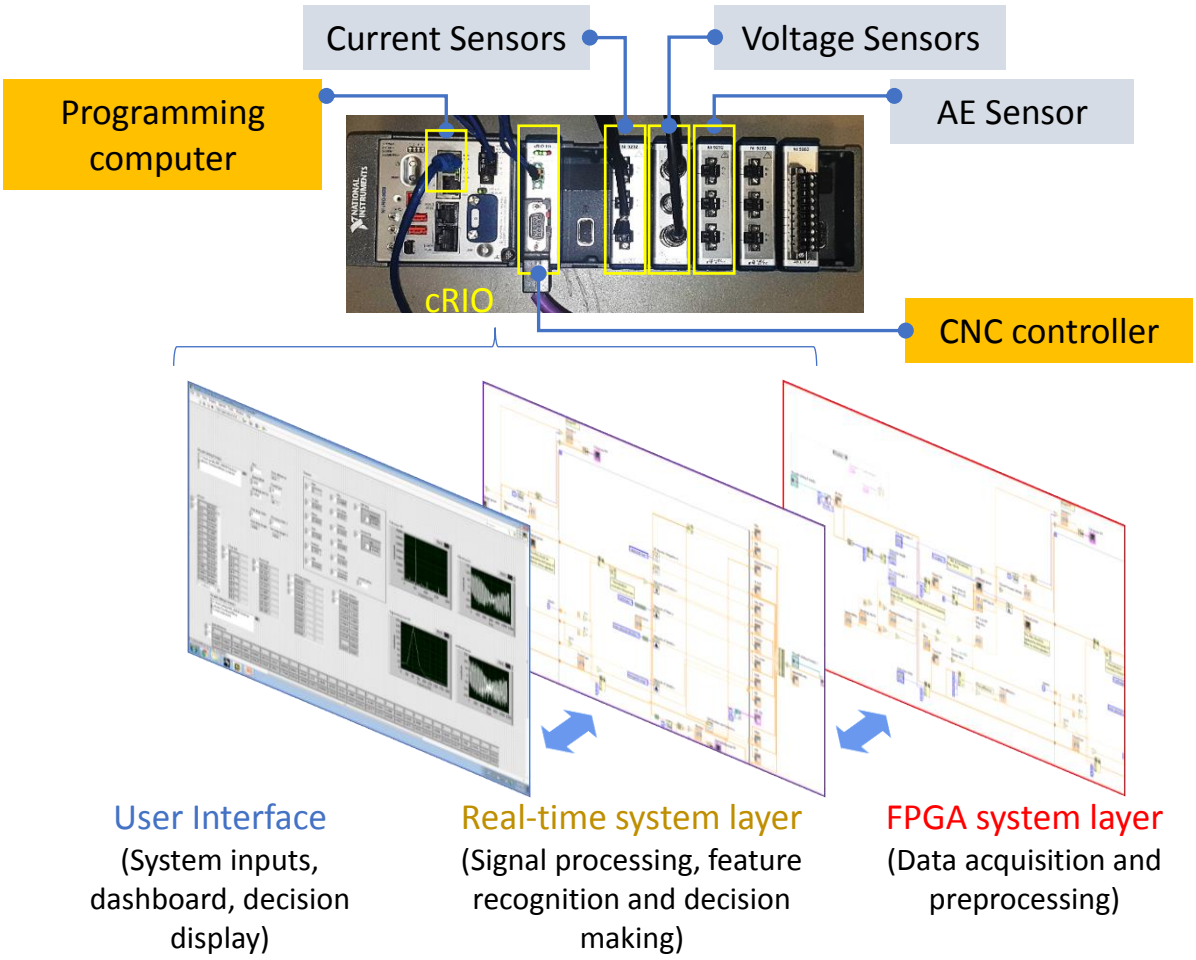

Figure 3-9 System configuration for online implementation

Figure 3-9 shows the system hardware configuration for online implementation of the TCM systems. Three channel 102.4 kS/s input modules were used for signal acquisition. Signal segmentation and conditioning were programmed on the FPGA while data processing and decision making were programmed on the real-time processor. The LabView programming language was used to build the real-time TCM system software. The integration of the LabView language helped to reduce the signal processing time by ~50%, thanks to its parallel programming environment. A PROFIBUS Interface Module was used for data transfer between the controller and the CNC machine. The CNC milling center was equipped with a 2-way communication

interface for real-time control of the process parameters. This is an interface between the cRIO system and the CNC SINUMERIK 840D system using PROFIBUS DP (Decentralized Peripherals) protocol, which allowed a high communication speed rate, based on the Remote Procedure Call communication mechanism. It allowed reading, writing and overriding of the machine control parameters during the machining process with a speed rate of 1.5 Mb/sec.

3.9. Summary

This chapter described the machine tools, cutters and workpiece materials used in this research. Powerful machine tools with the capability of high speed machining were used. A variety of milling and turning tools were employed in this work to test the effect of the tool geometry on the developed TCM system. In addition, four different types of workpiece materials were used for TCM system testing and validating as well as for accelerated generation of tool failure. The machine tools, cutters and workpiece material properties were listed and described.

The selection process of the means of sensing cutting forces, vibrations, acoustic emissions and motor feedback signals were demonstrated. During this process, the applicability, practicality, measuring range, sensitivity and response time of these sensing systems were considered. The specification of these systems as well as the position and orientation of mounting were shown.

The tool deterioration criteria and limits for tool wear and chipping were defined. A tool analyzer was used to analyze and measure tool failure offline at the end of each test. Additionally, the tool condition was assessed in real-time during the cutting processes using a high-speed camera. The imaging of this camera was used to assess the TCM system performance as described in this chapter and shown in Chapter 5.

The hardware and software used to implement the developed TCM system in real-time were demonstrated. An ultra-high-speed controller and a 2-way communication system were integrated to control high speed cutting processes in real-time.

CHAPTER 4
TOOL PREFAILURE CHARACTERIZATION AND DETECTION DURING INTERMITTENT MACHINING PROCESSES

4.1. Introduction

The objective of this work is to develop an integrated TCM system approach to reliably detect tool prefailure and to stop the intermittent turning operation in real-time before tool chipping and part damage occur. No such system is presently available. Therefore, a novel, multi-sensor signal processing approach for online prediction and prevention of tool chipping during intermittent cutting is presented. It identifies the unstable crack propagation features of the prefailure phase using feedback signals, independent of the cutting parameters and workpiece material. In this chapter, the ability of using the process monitoring signals to detect tool prefailure and failure by chipping and/or breakage during intermittent cutting operations is investigated. The processing approach is introduced, and then tested using artificial signals.

4.2. Experimental Investigation of the Monitoring Signals Ability to Detect Tool Prefailure and Onset of Failure

This section focuses on testing the ability of signals acquired by various types of sensors to capture the unstable crack propagation phase, which precedes the chipping and/or breakage event, as an indicator of tool prefailure. The research mainly focuses on cracks due to mechanical loads only, while avoiding the occurrence of tool wear. Therefore, a method was devised to induce a cyclic impact load on the cutting tool tip during an intermittent turning operation. This simulated the loading conditions during milling as well. A full description of this intermittent turning method and its experimental setup can be found in Section 3.7. This type of test allowed characterizing the features of the signals collected by various sensors (forces, vibrations, AE and drive motor power) due to unstable crack propagation and tool edge chipping, while ensuring minimal tool wear.

The cutting speed, feed and depth of cut were 70 m/min, 0.14 mm/rev and 2 mm, respectively. The turning operation was performed in 100 mm passes. After each pass, the insert was periodically removed from the tool holder and inspected for any sign of chipping or wear on the flank and rake faces using a Winslow cutting tool inspection system model 560.

4.2.1. Experimental Results

An edge chipping of 0.1 mm width was observed after the fourth turning pass, as shown in Figure 4-1 (a), while no sign of significant wear was observed. The corresponding resultant cutting force was processed and analyzed to detect any peak corresponding to tool failure, as shown in Figure 4-1 (b). The figure shows that a peak of the normalized force occurred after a total cutting length of 315.5 mm. This event can be causally related to tool failure by observing chipping as the trend of the resultant forces increased after its occurrence.

Figure 4-2 shows the normalized feedback signals of the (a) resultant force F_r, (b) vibrations in the feed direction V_f, (c) spindle motor power P, (d) acoustic emission raw signal AE and (e) acoustic emission root means square (AE_{rms}) for the prefailure, failure and post-failure stages. Figure 4-2 (a) and (b) show a burst in the resultant force and vibration signals, respectively, which coincide with the tool failure evidence shown in Figure 4-1. The cutting power (Figure 4-2 (c)) has increased slightly as well at the chipping event. The sensitivity of the cutting forces to the breakage event is due to their sensitivity to tool geometry changes [36]. While the high vibrations generated due to the tool chipping caused an instant high burst in the acquired vibration signals, regardless of the vibrations coming from the tool/workpiece engagements. This shows the cutting force and vibration signal capabilities to capture tool chipping as small as 0.1mm. However, these raw signals did not show any changes during the prefailure phase (i.e., during unstable crack propagation).

On the other hand, no corresponding bursts were observed in the AE and the AE_{rms} signals at the onset of chipping (Figure 4-2 (d) and (e)). However, high bursts in the AE and the AE_{rms} were captured earlier by three sequential engagements between tool and

workpiece, as shown in Figure 4-2 (d) and (e). This event can be related to the tool prefailure stage, which is characterized by crack propagation. This peak was not observed in the other measured signals.

The forces, vibrations, AE and power signals were generated during the cutting process due to the tool/workpiece engagement. The variation in these signals due to chipping is uncertain. For example, the cutting forces depend on the force coefficients of the cutting tool and the material removal rate *MRR*. Such a relation may alter the resultant forces generated during tool chipping or breakage. Based on the chipping size, position and shape, the cutting forces may increase, decrease or stay unchanged. Assuming one tool/workpiece engagement per revolution, if the chipped part of the cutting tool edge is higher than the cutting feed rate per tooth f_z, the tool is no longer engaged in cutting, which reduces the *MRR* to zero. On the other hand, if the chipped edge segment is smaller than f_z, the tool cuts the workpiece with the chipped edge, where its force coefficients are greater than those of a normal edge. Hence, the integrated results between the *MRR* and the force coefficients of the chipped part control the value of the cutting force at the onset of fracture. Because of the high uncertainty of the chipping characteristics (e.g., size, position and shape), both increasing and decreasing the acquired signals are possible after chipping.

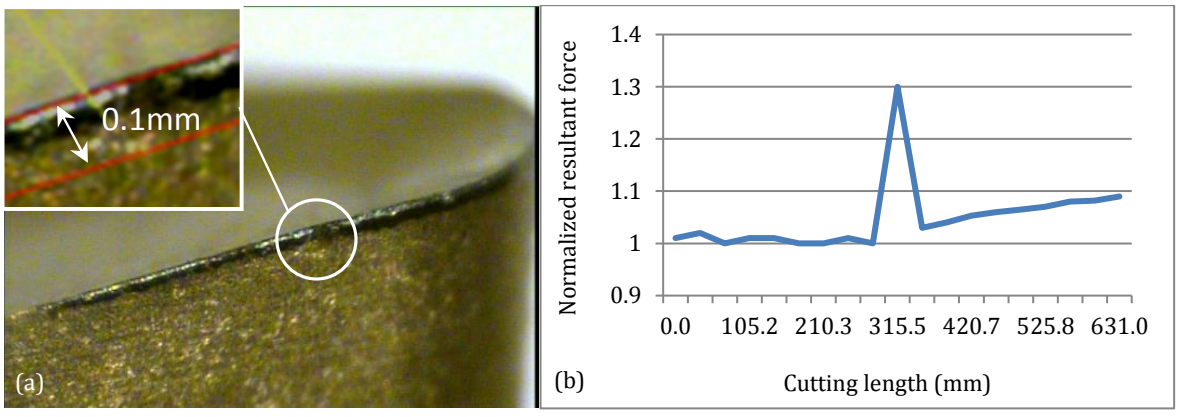

Figure 4-1 (a) Edge chipping after the fourth pass (b) Normalized resultant force through all turning passes

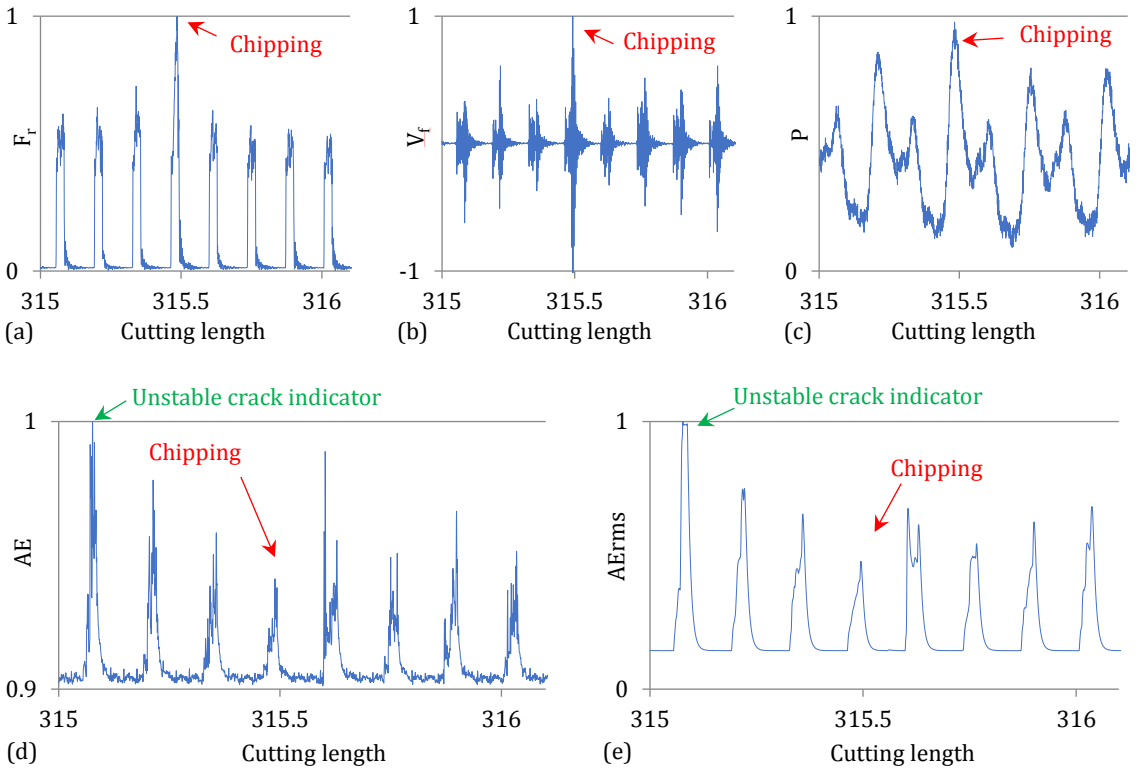

Figure 4-2 Normalized signals of (a) resultant force 'F_r' (b) vibrations in feed direction 'V_f' (c) drive motor power 'P' (d) acoustic emission AE and (e) acoustic emission rms 'AE_{rms}'

However, there are other sources of AE signals during the cutting process. One of them is attributed to the elastic stress waves produced by the release of strain energy because of the new surface generation during the course of crack propagation. Such sensitivity explains the first burst in the AE and AE_{rms} signals observed before chipping as an indicator of new surface generation on the tool edge and as an indicator to unstable crack evolution, as seen in Figure 4-2 (d) and (e). In addition, they showed sensitivity to changes in tool geometries after chipping. This sensitivity can be seen in the high burst in the AE signals and the high energy in the peak of the AE_{rms} signal after chipping, as seen in Figure 4-2 (d) and (e). These characteristics and the response of the AE and AE_{rms} signals recommends using them for real-time tool prefailure detection due to:

1- Their sensitivity to unstable crack propagation, which precedes tool chipping/breakage,

2- Their sensitivity to changes in cutting-edge geometry due to chipping/breakage,
3- Allowing a sufficient time window (e.g., three tool/workpiece engagements) during intermittent cutting operations to take the appropriate corrective action.

Such characteristics can be employed to prevent any damage to the workpiece and the machine tool as a result of tool sudden failure.

It should be noted that the peak value of the spindle motor power signal (Figure 4-2 (c)) did not show a significant increase at the chipping event compared to the normal cutting peak value, which disagrees with reported findings in the literature [27, 50, 91]. This can be linked to the small chipping size (0.1 mm) and the limited sensing bandwidth due to the inertia of the drive motor rotor, which acts as a low pass filter at the same motor frequency [45], whereas abrupt failure is a high frequency event.

4.3. AE Signal Characteristics in the Prefailure Phase

The findings in Section 4.2 show that the AE waves associated with the generation of new surfaces during unstable crack propagation have high potential to be used as a tool prefailure indicator. It is clear that the AE_{rms} signals have the same time-domain sensitivity to the prefailure phase as the raw AE signals, as shown in Figure 4-2 (d) and (e). However, the AE_{rms} signals have the advantage of reducing the required sampling rate, which minimizes data storage. As a result, the AE_{rms} signals were investigated further to be implemented in the tool prefailure detection system.

An FFT was calculated for the AE_{rms} signal to study its characteristics in the frequency domain. The signal was segmented per each tool/workpiece engagement before, during and after the prefailure phase, as shown in Figure 4-3 (a). In total, 13 segments were analyzed to determine their FFT power and mean frequency f_{mean}, as shown in Figure 4-3 (b). Additionally, the mean frequency of all the peaks, as one segment, was calculated and referred to as ft_{mean}. As seen in Figure 4-3, the AE_{rms} signal showed the highest FFT power at the unstable crack indicator (peak No. 6). This was followed by peak No. 10, which indicated the first engagement between the tool and the workpiece after chipping. Additionally, the highest f_{mean} values were found during the prefailure phase; the f_{mean} of individual peaks only exceeded the ft_{mean} at the prefailure

stage (i.e., peak No. 6, 7 and 10). Such findings show that the prefailure phase induces high relative frequency and density in the frequency domain in addition to their high relative peak values in the time domain of the AE_{rms} signal, expressly at the unstable crack indicator.

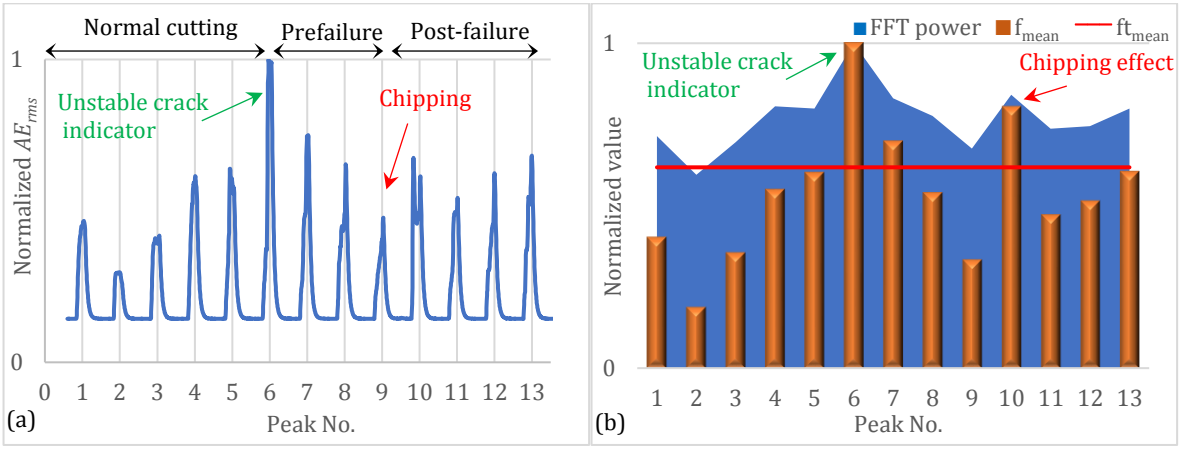

Figure 4-3 AE_{rms} before, during and after prefailure in (a) time domain and (b) frequency domain

During intermittent complex cutting processes, identifying the prefailure phase is challenging due to the bursts coming from other process sources. These sources can be classified into two groups [92]: steady-state operation AE waves such as formation and collisions of chips and rubbing between cutting tool, workpiece and formed chips, and abnormal AE waves that can be generated due to cutting tool vibrations and damage. The indeterminateness of some of these events in addition to the stochastic nature of the unstable crack propagation and its generated AE waves cause a non-stationary nature to the AE_{rms} signals.

To describe the generated AE_{rms} signals during cutting, a quantitative model of the AE_{rms} peak voltage in machining using carbide inserts was successfully developed [93]. This model was developed in order to understand the AE signal response to the fracture of carbide inserts during intermittent cutting. The model describes the AE_{rms} voltage as a function of the cutting tool material properties, wave propagation properties, crack propagation and cutting forces as follows:

$$AE_{rms} = K_1 \sqrt{\frac{E}{(1+v)^2.(1-v^2)}} \sqrt{\frac{\omega^2.\delta^2}{(k^2+\omega^2)}} F_r \sqrt{\alpha a^{\beta}.\Delta a.\Delta A_c{}^2} \qquad \textbf{4.1}$$

where K_1 is a constant, E and v are the modulus of elasticity and Poisson ratio of the tool material, respectively. k, ω and δ are the crack AE wave decay constant, frequency of decaying and stress propagation factor, respectively. F_r is the resultant cutting force at tool fracture, α and β are constants related to tool geometry, and a and A_c are the crack length and area, respectively. This equation can be simplified, for the same tool material, after assuming ΔA_c is a linear function of Δa as follows:

$$AE_{rms} \approx C F_r (\Delta A_c)^{1.5} \qquad 4.2$$

where C is a material and geometry dependent constant. Equations 4.1 and 4.2 show the nonlinear relationship between the AE_{rms} signal and cutting forces. The AE_{rms} signal variation through the course of the intermittent cutting operation for the same insert depends mainly on the resultant force variation and new generated crack surfaces. Furthermore, as the AE_{rms} depends on the instantaneous F_r, it is highly expected that the crack propagation bursts could be contaminated by the bursts coming from the force variation during intermittent cutting.

4.4. AE Signal Processing Approach for Real-Time Prefailure Detection

The prefailure phase induces high frequency/amplitude bursts in the AE_{rms} signals. However, the main challenges of detecting the unstable crack propagation phase, preceding tool chipping, using the AE_{rms} raw signal are: (i) the nonlinear relationship between the AE_{rms} response and the change in the crack area ΔA_c, as shown in Equation 4.2, (ii) the non-stationary nature of the AE signal and the stochastic nature of the unstable crack propagation process, (iii) the contamination of the crack propagation bursts in the AE_{rms} signal by the bursts coming from the force variation during intermittent cutting, and (iv) the infinitesimal time spans of the high frequency bursts inherent in unstable crack propagation. This leaves a relatively short time (on the millisecond-scale) for taking corrective action after detection. As the AE_{rms} raw signal is *insufficient*, by itself, to be an indicator for tool prefailure detection, a special signal

processing approach is required to accentuate the high frequency/amplitude events in the signal to ensure a reliable and robust tool prefailure indicator.

4.4.1. Signal Processing Approach

To emphasize the crack propagation effect on the AE_{rms} signal and to depress the steady state cutting effect, a two-stage novel approach was developed to detect the prefailure evolution phase. It can deal with the aforementioned challenges of using the AE_{rms} raw signal for tool prefailure detection. Challenges (i) and (ii) are overcome by the first stage of the proposed approach, which is based on direct extraction of the energy associated with the intrinsic time scales in the signal by applying the HHT [94]. In the second stage, the Teager–Kaiser Energy Operator (TKEO) [95] is applied to highlight the prefailure phase and to suppress the bursts coming from the force variation and signal noise in the cutting process, thus overcoming challenge (iii). This provides an outcome proportional to the multiplication of the instantaneous frequency and the peak value of the AE_{rms} signal. Hence, physical events with a relatively high frequency and high energy nature are accentuated, whereas events with high energy only or high frequency only are depressed.

The HHT is a non-linear and non-stationary empirically based signal processing method that can recognize abnormal signal changes and can indicate the instantaneous frequency changes within one oscillation cycle. It can represent the data in a physically meaningful way by analyzing the signal in the time-frequency domain, in which, a peak means that a wave of the corresponding frequency has appeared at that particular time interval. In addition, the TKEO gives the estimated energy content in the processed signals and accentuates the high-frequency content [95]. The adopted approach can be mapped out in four steps:

1. Signal sifting to decompose the signal into a superposition of natural modes termed the 'intrinsic mode functions' (IMFs), using the 'mode decomposition' method [94]. This is a direct and adaptive method with posteriori defined basis used to define the linear and nonlinear harmonics of the processed signal. Each mode represents a frequency range, varying from signal noise to the main signal trend. To find the IMFs, first the local

maxima and minima in the time domain AE_{rms} signal are located. Then, two cubic splines are used to define the upper and lower envelopes by linking the signals local minima and maxima respectively, as shown in Figure 4-4 (a) for an arbitrary signal *x(t)*. These two envelopes must contain all the signal data in between. The first component of the sifting process h_1 is the difference between the input signal *x(t)* and the mean of these two envelopes m_1, shown in Figure 4-4 (b). The sifting process is repeated *k*-times using the extracted component $h_{1(k-1)}$ as the input signal until the sifted signal is reduced to the first IMF component as follows:

$$IMF_1 = h_{1(k-1)} - m_{1k} \quad \textbf{4.3}$$

where m_{1k} is the mean of the two envelopes after *k*-times. The sifting stoppage criterion can be found in [94]. IMF_1 is subtracted from the original signal *x(t)* and the output is treated as a new input signal for the sifting process. Hence, the original signal can be represented as:

$$S(t) = \sum_{j=1}^{n} IMF_j(t) + r(t) \quad \textbf{4.4}$$

where r is a residue. Each of these IMFs can be analyzed for their instantaneous frequencies.

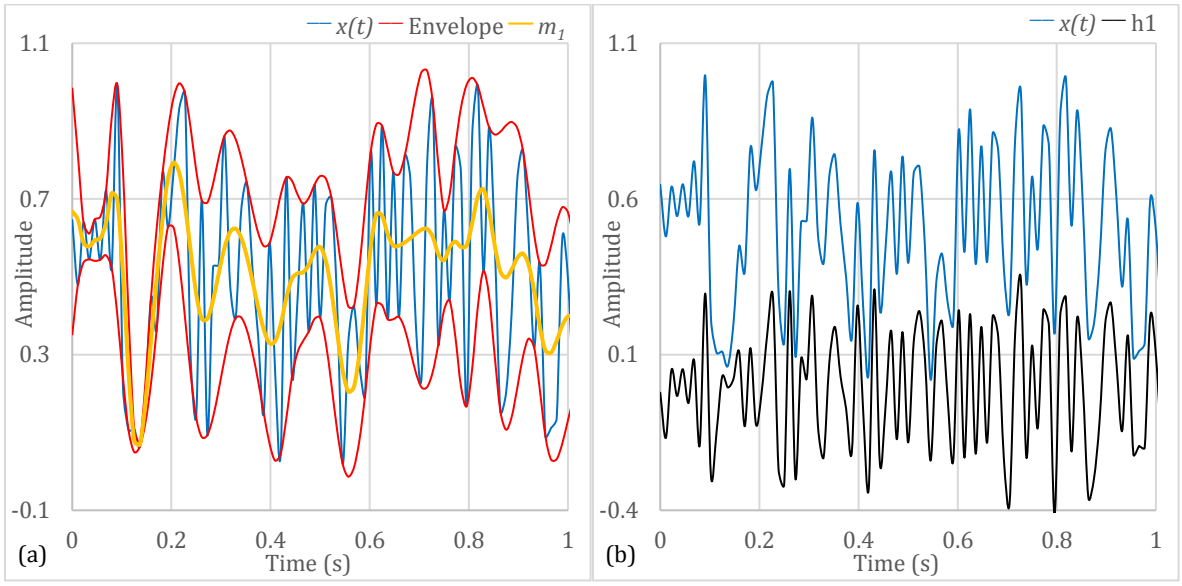

Figure 4-4 (a) Input signal x(t), upper and lower envelopes and their mean value m_1 (b) Input signal and first sifting component h_1

2. Application of the Hilbert transform $y_j(t)$ to the IMF(s) [94]. The instantaneous frequency is calculated for each IMF, in the time domain, using the HHT to identify the intra-frequencies of the prefailure phase.

$$y_j(t) = \frac{1}{\pi}\int_{-\infty}^{\infty} \frac{IMF_j(\tau)}{t-\tau} d\tau \quad 4.5$$

with a definition of the complex function of the analytic signal as:

$$S_j(t) = IMF_j(t) + iy_j(t) = a_j(t)e^{i\theta_j(t)} \quad 4.6$$

where $a_j(t) = \sqrt{IMF_j^2(t) + y_j^2(t)}$ is the processed signal instantaneous amplitude and $\theta_j(t) = \tan^{-1}\left({y_j(t)}/{IMF_j(t)}\right)$ is the phase function for each IMF.

The HHT spectrum, generated by the summation of the IMFs' transforms, is a function of the IMFs instantaneous amplitude, frequency and the phase between them. The original signal can now be represented as:

$$S(t) = Re\left[\sum_{i=1}^{n} a_i(t)e^{i\int \omega_j(t)dt}\right] \quad 4.7$$

where $\omega_j(t) = \frac{d\theta_j(t)}{dt}$ is the instantaneous frequency. This identifies the instantaneous signal energy and frequency in the time domain. Hence, a peak in the Hilbert spectrum represents the *abnormal events* in the considered time interval.

3. Application of TKEO to the transformed signals [95]. This emphasizes the relatively high frequency/amplitude events of crack propagation and suppresses the effect of the impact cutting forces on the AE_{rms}. The TKEO is applied for discrete signal of *n* points as follows:

$$\boldsymbol{\Psi}(S(n)) = S^2(n) - S(n+1) \times S(n-1) \quad 4.8$$

This operator has high sensitivity to instantaneous changes in frequency dependent energy, as its output is proportional to the product of the instantaneous amplitude and frequency of the input signal. Hence, physical events with relatively high frequency and high amplitude are accentuated, whereas events with relatively high energy only or high frequency only are depressed. The instantaneous nature of the TKEO and its very low computational time make it an ideal tool for a real-time application [95].

4. Application of a window function to the TKEO output to localize local maxima [95]. The Bartlett window function with an integer filter implementation was chosen to keep the complexity of the algorithm as low as possible.

$$\Psi_B(S(n)) = \Psi\big(S(n)\big) \otimes w(n) \tag{4.9}$$

where $w(n)$ is the window function and $\otimes$ is the convolution operator. The window output is proportional to the square of the product of the instantaneous amplitude and the frequency of the input signal [95]. Hence, the implementation of this function increases the unstable crack indicator uniqueness in the output signal.

4.4.2. Implementation of the Signal Processing Approach in a Real-Time Application

For real-time implementation of the proposed signal processing approach, challenge (iv), detecting the unstable crack propagation phase, preceding tool chipping, using the AE_{rms} raw signal as stated in Section 4.4.1, needs to be addressed. The processing time is affected by the signal segment length and sampling rate. As the proposed processing approach accentuates the *relative* high frequency/energy events, short windows may not contain enough relative data to process. Furthermore, a low sampling rate may cause the loss of some of the high-frequency information in the prefailure phase. On the other hand, long time windows and/or high sampling rates increase the signal-processing time. Hence, to select a representative segment for the repetitive load on the cutting tool, a full workpiece rotation window was used. To ensure no loss of information related to the relative changes in the instantaneous amplitude and frequency of the processed signal interval, a 50% overlap between segments was implemented. This assures that the beginning and ending of the prefailure phase is captured and compared to steady state cutting. Additionally, the AE_{rms} was calculated from the analogue raw AE signal, before digitalization, in order not to lose signal content, and to minimize the required sampling rate and data storage. AE raw analogue signals were filtered using a band from 100 kHz to 900 kHz to isolate the high frequency sound emission signals and to improve the signal to noise ratio. Moreover, signal linear de-trending was applied to remove the signal gradual change due to the tool path.

The main feature that represents an abnormal event in the processed signal is the maximum peak value for each window $\boldsymbol{\Psi}_{BW}=\max(\boldsymbol{\Psi}_{B})$. Hence, it was extracted and used as a prefailure detection parameter. A static threshold was defined experimentally based on $\boldsymbol{\Psi}_{BW}$ to predict tool prefailure.

4.5. Testing the Developed Approach Using Artificial Signals

To demonstrate the performance of the proposed approach, Figure 4-5 (a) shows an ideal nonlinear periodic signal, which represents the AE_{rms} signals during cutting operations. This signal has been contaminated by an artificial fault signal, shown in Figure 4-5 (b). This is a sinusoidal decaying signal that simulates a sudden AE burst generated by a non-stationary crack propagation process. The contamination signal has been added to the original signal, as seen in Figure 4-5 (c). To apply the HHT method, the signal has been first decomposed into its intrinsic mode functions IMFs using the empirical mode decomposition method, described by Equation 4.3 and 4.4. In total, the contaminated signal was decomposed into 10 superposition natural modes IMF, as seen in Figure 4-5 (d). These IMFs can be grouped into two categories, a high frequency range (e.g., from IMF_1 to IMF_5) and a low frequency range (e.g., IMF_6 to IMF_{10}), where IMF_{10} represents the signal residue *r*.

The Hilbert Huang transformation was applied to all the generated IMFs to calculate their frequencies in the time domain and to define the intra-frequencies during the abnormal event. Equations 4.5, 4.6 and 4.7 were used to find the HHT spectrum of the contaminated signal by calculating the processed signal instantaneous amplitude, frequency and the phase function of each IMF. The HHT spectrum was generated by the summation of the IMF transforms. To emphasize the instantaneous changes in frequency-dependent energy in the HHT spectrum and to suppress the normal signal peaks, the TKEO was applied using Equation 4.8 to find the $\boldsymbol{\Psi}_{B}$ vector. This was followed by applying the Bartlett windowing function, shown in Equation 4.9, to highlight the abnormal event peak in the processed signal, as shown in Figure 4-5 (e). The applied approach successfully accentuated the fault induced in the 3rd peak (i.e., at ~0.6 s) and depressed all the other signal peaks. During the real-time application of this processing

approach, the signal was segmented and processed as shown in the previous section. First, the signal was segmented for each 2 workpiece/tool engagements (i.e., two sequential signal bursts) with a 50% overlap between segments. Then, the processing approach was applied to each segment individually and the maximum peak value of each processed segment was extracted to represent the prefailure detection parameter Ψ_{BW}, as shown in Figure 4-5 (f), where a static threshold was applied to define the onset of prefailure phase evolution.

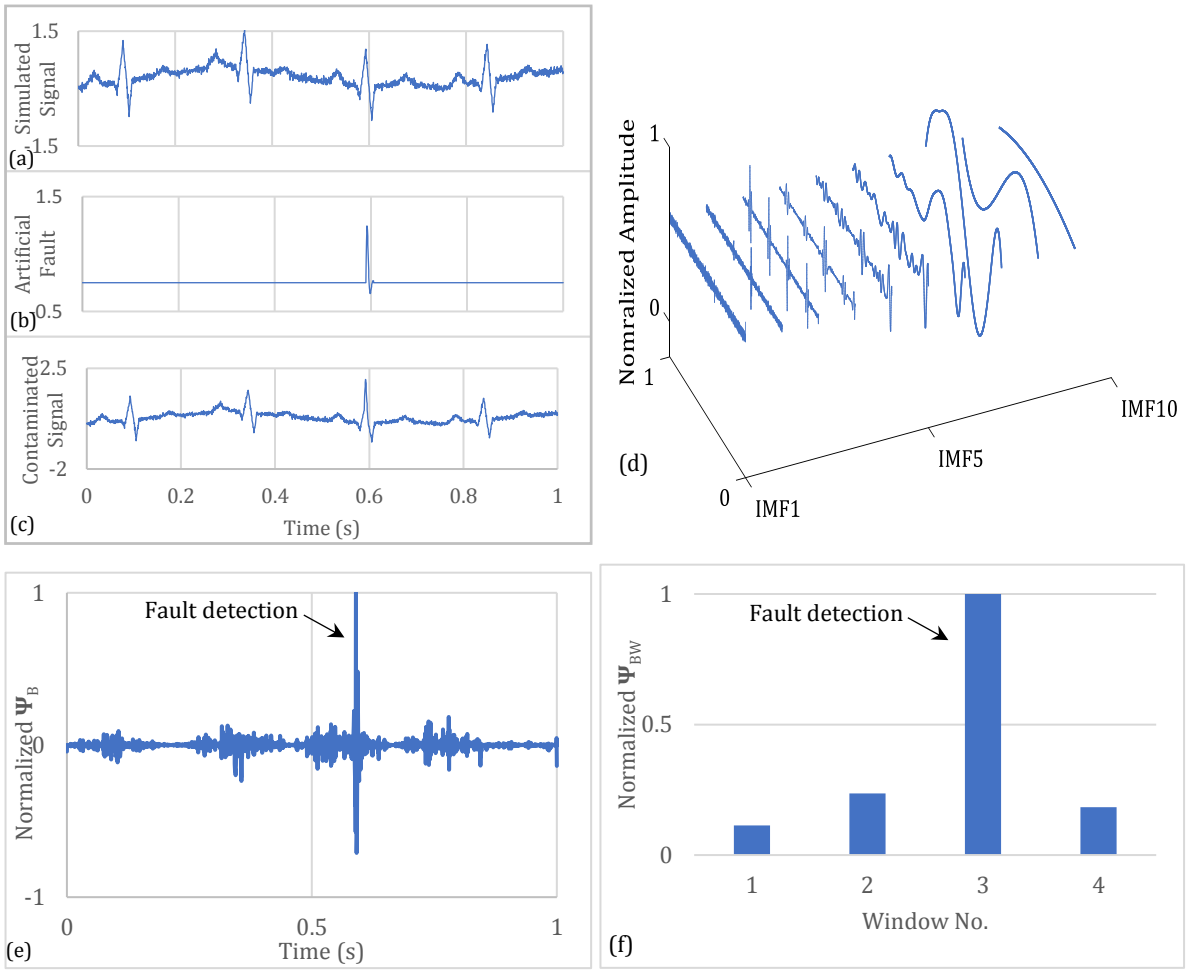

Figure 4-5 (a, b and c) Simulated signals (d) normalized IMFs (e) normalized Bartlett-TKEO-HHT Ψ_B (f) maximum peak value of Ψ_B for each window Ψ_{BW}

To reveal the capability of the developed processing approach to capture both tool prefailure and the onset of chipping, the approach was applied to the acquired signals during the experimental investigation of the monitoring signal ability to detect the tool prefailure and failure as showed in Section 4.2. Figure 4-6 shows the acquired data and

the calculated Ψ_B for (a) resultant forces, (b) vibrations, (c) AE_{rms} and (d) power signals before, during and after chipping. As seen in the AE_{rms} processed signal, the processing approach successfully localized the crack evolution phase. Furthermore, it depressed the AE_{rms} peaks before and after the chipping event period, which could have the same amplitudes, but low relative frequencies. The processed AE_{rms} signals captured the onset of the prefailure stage four engagements earlier before fracture, compared to three engagements using the raw signal. This response provided an earlier time window to stop the machine before any damage could happen to the machined part. The AE_{rms} response can be directly related to the elastic stress waves produced by the release of strain energy during the course of crack propagation and the generation of new surfaces. Additionally, mounting the sensor on the tool has significantly enriched the acquired signal by the waves generated from the tool material rather than the workpiece. This outcome shows the approach capabilities to indicate abnormal events during intermittent cutting operations using the AE_{rms} signals.

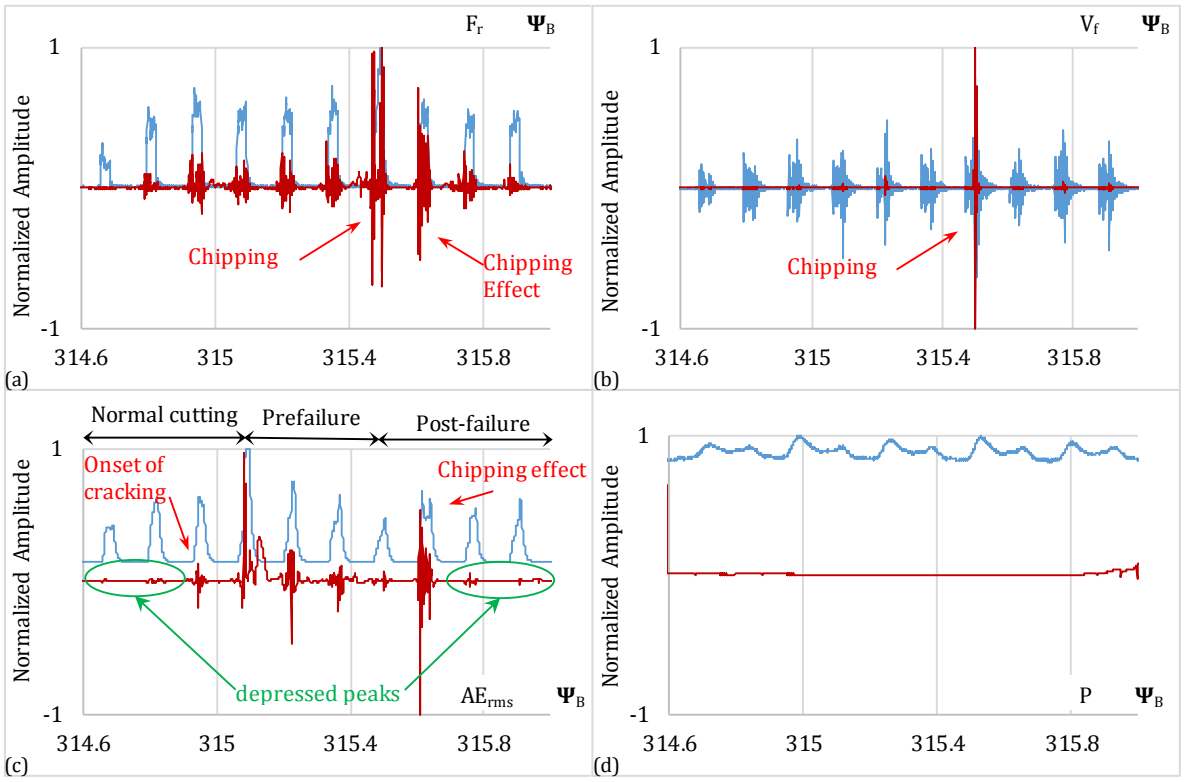

Figure 4-6 Normalized signals and corresponding TKEO-HHT responses of (a) resultant force 'Fr' (b) vibrations in feed direction 'Vf' (c) acoustic emission rms 'AE_{rms}' and (d) drive motor power 'P' during the prefailure phase and the chipping event.

This processing approach also showed the resultant force and the vibration signals suitability to capture the onset of chipping only as the processed signal bursts during the prefailure period were comparable to the ones after chipping, as shown in Figure 4-6 (a) and (b). On the other hand, the processed power signals did not show any peaks in the time-frequency spectrum, which confirmed the signal insensitivity to the crack evolution and the chipping event.

The output nature of the signal processing approach allowed the application of a static threshold experimentally. Once the processed signals were calibrated with the tool condition, a threshold limit could be defined by comparing the processed signal peak values in the prefailure phase to the ones during normal cutting.

4.6. Summary

A method was devised to induce cyclic load on the cutting tool tip to study the effect of unstable crack propagation, which preceded tool chipping, on indirect sensing methods using cutting forces, vibrations, power and AE signals.

Forces and vibrations were shown to be sensitive to the onset of tool chipping, whereas the power was shown to be insensitive to the event in contrast to the literature. This insensitivity can be related to the small chipping size of 0.1 mm. These signals did not show any change during the prefailure phase

The AE raw signal and the AE_{rms} were shown to be sensitive to the elastic waves generated in association with the generation of new surfaces during the unstable crack propagation phase. The phase was captured before the onset of chipping by three sequential engagements between the tool and workpiece. However, this left a relatively short time (on the millisecond scale) for taking corrective action after detection.

During the prefailure phase, the unstable crack indicator in the AE signals was characterized by infinitesimal time spans of high energy/frequency bursts. In addition, the AE signals generated were nonlinear, non-stationary and contaminated by bursts coming from the force variation in the intermittent cutting processes.

To emphasize the crack propagation effect on the AE_{rms} signal and to depress the steady state cutting effect, a two-stage novel approach was introduced to detect the

prefailure evolution phase. The first stage analyzed the AE signal in the time-frequency domain using the non-stationary and nonlinear Hilbert-Huang Transform. In the second stage, the prefailure indicator was emphasized using the Teager-Kaiser Energy Operator and Bartlett widowing function.

A method was developed to implement the signal processing approach for real-time applications. The method was optimized to minimize the computational time while ensuring no loss of information related to the relative changes in the instantaneous amplitude and frequency of the processed signal.

The capability of the signal processing approach to capture induced artificial faults in ideal nonlinear periodic signals has been tested using artificial signals. The approach was further applied to real forces, vibrations, AE_{rms} and power signals, which were acquired during the characterization test. The approach successfully captured the prefailure phase earlier by 4 tool/workpiece engagements. This was one engagement earlier than when using the raw signals. In addition, the approach depressed the AE peaks coming from normal cutting status. The approach emphasized the onset of chipping on both the force and vibration signals, and proved the insensitivity of the power signals to the chipping event.

CHAPTER 5
EXPERIMENTAL TESTING, VALIDATION AND ONLINE IMPLEMENTATION OF THE DEVELOPED TOOL PREFAILURE DETECTION SYSTEM

5.1. Introduction

In this chapter, extensive experimental testing and validation of the proposed signal processing approach for tool prefailure detection were carried out in both intermittent turning and milling applications. Different cutting parameters, tools and workpiece materials were used to investigate and validate the generalization capability of the proposed approach. Additionally, correlation between the chipping size and the prefailure phase features was developed for decision making. A thresholding function was introduced as well to avoid any tool chipping in order to protect the machined surfaces. A real-time data acquisition and signal processing controller were developed to implement the developed system online. This system acquired and processed the AE_{rms} signal in real-time to detect tool prefailure. The system was featured by a 2-way communication controller that was developed to overwrite the machine cutting parameters to safeguard the machined part in case of prefailure detection. Extensive experimental validation confirmed the accurate prediction of tool failure. The time required for signal processing, decision making and communication with the machine controller allowed stopping the operation before part damage. Such a system has not been created before.

5.2. Design of Experiments

To test the developed signal processing approach during intermittent turning applications, the same method devised in Section 3.7 and used in Chapter 4 was used to focus only on cracks due to mechanical loads and to avoid the occurrence of tool wear and build-up edges. Dry turning operations were carried out using carbide inserts on the 6-axis Boehringer-NG200 CNC turning center. The experiments were designed to

validate the independence of the proposed approach of the cutting parameters and workpiece material. The insert types, workpiece material, and cutting conditions are given in Table 5-1. Inserts 1 and 2 have the same geometry, coating (CVD $TiCN/Al_2O_3/TiN$), and nose diameter of 0.4 mm, but from different suppliers, whereas insert 3 has a PVD (Ti, Al) N/TiN coating and a 0.8 mm nose diameter. Additionally, three different types of steel and aluminum materials were used. The high speed camera HSC imaging was used for synchronization with the acquired cutting forces, vibrations and AE signals to record the chipping events in real-time during cutting. In addition, the imaging of this HSC was used to measure the chipping size at the insert nose. The chipping area A_c of the new generated surface was calculated as the product of the chipping size and depth, as shown in Section 3.6. The time of onset of chipping captured by the HSC imaging and the cutting force and vibration signals was compared to $\boldsymbol{\Psi}_{BW}$ peak location.

For milling tests, the experimental setup shown in Section 3.7 was employed to investigate the prefailure detection approach in different cutting parameters and tool paths. Slotting and side milling experiments, which represent the main operations in any milling tool path, were carried out using endmill cutters on the 5-axis DMU 100P duoBlock machining center. Five solid tungsten carbide end milling tools and inserts with different diameters and corner radii were used to machine 200 mm long slots in different steel and aluminum workpieces under dry cutting condition. The 3-component cutting forces, vibrations and AE signals were acquired during the tests in synchronization with high speed camera imaging. In milling applications, the width of the chipped edges W_c, shown in Figure 5-1, was employed as the chipping measurement criterion.

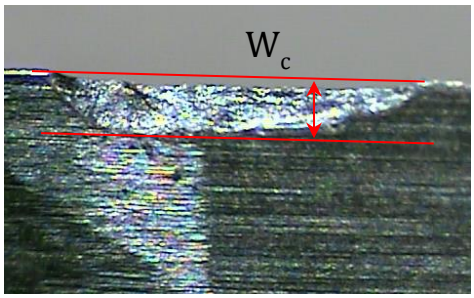

Figure 5-1 Chipping on an endmill edge

Table 5-2 shows the tools, the cutting conditions (rotational speed n, feed rate f and axial depth of cut a_p) and the workpiece materials used in these tests. The tools and workpiece material properties are described in detail in Section 3.3 and 3.4. Due to the difficulty of using the HSC imaging to assess the tool condition, a Winslow tool analyzer model 560 was used to measure the chipping width and the generated new surfaces at the end of the cutting paths.

Table 5-1 Cutting conditions for intermittent turning operations

Test	Insert type (number)	Workpiece material	n (rpm)	f (mm/rev)	a_p (mm)
1 2	DCMT11T304 (1)	ASTM A514-B	200	0.08 0.1	2
3 4	DCMT11T304 (2)	ASTM A514-B	450	0.15 0.2	1
5 6 7	DCMT11T304 (2)	AISI1018	450	0.2 0.3 0.45	1
8 9	DCMT11T308 (3)	ASTM A514-B	900	0.47 0.5	2

Table 5-2 Cutting conditions for milling operations

Test	Tool	Workpiece material	n (rpm)	f (mm/tooth/rev)	a_p (mm)	a_e (mm)
10 11	T16F2R40	AISI1018	900	0.08	4	2 3
12 13	T20F2R40	AISI1018 AL7075	900 16000	0.08 0.25	4 6	2.5 20
14	T25F2R04	ASTM A514-B	900	0.1	6	3
15 16	T25F2R40	ASTM A514-B AISI1018	900	0.1 0.08	6	3
17	T50F4R40	AISI1018	900	0.08	6	6

5.3. Experimental Results and Discussion

5.3.1. TKEO-HHT Processing Approach Capabilities

The results of test number 6 are demonstrated as a representative case of the turning tests in order to show the capabilities of the TKEO-HHT approach to deal with the non-stationary and nonlinear AE_{rms} signal in the prefailure phase. Figure 5-2 (a), (d) and (e) show the normalized raw vibration, AE_{rms} and the corresponding output of the Bartlett function of the TKEO-HHT ($\mathbf{\Psi}_B$), respectively, for eight engagements. These signals

were acquired during the prefailure phase and the chipping of the cutting tool. In this test, a chipping area of 2.46 mm^2 was observed on the cutting insert tip using the HSC after 6 cutting engagements, as shown in Figure 5-2 (b) and (c). Only the chipping event was captured by the vibration signals in the cutting direction, as shown in Figure 5-2 (a). On the other hand, the acoustic emission raw signals, Figure 5-2 (d), showed relatively high peak values in the prefailure phase (i.e., engagements 2 to 5) followed by the highest peak value at engagement 6. These peaks were, however, not highly indistinguishable compared to the rest of the cut, e.g., the peak of engagement 8 occurred after chipping, and had almost the same value. The peak of engagement 7 was relatively low due to the reduced contact between the chipped tool tip and workpiece.

The TKEO_HHT approach discriminated the high energy events of the prefailure phase, while depressing any other low energy signal variation, as shown in Figure 5-2 (e). The proposed approach was thus able to distinguish between the signals inherent to the cutting process, even at impact load conditions, and the non-stationary signals associated with the stress waves released by the surface's formation, before and at chipping. The onset of fracture was predicted during this pass *four engagements earlier*.

For the milling operations, a high-speed high-feed roughing test (test number 13) is presented to demonstrate the characteristics of the acquired signals in harsh cutting conditions. Figure 5-3 (a) and (b) show the raw acquired V_f and AE_{rms} signals for a period of 200 seconds (~ 55 tool rotations). A chipping width W_c of 0.05 mm was observed after only 593 ms of cutting. The event was not captured by any of the raw signals, as seen in Figure 5-3 (a) and (b), due to the high rotational speed and the multi-engagements between the tool teeth and the workpiece per rotation. However, by applying the TKEO-HHT approach to the V_f signals, the event was accentuated, as seen in Figure 5-3 (c). The processed AE_{rms} signal $\boldsymbol{\Psi}_B$ (AE_{rms}) successfully predicted the prefailure stage at 574 ms, which was five rotations before the onset of chipping, as seen in Figure 5-3 (d). This provided a 20 ms window to process the signal, to make a decision and to take an action before chipping during this high speed milling application.

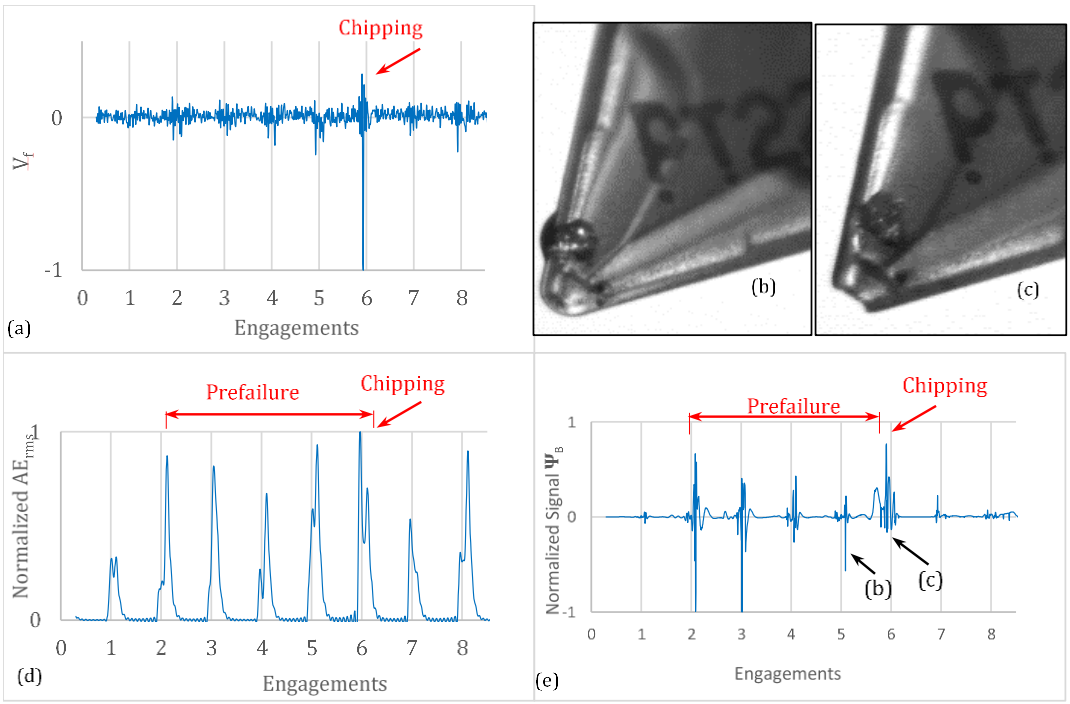

Figure 5-2 (a) Normalized filtered vibrations, (b and c) high speed camera photos, (d, e) raw and processed AE_{rms} signal (ΨB) of test number 6

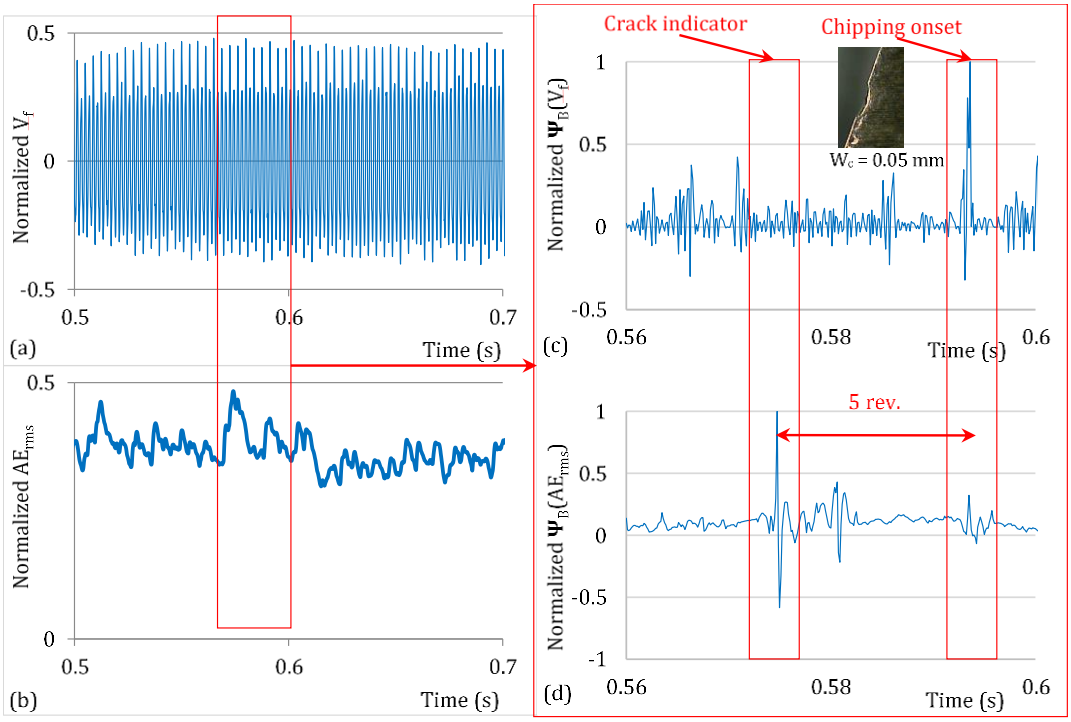

Figure 5-3 (a and b) Normalized raw vibrations and AE_{rms}, (c and d) processed vibrations and AE_{rms} signal (ΨB) respectively of test number 13

5.3.2. Online Implementation and Threshold of the TKEO-HHT Approach

The acquired AE_{rms} signals were conditioned, segmented and processed, as described in Section 4.4 in order to be implemented in real-time applications. A static threshold per tool was defined experimentally, based on the processed signal value during normal cutting conditions, to indicate the tool condition. The threshold function was independent of the cutting conditions, tool path, workpiece material and tool diameter. Figure 5-4 (a) and (b) and Figure 5-5 (a) and (b) show the prefailure detection parameter $\boldsymbol{\Psi}_{BW}$ of the AE_{rms} signals, the corresponding chipping size, and the real-time HSC tool imaging acquired during intermittent turning tests (Tests 1 to 9) and milling tests (Tests 10 to 17), respectively. Due to the complexity of the milling process and the nature of the tool/workpiece engagement in the milling process, it was difficult to acquire tool imaging in the real-time. Therefore, Figure 5-5 shows the tool condition, captured by a WINSLOW 560 tool analyzer, after each cutting path, and the corresponding chipping width. Hereafter, the onset of tool chipping in milling tests was detected by processing the vibration signals in the feed direction, as shown previously in Sections 4.5 and 5.3.1. The response of the processed vibration signals was compared to the AE_{rms} response to measure the prefailure time window. As seen in these figures, the developed signal processing approach achieved a 100% accuracy, predicting all the chipping events during both the turning and milling tests, regardless of the cutting speed, feed rate, depth of cut, tool geometry, tool material, cutting path and workpiece material. It also suppressed any AE_{rms} signal peaks caused by other sources that were not related to the prefailure phase. Additionally, the approach demonstrated a high ability to predict the chipping of an already chipped tool, as seen in tests numbered 1, 3, 5, 7, 10, 11, 12, 14, 15 and 17. Moreover, the approach predicted overlapping chipping events, where two or more chipping events occurred on the same location on the cutting edge as in most of the cases, as shown in Figure 5-4 and Figure 5-5. Furthermore, the approach also predicted overlapping prefailure stages for different chipping events, where more than one crack unstably propagated at the same time, such as in tests numbered 1, 3, 7 and 17. Additionally, the approach also detected the onset of tool chipping for several events, such as tests numbered 5, 8 and 9. The proposed approach

was also able to detect chipping events with a width as small as 0.05 mm, even during high speed roughing operations, as shown in tests numbered 10, 12 and 13.

The window size is mainly dependent on the unstable crack propagation rate. Such a stochastic phenomenon depends on controllable parameters, such as the cutting forces and the tool material and geometry properties, as seen in Equation 4.1, and other uncontrollable features, such as the existence of minor cracks and material imperfections. However, the proposed approach provided a window ranging from 4 to 6 engagements between one tooth of the cutting tool and the workpiece for different cutting parameters and tool materials in both turning and milling applications.

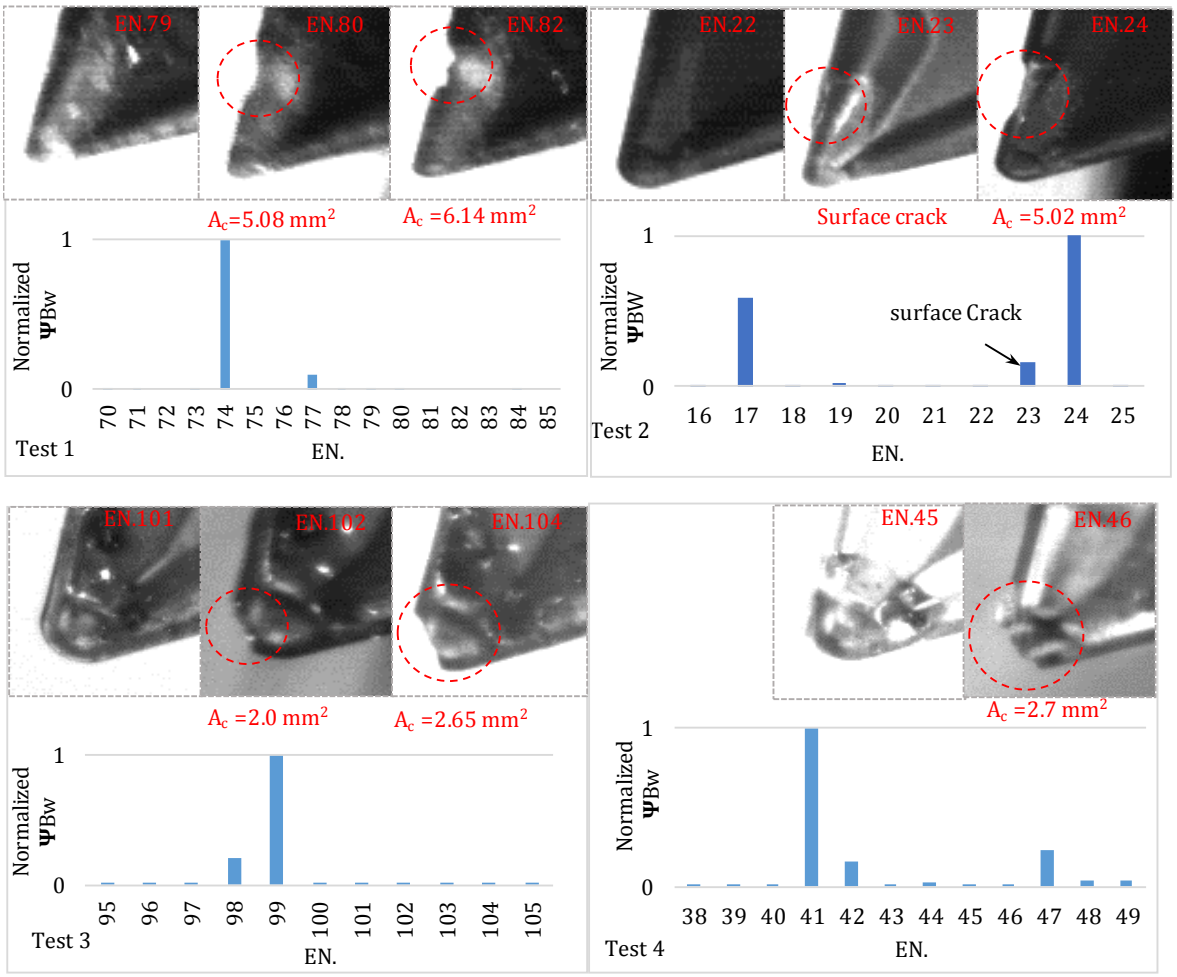

Figure 5-4 (a) Prefailure detection parameter Ψ_{BW} for turning tests 1 to 4 with respect to the tool/workpiece engagement number EN and the corresponding tool condition and chipping area A_c

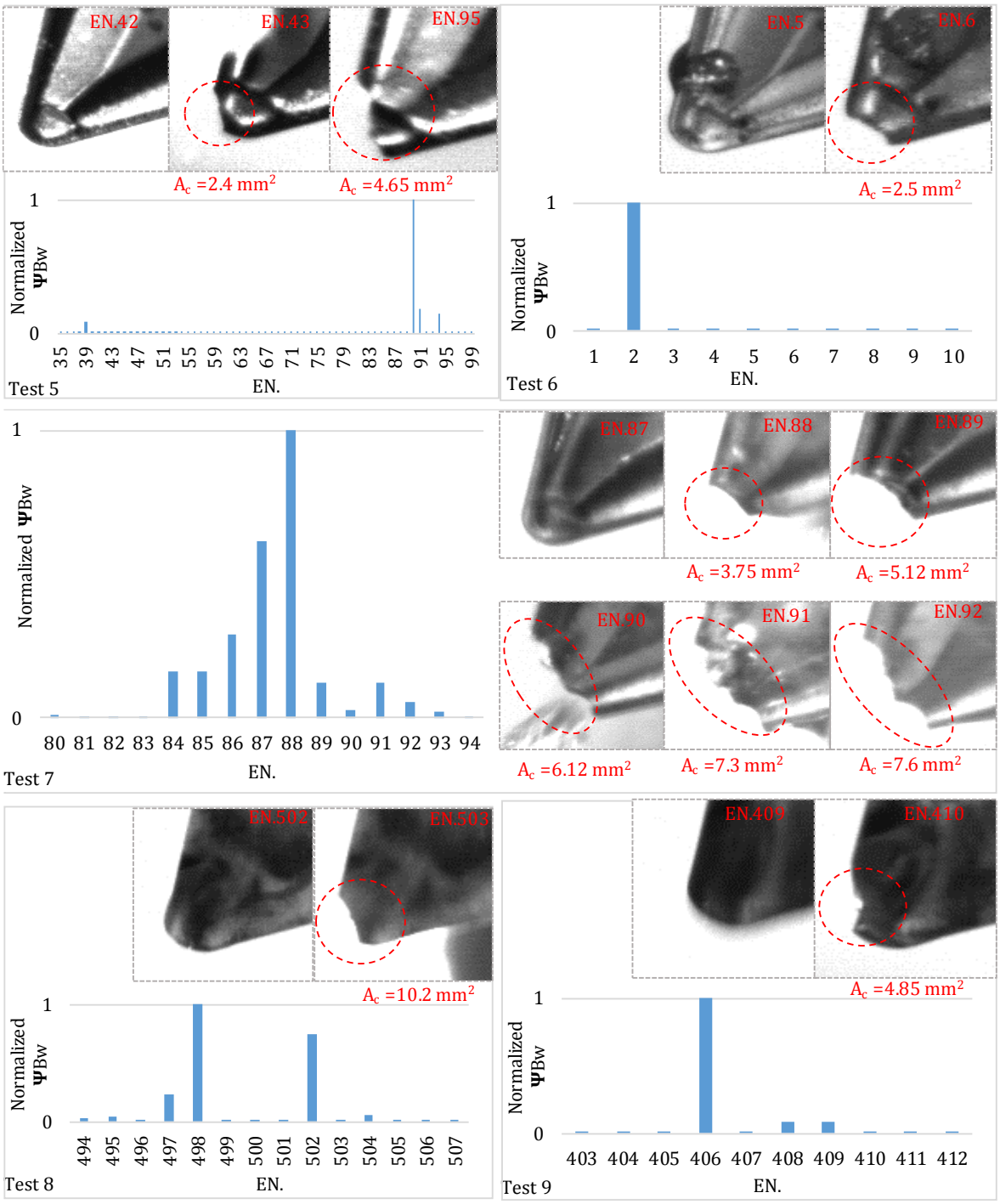

Figure 5-4 (b) Prefailure detection parameter Ψ_{BW} for turning tests 1 to 4 with respect to the tool/workpiece engagement number EN and the corresponding tool condition and chipping area A_c

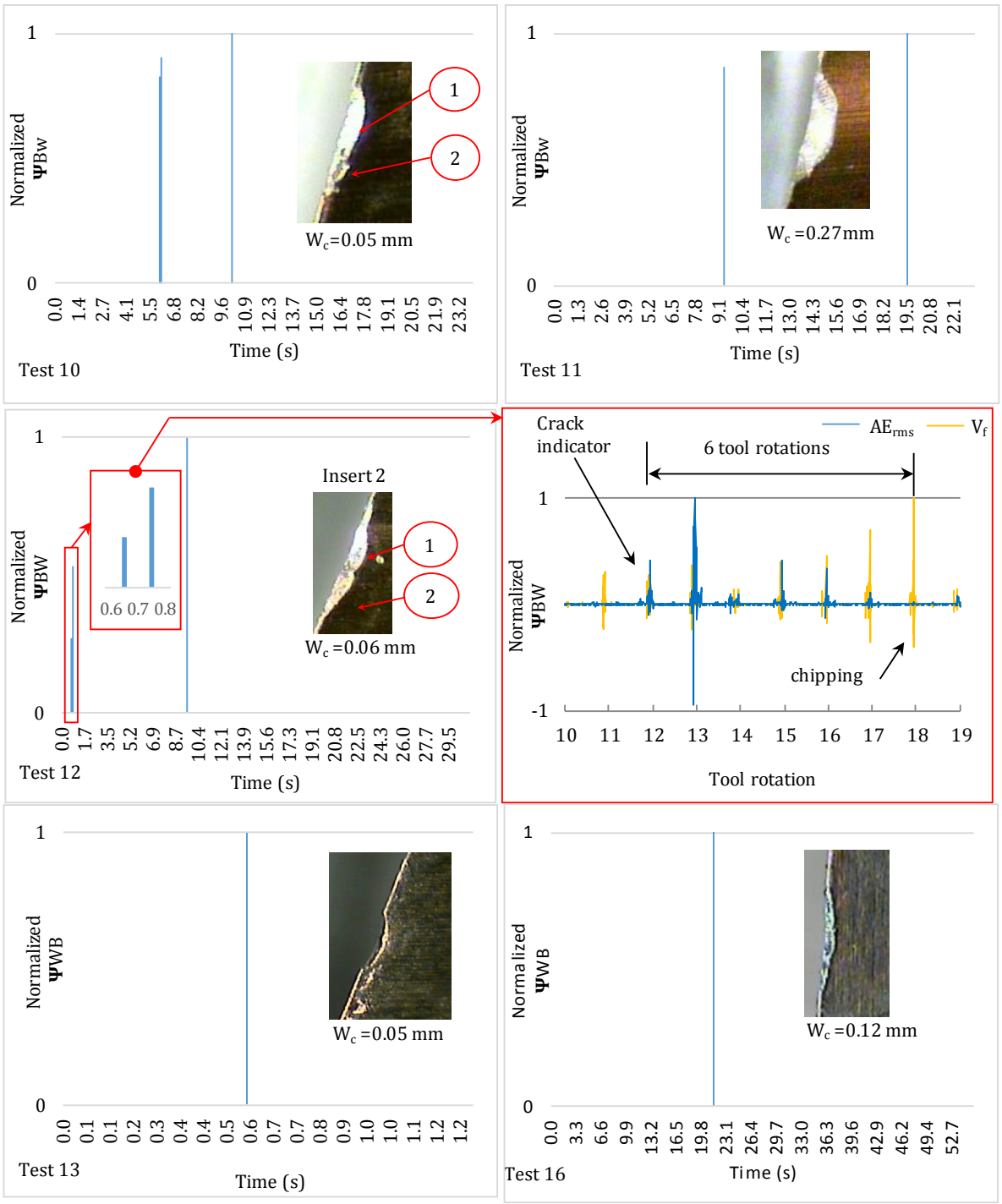

Figure 5-5 (a) Prefailure detection parameter Ψ_{Bw} for milling tests 10, 11, 12, 13 and 16 with respect to cutting time and the corresponding tool condition and chipping width W_c.

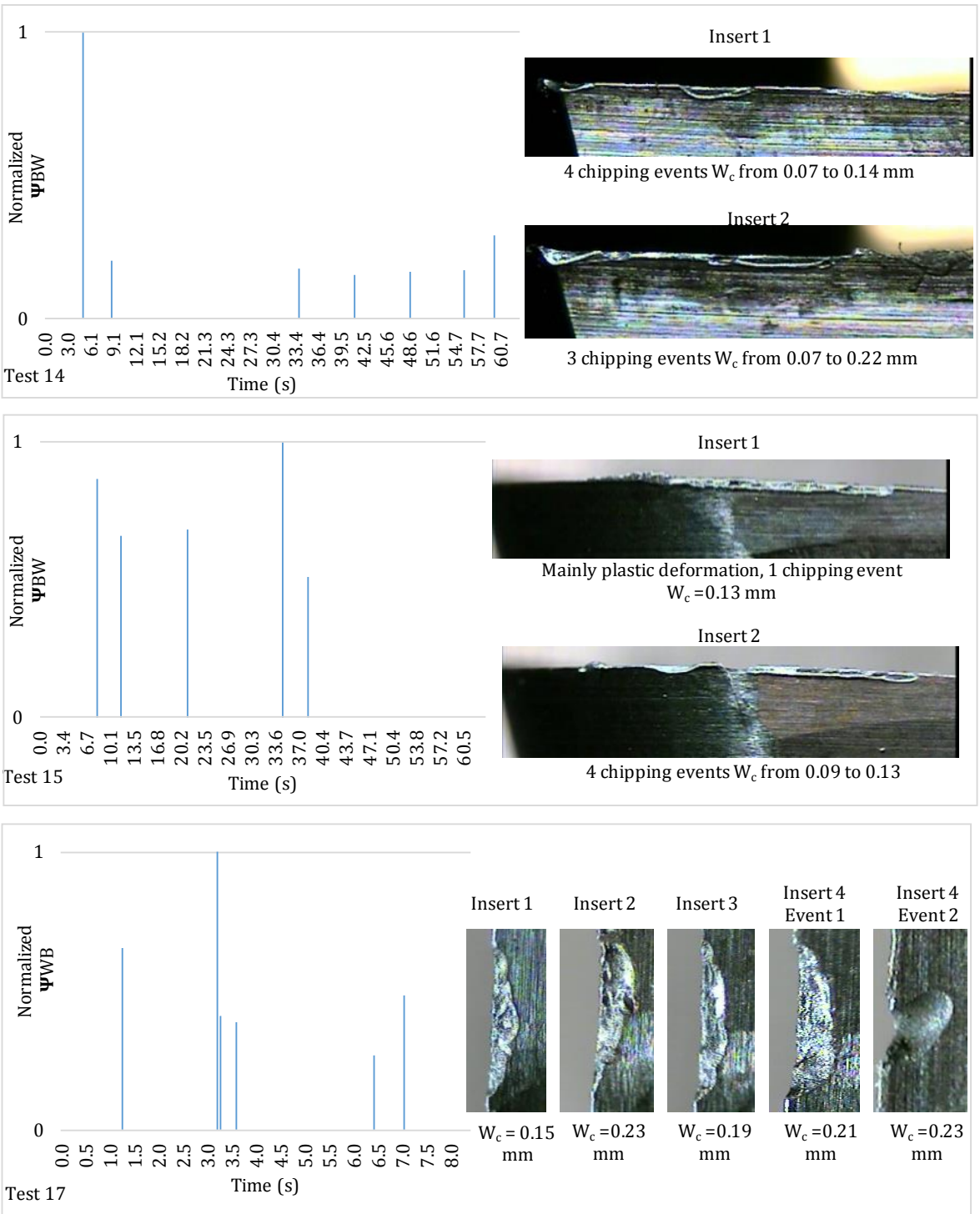

Figure 5-5 (b) Prefailure detection parameter Ψ_{Bw} for milling tests 14, 15 and 17 with respect to cutting time and the corresponding tool condition and chipping width W_c.

Table 5-3 shows the range of the prefailure detection window for the turning and milling tests and the corresponding processing time. For aerospace applications of high speed milling, typically the cutting speed varies between 6,000-20,000 rpm, which provides a window of 12 to 60 ms to predict tool chipping/fracture and take corrective action before a complete tool failure. The proposed approach successfully predicted all the chipping events with a maximum processing time of 2 ms. The processing time mainly depends on the cutting speed, signal sampling rate and the sifting process to extract the IMFs. The sifting process and its stopping criterion in addition to the sampling rate were optimized to minimize the processing time to a range between 0.8 to 2 ms. This time is equivalent to approximately 0.25 to 0.65 of a tool rotation at a speed of 20,000 rpm. The prefailure window was *insensitive* to the cutting conditions, workpiece material as well as insert geometry and coating.

Table 5-3 Ranges for prefailure detection window and the corresponding processing time

Test	1	2	3	4	5	6	7	8	9	10	11	12	13	14	15	16	17
No. of chipping event	2	2	2	1	2	1	5	1	1	2	2	2	1	7	5	1	5
Prefailure window range	5-6	6	4-5	5	4-5	4	4	5	4	6	4-5	4-6	5	4-6	4-6	4	4-6
Processing time/Engagement (ms)	1.9-2	1-1.5						0.8-09		0.8-0.1			0.75	0.75-1.5			

The prefailure detection parameter $\mathbf{\Psi}_{BW}$ showed a quantitative relationship with the chipping size. Figure 5-6 (a) shows the prefailure detection parameter $\mathbf{\Psi}_{Bw}$ for the chipping events of test 7 as a representative case of successive tool chipping. This parameter is sensitive to the generated new surface area only regardless of the tool condition preceding the prefailure phase (i.e., healthy or chipped tool condition). The parameter $\mathbf{\Psi}_{Bw}$ showed an exponential relationship with the chipped area A_c. The same relationship was observed for the milling tests for two tools with the same geometries, but different diameters, namely, T20F2R40 and T25F2R40, as seen in Figure 5-6 (b). The sensitivity of the processing approach to the chipping area was not affected by tool diameter, tool path, cutting conditions and workpiece material. In some industrial applications, chipping does not prevent cutting totally and can be tolerated depending on the chipping level. Hence, this relation can be used to define a threshold of $\mathbf{\Psi}_{Bw}$ depending on the acceptable tool chipping. If $\mathbf{\Psi}_{Bw}$ exceeded this threshold, the process

should be stopped immediately to prevent part damage. However, the application of a global threshold using the Ψ_{Bw} directly for industrial applications has some challenges. The 'Ψ_{Bw}–A_c' relationship is affected by the tool coating, geometry, boundary conditions and cutting conditions, which requires more learning effort to determine this exponential relationship for each tool. To overcome this limitation and to provide a general rule for a tool prefailure detection threshold, the relative percentage increase in Ψ_{Bw} at prefailure with respect to steady state cutting was calculated and found to be always significantly high and distinguishable. Figure 5-6 (c) shows the percentage increase in Ψ_{Bw} versus the chipped area at the prefailure detection of the first chipping event of each test. It can be shown that the percentage increase in Ψ_{Bw} follows the same 'Ψ_{Bw}–A' relationship, as shown in Figure 5-6 (a), although it was obtained at different cutting conditions and insert coating (inserts 1 and 2). This shows the dominant effect of the chipping area on the *percentage increase* in Ψ_{Bw}. Although this is still sensitive to the tool geometry, as shown for insert 3, the percentage increase in Ψ_{Bw} at prefailure detection was always higher than 10 times the normal cutting response under all circumstances. This percentage can be used in cutting applications that do not tolerate chipping as a reliable prefailure detection indicator with minimum learning effort. The aforementioned observations of the proposed approach clearly demonstrate the method's capability to capture tool prefailure in real-time for industrial applications.

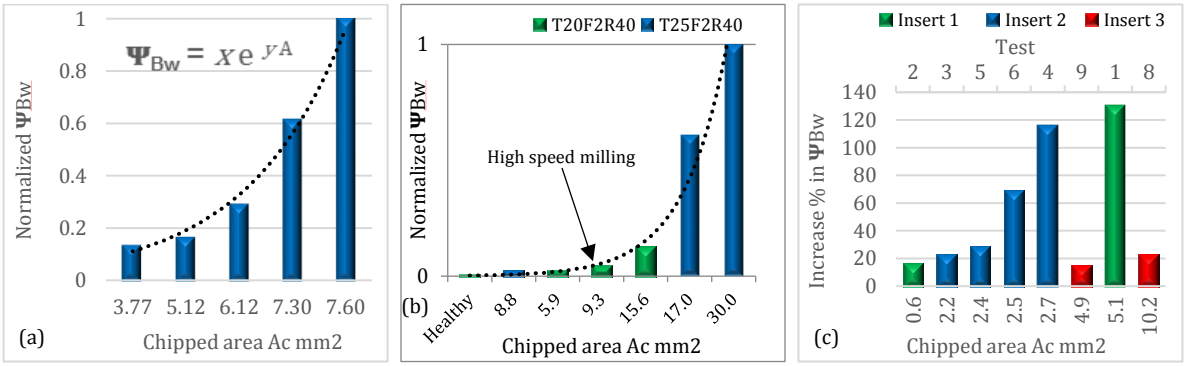

Figure 5-6 Prefailure detection parameter Ψ_{Bw} for chipping events in (a) test number 7 and (b) milling tests using different tool diameters and (c) percentage increase in Ψ_{Bw} at prefailure for different inserts during turning.

It should be noted that, due to the AE_{rms} signal segmenting and overlapping, the $\boldsymbol{\Psi}_{Bw}$ mainly indicates the beginning of the prefailure phase and the chipping onset, while the intermittent peaks (i.e., peaks occurred during the prefailure phase) of $\boldsymbol{\Psi}_{B}$, are suppressed. This is because, at the prefailure phase limit, the approach emphasizes the *relative* change between the prefailure phase and the steady state cutting. Although within the prefailure phase peaks, the *relative* change in the frequency/amplitude are insignificant, and hence, they are suppressed by the processing approach, which does not affect the prefailure detection accuracy. For example, Figure 5-4 (Test 2) shows the $\boldsymbol{\Psi}_{Bw}$ during the prefailure phase of chipping event 4. It is clear that the $\boldsymbol{\Psi}_{Bw}$ is significantly high at the prefailure phase limits only, even when a surface crack was induced at engagement 23.

5.3.3. Cutting Operation Stopping Time

The total time needed to stop a machine, in the case of prefailure detection, can be divided into the time needed for (a) acquiring data, (b) conditioning and processing of the AE_{rms} signal, (c) communicating with the machine automation system, and (d) executing a stopping command and deceleration of moving the spindle/table. Despite the limited control on (d), the time needed for (a), (b) and (c) can be optimized. Hence, an ultra-high-speed processor was integrated in the TCM system for real-time signal acquisition, decision making and communication within a short time span. A National Instrument real-time embedded industrial compact controller chassis cRIO with an FPGA and a real-time processor were used as the TCM system hardware. Full description of the developed hardware and communication system can be found in Section 3.8.

The developed TCM system was used to send a feed-hold command to the CNC controller during slot milling tests using a T25F2R04 tool with a rotational speed of 16,000 rpm and different cutting feed rates and depth of cut (a_p). The tests were monitored using a high speed camera to measure the communication time between the developed TCM system and the CNC machine as well as the machine response time. A 5v TTL signal was sent to the HSC in synchronization with the feed-hold command,

which was sent to the CNC machine. This signal was used to mark the event time on the HSC camera. Figure 5-7 shows the time elapsed between sending a feed-hold command and the total stop of the table feed drive of the DMU-100P duoBlock CNC machine center. Regardless of the cutting feed rate, the drive stopping profile showed a linear relationship with the cutting feed rate. The deceleration function, which is the slope of the curves in Figure 5-7 (a), was a constant of approximately 0.6 G for all the tests. The time elapsed during communication and machine response ranged between 1 to 2 ms, as seen in Figure 5-7 (b). These measurements represent only the tested DMU CNC machine, which is driven by a SIMATIC S7-300, 317-2 DP central processing unit CPU. Faster response time can be achieved using a faster machine tool CPU, which has a response time. i.e., as low as 500 μs [96]. Overshooting took place at the end of the stopping procedure that resulted in contact between the cutting tool and the workpiece (i.e., positive feed rate) during the settling time, as shown in Figure 5-7 (c). A maximum feed rate of 170 mm/min was observed during this time that lasted for only 35 ms. This is equivalent to a feed rate of 0.016 mm/tooth/rev which limits the contact between the chipped surfaces of the cutting edge and the machined part. In addition, during this event, a total length of only 100 μm was cut. Such conditions have minimal influence on the surface integrity of the machined part and can be tolerated.

Figure 5-8 shows the total time needed to completely stop the CNC machine using the developed, novel integrated TCM system. This includes time for acquiring the signal, processing it, sending the command to controller and completely stopping the feed motion. The figure shows the minimum W_{min} and the maximum W_{max} prefailure detection window limits (i.e., 4 and 6 tool revolutions respectively) of the cutting feed rate over a typical range of high speed cutting conditions of aluminum alloys in aerospace applications, where the cutting speed and feed rate varies between 6,000 to 20,000 rpm and 0.05 to 0.127 mm/tooth/rev, respectively. This graph was generated assuming one tool/workpiece engagement per rotation, which is generally the case in milling, and a single flute tool. Under these conditions, a cutting process at a rotational speed of 16,000 rpm can be operated safely with a feed rate of up to 0.13 mm/rev. Additionally, due to the prefailure window independence of the cutting conditions, the tests data can be extrapolated to a maximum rotational speed of the testing CNC

machine (i.e., 18,000 rpm). Despite diminishing W_{min} and W_{max} to 13.4 and 20 ms, respectively, at this speed, the extrapolated stopping time of the operation is 14.5 ms, approximately 1.2 ms after chipping, assuming the lowest prefailure window provided by the proposed approach (i.e., 4 revolutions). This is equivalent to a 0.5 tool rotation; by which time, the chipped tool would not encounter the machined part. The proposed approach responds to the industrial need in a real working environment and can be retrofitted to existing machine tools. It is worth noting that no such system is currently available.

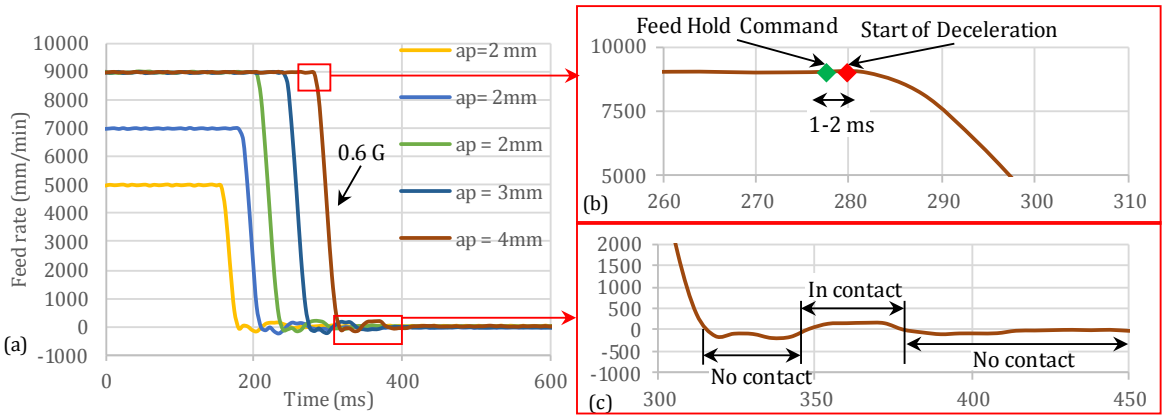

Figure 5-7 (a) Stopping profile of DMU CNC center at a speed of 16,000 rpm (b) communication time measurement and (c) settling time

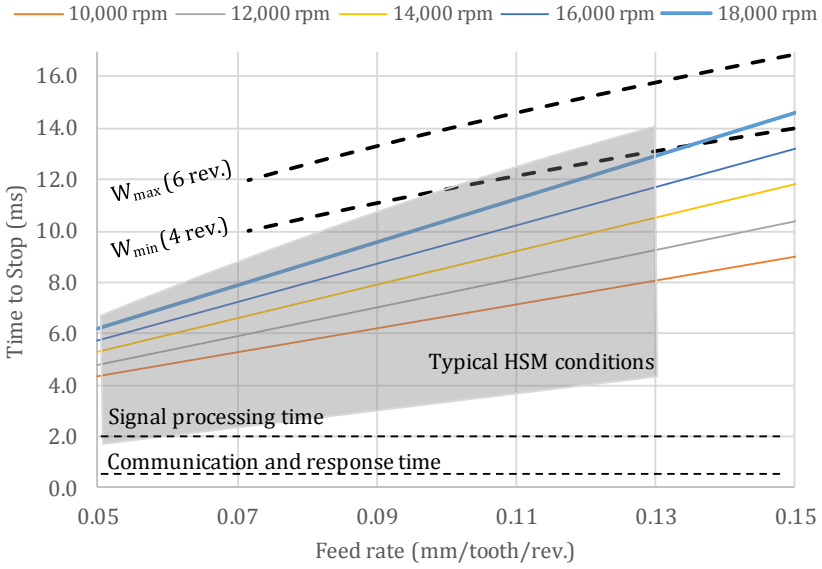

Figure 5-8 Safe region to stop the cutting process before chipping at typical HSM cutting conditions of aluminum alloys in aerospace applications

5.4. Summary

Intermittent turning and milling tests were conducted to test and validate the proposed signal processing approach under a wide range of cutting parameters, tools and workpiece materials. The onset of tool failure was captured using a high speed camera as well as force and vibration signals to be compared to the prefailure detection parameter of the AE signals.

The developed signal processing approach was able to accentuate the prefailure phase in the AE_{rms} signals and depress the signal bursts that were generated during normal cutting. In addition, it detected tool prefailure even when there was no straightforward evidence of the unstable crack indicator in the raw AE signals in the time domain. This was shown in an analysis of signals acquired during a high speed milling application.

The signal processing approach accurately predicted tool chipping in all the validation tests regardless of the cutting parameters, tool path or workpiece material, using a maximum processing time of 2 ms. Moreover, the approach captured overlapping chipping events, where two or more chipping events occurred on the same location of the cutting edge, and overlapping prefailure stages for different chipping events, where more than one crack were unstably propagating at the same time.

The developed approach provided a window between 4 to 6 tool/workpiece engagements to take corrective action by stopping the machining process before tool failure happened. This is equivalent to a window of 12 to 60 ms. The approach was optimized to be implemented in real-time to predict tool chipping/fracture and to take corrective action before a complete tool failure in high speed milling applications.

The prefailure detection parameter showed an exponential quantitative relationship with the chipping area. This relationship was insensitive to the tool diameter, tool path, cutting conditions and workpiece material. Therefore, it can provide a threshold to tolerate acceptable chipping size. In addition, the percentage increase in the prefailure detection parameter is always significantly high and distinguishable, regardless of the cutting conditions, workpiece material or tool coating.

A static threshold was found which can be applied with minimum calibration effort to prevent tool chipping during intermittent cutting operations.

A real-time tool prefailure detection and tool failure prevention system was developed. The system uses an innovative approach and a 2-way communication interface for real-time control of the process parameters. The system provides an adequate time window to stop the machine before any damage to the machined part. The developed system was able to prevent tool chipping and safeguard the surface integrity of the machined part in high speed applications to a spindle rotational speed of up to 18,000 rpm. The proposed approach responds to industrial needs in a real working environment and can be retrofitted to existing machine tools. It bridges a gap in the current state of knowledge, since no such system is presently available.

CHAPTER 6
DEVELOPMENT OF A REAL-TIME TOOL WEAR MONITORING SYSTEM

6.1. Introduction

In this chapter, an innovative signal processing approach is developed to deal with the limitations of using spindle drive feedback signals. This novel, rapid and effective approach is proposed to extract generalized features that can describe the tool condition under different cutting conditions and optimize the learning process time during intermittent cutting operations. The approach masks the effect of the cutting feed rate and depth of cut, and emphasizes the effect of the tool condition on the extracted features. Extracted features were analyzed using an N-way ANOVA test and then ranked, according to their sensitivity to the tool condition. In addition, an approach is proposed to benchmark six widely used pattern recognition classification methods with respect to their characteristics and computational efficiency to optimize the learning effort, the classification accuracy and the calculation time for TCM systems. A reassessment of the performance and accuracy of the classification methods was done using generalized extracted features (i.e., non-determined problem data) to provide a general judgment on the performance of these methods. These methods were selected due to their potential in the broad literature, namely, Binary Support Vector Machine (SVM), Linear Discriminant Analysis (LDA), K-Nearest Neighbor (KNN), Neural Network (NN), Naïve Bayes (NB), and Decision Trees (DT). The following sections describe the feature extraction and generalized processing approach, the N-way ANOVA for feature ranking, and the methods used for classification, and they discuss the benchmarking approach as well as the feature selection and optimization techniques for online TCM.

6.2. Nature of the Problem

As shown in Chapter 2, available TCM systems suffer from the lack of standardization, generalization and the need for extensive learning effort. Additionally, the TCM challenges increase with the recent trend of applying adaptive control systems. The critical literature review showed the high potential of using feedback signals from the spindle and feed motors compared to force and vibration signals for industrial applications. This is due to their non-intrusive nature and applicability for monitoring HSM processes of large parts. In the literature, signals acquired from spindle and feed motors have shown the capability to capture tool wear, and there has been no evidence that one of them is more sensitive to the tool condition than the other. In this work, the spindle drive feedback signals were selected over the feed motor feedback. This was to minimize the number of sensing systems, and the associated computational effort, to monitor all the feed motors in multi-axis CNC machines.

The information content of the force signals is the best way to describe the cutting process. The cutting power, for instance, has an adequate amount of this information as well. This is because the power needed in the cutting process is a function of the resultant cutting forces and the spindle speed. For the same cutting parameters, there is a linear relationship between tool flank wear VB1 and cutting power as shown in Figure 6-1 (a) [97]. The same relationship can be found for the cutting current. However, power also increases by increasing the metal removal rate (MRR) during the cutting process. Figure 6-1 (b) shows the normalized power measured during a slot milling process using the same tool and workpiece material versus the MRR. The MRR was increased from MRR_1 to MRR_4 by increasing the depth of cut. Due to MRR dependency on the feed rate, speed and depth of cut, the power-wear relationship cannot be generalized. Therefore, time domain trend analysis techniques cannot be applied. On the other hand, advanced frequency domain processing techniques, which have been reported as a powerful processing tool in the literature for wear detection, are time consuming. Thus, they cannot be applied for HSM TCM applications as well. Hence, in this work, pattern recognition methods were investigated to detect the tool wear condition based on feedback signals of the spindle motor.

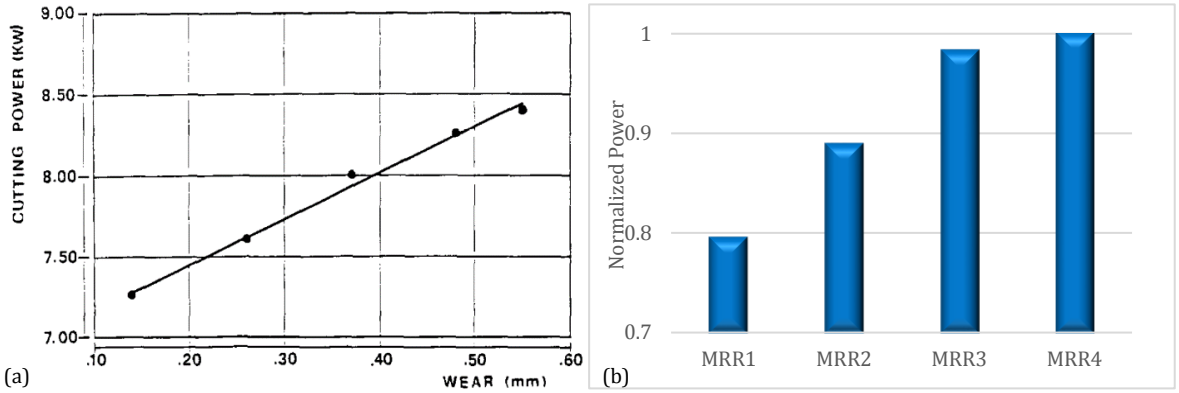

Figure 6-1 (a) Cutting power vs. wear, turning operation for C45 steel using a P30 tool, v=165 m/min, f=0.45 mm/rev, a_p=2.5 mm [97] (b) normalized cutting power vs. metal removal rate, milling operation of AL7075 using T25F2R04

In modern CNC machines, 400 Hz 2-pole induction motors are usually used as a spindle motor. These motors are controlled by a pulse width modulation (PWM) module to control the spindle torque and speed. As the spindle is subjected to cyclic torque during the milling process, a PWM module changes the supplied frequency and voltage to maintain constant speed. Unfortunately, there is no single standard PWM controlling strategy that can be applied for CNC spindle control among the wide range of cutting speeds and torques. As a result, to maintain the same spindle torque and speed, different combinations among the drive motor voltage, current and the phase between them can be found. To illustrate the effect of the PWM controller on the acquired spindle feedback signals (i.e., power, voltage and current), Figure 6-2 shows the current and voltage during machining tests that were acquired simultaneously with the power as shown in Figure 6-1 (b). The cutting power showed a gradual increase from MRR_1 to MRR_4. However, from MRR_1 to MMR_2, there was a slight increase in the voltage whereas the current contributed mainly to increase the power, as shown in Figure 6-2. In contrast, from MRR_2 to MRR_3, the increase in power was mainly dependent on voltage increase. Furthermore, from MRR_3 to MRR_4, although the power increased, both current and voltage decreased. This can be related to decreasing the phase between the generated signals. As a result, in this work, features extracted from all the feedback signals, namely, voltage, current and power, are studied and analyzed to select the most sensitive features to the tool condition. Subsequently, they are fused using a pattern recognition method to detect the tool condition, as is shown later.

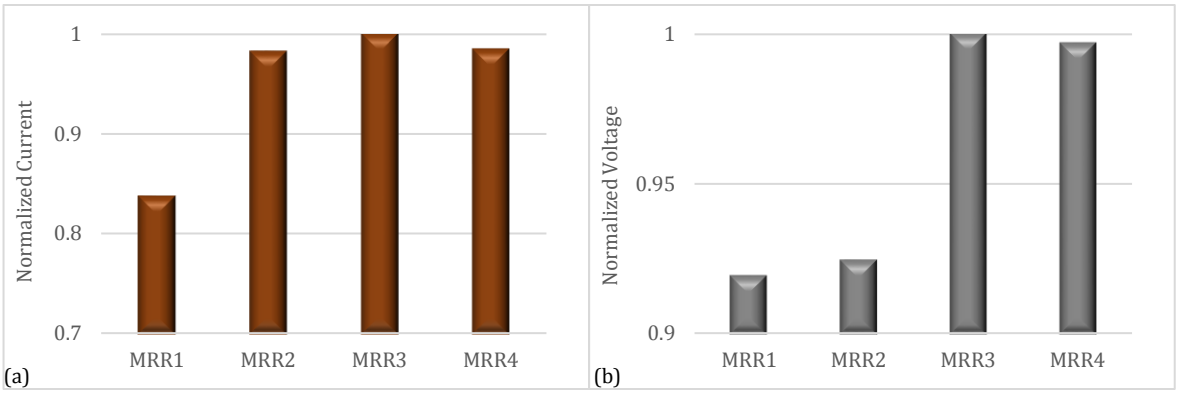

Figure 6-2 (a) Normalized current and (b) normalized voltage acquired during the tests shown in Figure 6-1 (b)

6.3. Proposed Generalized Method for Feature Extraction and Analysis

6.3.1. Proposed Signal Processing Approach

The signal processing approach introduced in this research significantly reduces the required system learning through masking the effect of the cutting conditions and emphasizing the effect of the tool condition. This approach was applied to the acquired force and spindle drive feedback signals to produce normalized patterns within scaled segments that have the same number of points per revolution. Producing such unified patterns is essential for adopting a deterministic approach for online pattern recognition and decision making, which reduces the processing time and improves system reliability. The use of forces is not practical for implementation in an industrial environment. Therefore, in this study, forces are only used as a reference to insure the validity of using spindle drive feedback signals, namely, the spindle motor current, voltage and power, for tool condition monitoring. In order to eliminate noises resulting from the spindle drive motors, the second passing frequency of the cutting tool was applied as a low pass filter for the acquired signals. This filtering reduces the signal noises and prevents aliasing problems due to sampling without affecting the fundamental features of the cutting process [42, 98].

Following signal filtering, the following two main consecutive operations are applied to spindle drive feedback signals prior to feature extraction:

1. Signal segmentation in the time domain: Owing to the repetitive nature of the milling process, the acquired signals were segmented per tool rotation to provide repetitive patterns of the extracted signal segments. This provided a fixed pattern independent of the cutting speed. An overlapping moving frame was also applied for segmentation in order to remove any constraints on the segmented pattern boundaries to match the starting and ending points of the tool/workpiece engagement. Such an action removed the constraints on the segmentation timing, and hence, provided more "generalized features".

2. Normalization: The cutting feed rate and depth of cut controlled the segment peak values during the cutting process. Therefore, each segment was normalized with respect to its maxima to mask the feed rate and depth of cut effects.

6.3.2. Feature Extraction

The obtained normalized segments contain the information required to detect the tool status. This is clearly demonstrated in Figure 6-3, which shows the change in the pattern of the normalized signals of the worn tool compared to the fresh tool within one revolution. For a worn tool, the change in the geometry of the cutting edge due to the developed wear resulted in a longer contact time between the tool and the workpiece. This alters the frequency spectrum and the statistical features of the standard pattern of a fresh tool, which can be used to detect the level of tool wear. In this study, 40 physical and statistical features were considered and tested. These features were selected because of their sensitivity to the physical tool condition change in the time and/or frequency domains of the force [33, 99-102] and spindle feedback [33, 103, 104] signals. However, only the most noteworthy features are reported in this chapter for simplification. These features are the segments: Energy E (represented by the area under the curve of the analyzed signal), Minimum min, Root Mean Square rms, Standard Deviation SD, Mean, Kurtosis K, Variance Var and Peak magnitude to rms ratio (P2rms) in the time domain. In the frequency domain, the mean and median normalized frequency of the signal power spectrum f_{mean} and f_{med}, the band power BP, the maximum peak value of the periodogram P_p and Welch power spectral energy P_w are extracted.

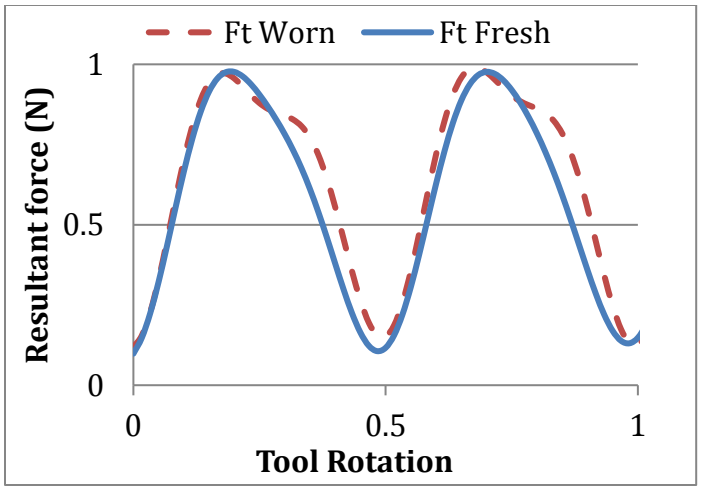

Figure 6-3 Normalized, filtered resultant force of a fresh and worn tool. n=14,000 rpm, f= 3,500 mm/min and a_p = 3 mm.

6.3.3. Data Analysis

In order to verify the significance of the processing method on masking the effect of cutting conditions, an N-way ANOVA analysis and f-test were carried out on the extracted features after applying each of the signal processing operations, namely, segmentation and normalization. The feature sensitivity to the tool condition, cutting feed rate and depth of cut was tested. Subsequently, a flag value was used to describe the change in the feature sensitivity to the tool condition after each processing operation. To ease the presentation of the ANOVA test results, and to test the plausibility and sensitivity of the tested features, which depended on the *p*-values and f-values of the feature, respectively, the following scheme was used.

- A value of '1' is assigned to any processed feature that has a *p*-value less than the ANOVA test significance level (i.e., 0.01) and the maximum f-value corresponds to the tool condition.
- Oppositely, a flag value of '-1' is assigned to any processed feature that has a *p*-value larger than the significance level (α= 0.01) or the tool condition f-value is not the maximum value.
- A flag value of '0' is assigned to any feature that does not satisfy any of the previous conditions.

6.3.4. Features Ranking

The extracted features were ranked according to their sensitivity to the tool condition and their insensitivity to the cutting conditions and tool size. A ranking function R_i was created to fulfill these qualities by sequentially feeding the p-values and f-values obtained from these analyses to the ranking function in order to select the most indicative features that correlate to the tool condition. The feature ranking score can be determined using the following equation:

$$R_i = \sum_{1}^{N} \frac{1 - \frac{f_F + f_{a_d}}{f_{TC}}\Big]_i + \frac{f_{TC_i}}{\max(f_{TC} \uparrow [N])}}{2N} \; ; \; \begin{cases} f_i = f & p_i \le \alpha \\ f_i = 0 & p_i > \alpha \end{cases} \; ; \; i \in \{1,2, \dots q\} \qquad 6.1$$

where f_F, f_{a_d} and f_{TC} are the f-values corresponding to the cutting feed rate, axial depth of cut and tool condition respectively, p_i is the p-value for different tested features, α is the ANOVA test significance level, and q is the number of features extracted. In Equation 6.1, N represents the number of similar tools of different sizes. The feature ranking score, R_i, varies from -∞ to 1. A value of R_i = 1 indicates ultimate sensitivity to the tool condition, while R_i = 0 shows extremely low sensitivity to the tool condition. On the other hand, a value of R_i< 0 denotes that this feature is insensitive to the cutting condition. The role of the assessment based on the p-value is to determine whether the extracted feature is applicable or not. Features with p-value less than 0.01 were the ones further ranked based on their f-values.

6.4. Pattern Recognition Classification Methods

The most frequently used pattern recognition methods, which were found in the literature, were considered in this study. These methods are the Binary Support Vector Machine (SVM), Linear Discriminant Analysis (LDA), K-Nearest Neighbor (KNN), Neural Network (NN), Naïve Bayes (NB), and Decision Trees (DT). To apply these methods, the machine learning toolbox of MATLAB© software was used. In addition, empirical prior probabilities were utilized as required depending on the relative incidences of the tool condition in the trained data. A small number of training samples may produce an

undefined classifier, whereas a high number may lead to an over-defined classifier. In both cases, the error increases. Therefore, different numbers of training samples were tested to reach near optimum classifiers. It should be noted that, due to the application of moving frame segmentation, the minimum number of segments to be used in the classifier training process should be at least equal to 1/(window overlapping percentage). This guarantees total coverage of all possible segment patterns in the learning process.

6.4.1. Support Vector Machine

The support vector machine solves the problem of separation of two classes by finding a linear function *f*, called *hyperplane*, that separates the classes and finds the widest margin between them by minimizing *w* as follows [61]:

$$f(x) = (x \cdot w) + b; \begin{Bmatrix} f(x) > 0 & for\ x \in class\ 1) \\ f(x) < 0 & for\ x \in class\ 2) \end{Bmatrix} \quad 6.2$$

This was done using the sequential minimal optimization technique. For nonlinearly separable data, a slack variable is allowed for samples from boundaries of the separation margin with a penalization parameter. A support vector machine proved to be less vulnerable for the overfitting problem and had a higher generalization ability since it was designed to minimize structural risk [105]. In addition, the method does not require a large number of training samples and can solve the learning problem even when only a small amount of training samples are available [61]. A linear SVM with a regularization parameter equal to 1 was used in this work.

6.4.2. Linear Discriminant Analysis (LDA)

Linear discriminant analysis is a mathematical model to classify multivariate data based on statistical analysis. It is based on assumptive Gaussian distributions of the learned data classes. The score function of the LDA model can be expressed as follows [106]:

$$Sf(\beta) = \frac{Var_{between}}{Var_{within}} = \frac{\beta^T \mu_1 - \beta^T \mu_2}{\beta^T C \beta} \quad 6.3$$

where β is the linear model coefficient, C is the pooled covariance matrix, and μ_1 and μ_2 are the mean vectors. This equation guarantees maximal separation between classes by maximizing the ratio of the 'between-classes' variance to the 'within-class' variance in the training data set. It predicts the tool condition by estimating the probability that a tested observation belongs to a tool condition class based on Bayes Theorem [106]. This allows fitting one of the pre-defined classes according to the mean and variance for each data class. The assumed distribution parameters are used to search for a linear combination of variables that best separate the learned data classes. This linear combination is used to determine the class of the tested data.

6.4.3. K-Nearest Neighbor (KNN)

K-Nearest Neighbor classification is a fundamental classification method that is recommended when it is difficult to determine reliable parametric estimates of probability densities [107]. It is based on learning by analogy. It measures the distance between the tested observation and the closest K-nearest neighbors in the learned dataset in an n-dimensional space. In this work, the Euclidean distance metric is utilized to determine neighbor closeness [107]. It is defined as the length of the line segments connecting the tested observation point P_o = ($Po_{1,}$ $P_{o2,\ ...,}$ P_{on}) by the nearest k-points P_k = ($Pk_{1,}$ $P_{k2,\ ...,}$ P_{kn}) in an *n* features domain. It can be calculated as follows:

$$d_k(P_o, P_k) = \sqrt{(P_{o1} - P_{k1})^2 + (P_{o2} - P_{k2})^2 + \cdots + (P_{on} - P_{kn})^2} \quad 6.4$$

The tested observation class is determined by using the assumption that objects near each other are similar. Hence, it categorizes tested data based on the classes of their nearest *k*-neighbors in the learned dataset.

6.4.4. Neural Network (NN)

Neural Networks are a computational model inspired by the neural structure of the human brain, which find data structures and algorithms for learning and classification of data. They consist of an interconnected group of multi-layers of neurons that relate the inputs to the desired outputs. The network is trained by iteratively modifying the strength of the structure connections based on the information flow through the network to map the inputs to the correct response [108]. Usually NN is used to model complex relationships and find patterns in nonlinear data. A one-layer NN of size 10 with one output was constructed using the Levenberg-Marquardt training algorithm [109] as well as the extracted features in this research.

6.4.5. Naïve Bayes (NB)

Naïve Bayes is a statistical method which is used to construct classifiers that predict the probabilities of each class feature. They are based on Bayes theorem with a strong (naive) independence assumption between the features. This assumption states that the conditional probability of a feature for a class is independent of the conditional probabilities of other features from the same class, and hence, all features are equally important and statistically independent. The joint probabilities of new data is used to predict their class, depending on the training dataset features probability distribution [110]. New data is classified based on the highest probability of its belonging to a particular class. Despite the incorrectness of this assumption, as regular features are dependent, NB classifiers are simple to apply and usually provide high accuracy [110]. Normal distribution was assumed to calculate the predictor distribution parameters within each class.

6.4.6. Decision Trees (DT)

A DT is a hierarchical model composed of decision rules that recursively splits independent variables into homogeneous zones [111]. It is a flowchart-like tree structure of decision rules to predict a new observation class from a set of input features. At each tree branching condition (node), the feature vector of a new observation is compared to a weight obtained from the training dataset. The number of

branches and the values of weights are determined during the training process. The DT method identifies and removes branches that may reflect noise in the training dataset to improve the classification accuracy. Decision trees have been applied successfully in many real-world situations for classification and prediction. The Gini diversity index was used in this work as a split criterion to classify the tool condition.

6.5. Benchmarking Approach of the Pattern Recognition Methods

The six pattern recognition models were trained and tested using the approach shown in Figure 6-4. The approach can be described as follows.

First, the top ranked time and frequency domain features were divided into training and testing sets. Depending on the capability of the processing approach to mask the cutting conditions, the training set was biased by selecting only one cutting condition per tool for this purpose and using the rest of the cutting conditions to test the developed models. This is done to test the model capability to accurately define the tool condition using the minimum training effort.

Next, in order to find the most suitable classifier for minimum training effort, the top ranked time and frequency domain features are divided into two distinct datasets for training and testing. Depending on the capability of the signal processing approach to mask the cutting conditions effect on the extracted features, a biased training dataset is generated from the features extracted from only one cutting feed rate and depth of cut combination per tool condition. The rest of the cutting conditions are used to test the developed models. This is done in order to test model capability to accurately define the tool condition using the minimum training effort, which is one cut per tool condition. It should be noted that, to achieve higher accuracy from the testing database, classifier underfitting is required. This is because in the proposed training and testing scheme, the classifier is tested using totally new data that has never been used for training. Hence, the more the classifier is fitted to the training data, the more it could misclassify new data. To illustrate, two curve fitting models, which are considered a machine learning model, are shown in Figure 6-5. These are a linear model and a six-degree polynomial model, which were generated using only 50% of the given data. As

seen, the polynomial model has provided higher accuracy than the linear one within the training data. However, for the total dataset, the linear model, which underfitted the training data, provided higher accuracy. Therefore, linear separation was applied in the tested classifiers when applicable.

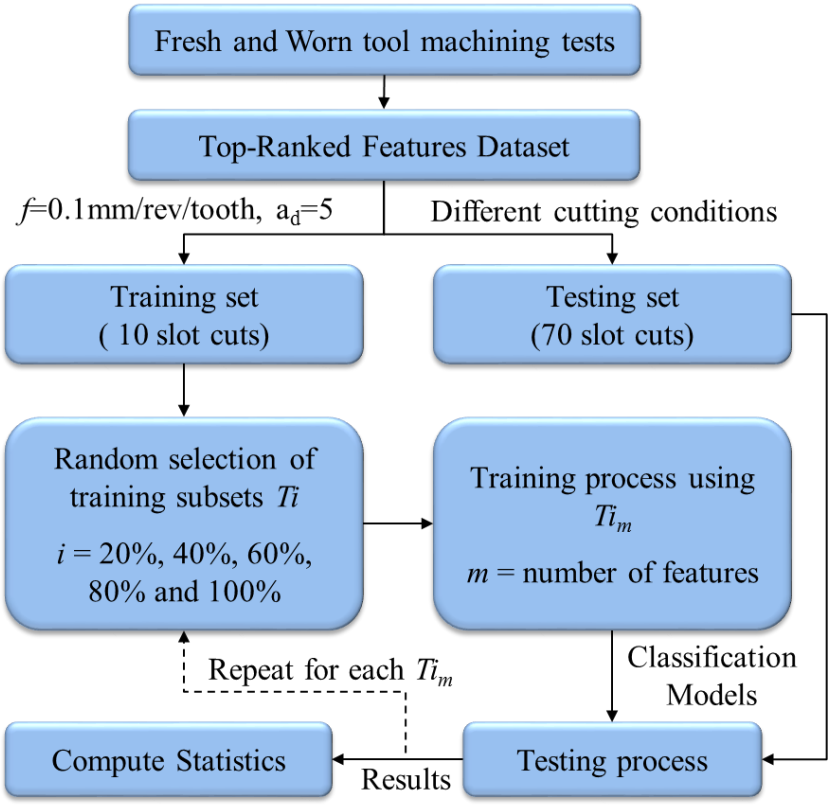

Figure 6-4 Benchmarking general approach

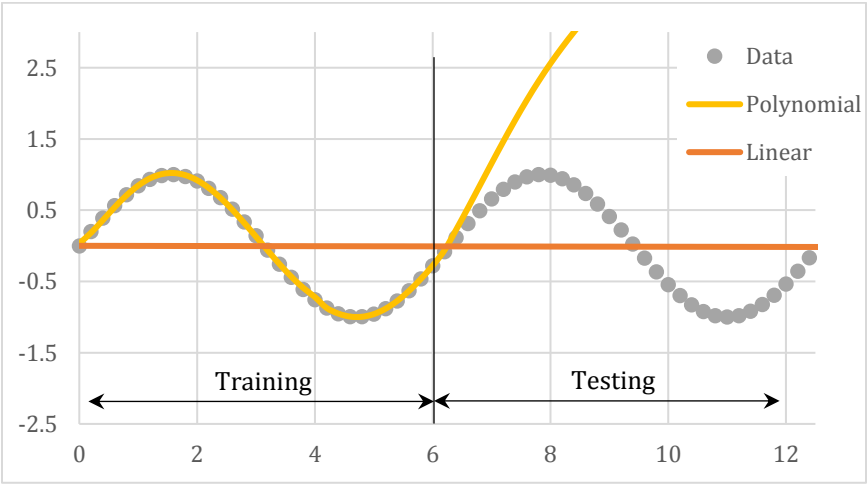

Figure 6-5 Curve fitting using 50% of the data for training

After that, for classification model training, five training subsets *Ti* were created randomly using 20%, 40%, 60%, 80% and 100% of the training dataset. Each subset was used for generating 11 different models of the same classifier method using an m number of features. Each size-feature subset Ti_m represents m number of features, where m varies from 1 to 11 according to their ranking score Ri in sequence. In total, 55 models were generated and analyzed for each pattern recognition method. A five-fold cross validation method was implemented in the training process in order to train the models by 5 stages/folds of the training data. Finally, the testing dataset was used to test and analyze the accuracy and computational time for the generated models.

The methods were compared according to classification accuracy, computational time and learning effort, which consisted of the number of training segments and the number of extracted features needed in the learning process. For a better representation of the classification method accuracy from a practical point of view, two types of false classification errors of the tool condition were introduced, namely, Safe False Alarm (SFA) and Unsafe False Alarm (USFA) rates. USFA occurs when the tool is worn, but the method classifies it as fresh. The SFA is the opposite where the tool is classified as worn while it is in a good state. Although SFAs may reduce productivity, they do not affect part quality. In contrast, the USFA condition could lead to more damage as the part surface integrity could be affected before tool replacement. Both errors rates were computed for all the classification methods

6.6. Feature Selection and Optimization

6.6.1. Feature Independency

The feature subset in the above benchmarking approach was generated in sequence, according to the ranking score for benchmarking purposes only. However, the combination of these features may not be the optimum feature subset and the level of accuracy may be increased by further optimization of the feature subset. In addition, the above feature selection algorithm does not consider interactions between features. For example, features selected from the list based on their relative ranking score may also contain redundant information, so that not all the features may be needed to

achieve the same level of accuracy. Hence, a more advanced feature selection algorithm is needed to identify the most characterizing features, to optimize the classification problem dimensionality (i.e., size of feature subset) and to improve the performance and accuracy.

To identify most characterizing features, redundant features are excluded from the positively ranked features. This is done by calculating the matrix of the pairwise correlation coefficient between each pair of features using Pearson's linear correlation method. The Pearson coefficient measure has a value from -1 to +1, where -1 is total negative linear correlation, +1 is a total positive linear correlation and 0 is no correlation. For a feature observation matrix $\mathbf{X}_{qn}$, where q is the number of features and n is the number of observations, the Pearson's linear correlation coefficient $\boldsymbol{r}$ between two features a and b (i.e., two columns in $\mathbf{X}$) is defined as [112]:

$$r(a,b) = \frac{\sum_{i=1}^{n}(X_{a,i} - \bar{X}_a)(X_{b,i} - \bar{X}_b)}{\left(\sum_{i=1}^{n}(X_{a,i} - \bar{X}_a)^2 \sum_{i=1}^{n}(X_{b,i} - \bar{X}_b)^2\right)^{1/2}} \qquad 6.5$$

where the mean value of the feature observations $\bar{X} = (\sum_{i=1}^{n} X_i)/n$. The practicality of the correlation is more vital than the statistical significance. Therefore, a threshold absolute r value of 0.95 is used to determine highly correlated features to be eliminated from the features' subset.

6.6.2. Feature Optimization

After filtering the features dataset by ruling out highly correlated features, it was optimized to reduce the classification problem dimensionality and to improve the performance and accuracy. This was done using the wrapper feature selection method, where one predetermined classification algorithm was used, and its estimated performance was implied as the evaluation criterion. A forward sequential feature selection SFS was applied. The minimum misclassification error rate (MCE) was employed as the cost function of the sequential feature selection method. It could be defined as the sum of misclassified segments over the total number of observations. Both techniques (i.e., forward and backward search) were applied on a training data

subset (i.e., *Ti*) to select the most expressive features with minimum MCE. The feature selection problem can be formulated as follows:

$$MCE(Ti_d) = \min_{Ti \in DB} MCE(Ti) \qquad 6.6$$

where Ti_d is a possible subset that contains *d* number of features and *DB* is the feature database. Hence, for the forward SFS method, starting from an empty feature set, the best individual feature, which generates the lowest misclassification error rate MCE_d, is selected to generate the initial subset Ti_d. Then, a candidate subset is created by sequentially adding each of the features not yet selected f^+ to obtain a new minimum MCE as follows:

$$f^+ = \arg\min_{f \in d} MCE^+(Ti_{d+1}) \qquad 6.7$$

where MCE^+ denotes that the error rate, obtained by Ti_{d+1}, is less than MCE_d. This process continues until adding more features does not decrease the error rate. For the backward SFS, the same procedure is followed in a top-down approach starting with the complete set of features, where redundant features are removed until *d* features remain. In this work, the forward sequential feature selection with a 5-fold cross-validation was applied to optimize the number of features.

6.7. Correlation between Fresh and Worn Tools

Worn tools were generated for the development of the tool condition monitoring system in a laboratory environment. However, it is more feasible to use the fresh tools only without the need for generating worn tools. This reduces the learning effort, the cost and the time required to implement the developed system for industrial applications. Hence, to further enhance the applicability of the developed system, an analysis was carried out to develop and validate a correlation between the features extracted from the fresh and worn tools. Such a correlation could further reduce the learning effort by 50% because only the fresh tool features would need to be used to develop the classification model.

6.8. Summary

The PWM spindle drive module controls the supplied voltage, current and the phase between them to provide the desirable power, torque and speed to the spindle. Therefore, features extracted from all the feedback signals, namely, voltage, current and power, were studied and analyzed to select the most sensitive features to tool wear, which was defined by uniform flank wear.

Based on the repetitive nature of the milling process, a robust and reliable signal processing approach was proposed to extract generalized features in both time and frequency domains. The approach filtered, segmented per revolution and normalized the signals to mask the effect of the cutting conditions on the extracted features and to accentuate the tool condition effect. The normalized segments showed that the developed tool wear resulted in a longer contact time between the tool and the workpiece, which altered the value of the extracted features.

An N-way ANOVA test and *f*-test were carried out to characterize the extracted features according to their sensitivity to the tool condition, feed rate and depth of cut. The outcome was used afterwards in a ranking function in order to select the most indicative features that correlate to the tool condition.

Using the features that had a high sensitivity to the tool condition, an approach was proposed for a systematic study of the widely used pattern recognition methods, namely, Support Vector Machine, Linear Discriminant Analysis, K-Nearest Neighbor, Neural Network, Naïve Bayes, and Decision Trees. The study benchmarked the methods based on their conservation characteristics as well as learning and computational effort, and they provided a general judgment on the classifying method performance.

The positive ranked features were optimized by first excluding redundant features, which had high correlations, then using the sequential feature selection method to develop a pattern recognition classification model with high accuracy. Such a process significantly reduced the number of features needed to identify the tool condition, and hence, reduced the computational effort. A correlation between the optimized features of fresh and worn tools was proposed to reduce the learning effort by 50% and to increase the flexibility of the developed system to be useful in industrial applications.

CHAPTER 7
EXPERIMENTAL TESTING, VALIDATION AND ONLINE IMPLEMENTATION OF THE DEVELOPED TOOL WEAR DETECTION SYSTEM

7.1. Introduction

In this chapter, the experimental results of testing and validating the proposed tool wear monitoring system are discussed. Generalized features that are independent of the cutting parameters and only sensitive to the tool condition were extracted, ranked and optimized based on the methods described in Chapter 6. The benchmarking results of six common pattern recognition classification methods, namely, Binary Support Vector Machine, Linear Discriminant Analysis, K-Nearest Neighbor, Neural Network, Naïve Bayes, and Decision Trees are discussed. The analysis of their characteristics and computational efficiency to optimize the learning effort, classification accuracy and calculation are demonstrated in this chapter. Based on the benchmarking results, the classification method with the best performance for real-time application was selected and used to build a tool condition classification model. A TCM system using this model was developed based on features extracted from the power, voltage and current signals of the spindle motor drive module. Experimental validation tests were carried out to demonstrate the robustness and high accuracy of the generated TCM system in real-time applications. The system capability to detect the tool condition was tested with respect to the cutting speed, feed rate, axial and radial depth of cut, tool diameter, tool corner radius, and number of flutes. The system generalization capability to detect the tool condition in different configurations of tool/workpiece engagement were tested as well. The following sections describe the experimental setup, sensor selection and the design of experiments; discuss the results of the N-way ANOVA test and feature ranking and selection; benchmark the methods used for pattern recognition; and demonstrate the validation results.

7.2. Design of Experiments for Tool Wear Monitoring System Development

7.2.1. Tool Wear Generation

According to ISO standards [2], a cutting tool reaches a severe wear condition when either or both of the acceptable flank wear VB threshold values (0.3 mm uniform or 0.5 mm localized) are exceeded [2]. In this research work, uniform flank wear was selected as the tool life criterion. Uniform worn tools, as shown in Figure 7-1, were distinguished compared to fresh ones. The tested tool conditions were categorized into two ranges, namely, a fresh tool (0 mm ≤ VB < 0.07 mm) and a worn tool (0.25 mm ≤ VB < 0.3 mm). This level of tool wear was generated on the cutting tool edges through controlled milling processes on steel workpieces prior to performing the TCM milling tests. Tool wear was measured using a Winslow cutting tool analyzer system model 560.

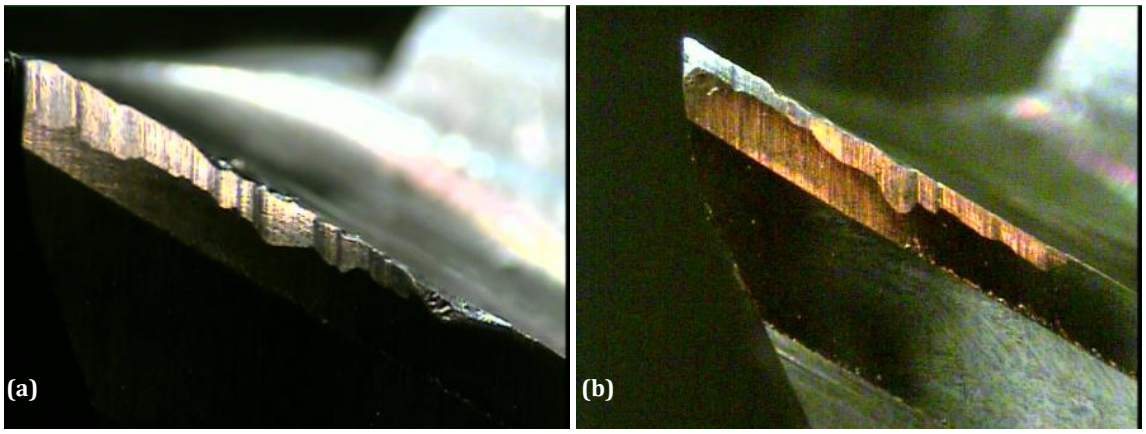

Figure 7-1 Tool wear generation (a) VB = 0.29 mm (b) VB = 0.27 mm

7.2.2. Design of Experiments for System Development

Experimental slot tests were performed on a 5-axis DMU 100P duoBlock machining center. The test setup, tools and workpiece material properties and chosen sensors are discussed in detail in Chapter 3. Seven solid tungsten carbide endmills with different diameters and corner radii were used to machine 100 mm long slots in the AL-7075 workpieces under flood cooling conditions. The 3-component cutting forces and the spindle drive motor current and voltage signals were acquired during the tests, and the tool condition was evaluated after each cut slot. The motor current and voltage signals

were used afterwards to digitally calculate the instantaneous motor power. Table 7-1 shows the full factorial matrix of the cutting conditions (rotational speed n, feed rate f and axial depth of cut a_p), as well as the wear levels used in the slotting tests. These tests were used in the development stage to analyze and select the most expressive features and classification method. A total of 112 slot tests were performed including one replicate of each set of cutting conditions. This section focuses on the cutting feed rate and depth of cut, as they have a direct relationship with the cutting energy, and hence, changing such parameters directly affects the monitored signals.

Table 7-1 Full factorial experimental design of the cutting conditions for TCM system development

Tool	VB (mm)	n (rpm)	f (mm/tooth/rev)	a_p (mm)
T12F2R00	0 - 0.07	14,000	0.1	3
T16F2R00				
T16F2R04				
T16F2R33				
T20F2R04	0.25 - 0.3		0.14	5
T20F2R33				
T25F2R04				

7.3. Experimental Results and Discussion

In this section, the ability of the processing approach to mask the cutting conditions is demonstrated, and the results of the N-way ANOVA test, the feature ranking, and the LDA model are presented. For simplicity, the results of the current signals only are presented and compared to the cutting force signals. The same processing procedures were applied to the spindle voltage and power, and equivalent results were obtained.

Figure 7-2 shows the normalized filtered signals of the (a) resultant force and (b) resultant spindle motor current. The cutting tests were performed at n =14,000 rpm, f= 3,500 mm/min, a_p = 3 mm, using tool T12F2R00. As shown in Figure 7-2 (a), the resultant force signals were steady and consistent through the repetitive tool/workpiece engagements. On the other hand, the resultant current signals showed

a repetitive, inconsistent pattern, as shown in Figure 7-2 (b). This inconsistency can be related to signal distortion due to the pulse width modulation that drives the spindle motor, which toggles the voltage/current signals on and off rapidly to control the motor speed and the delivered electrical power.

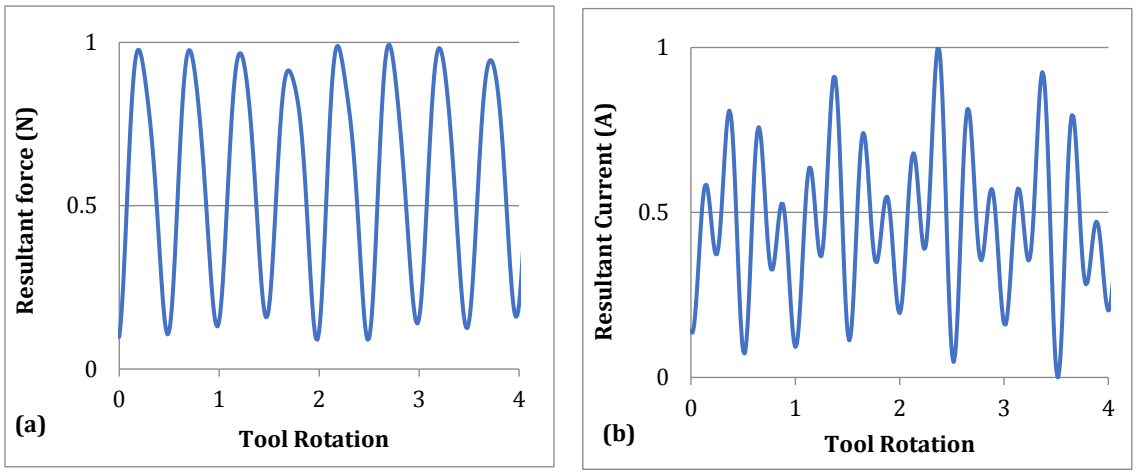

Figure 7-2 Normalized filtered (a) resultant force and (b) resultant current. n=14000 rpm, f= 3500 mm/min and a_p = 3 mm

After processing the acquired signals and extracting the desired features, N-way ANOVA tests were carried out using a confidence level of 99% (significance level α= 0.01) to test feature sensitivity to the cutting tool condition, cutting feed rate and depth of cut. The N-way ANOVA tests were performed using MATLAB's ANOVA routine from the Statistics and Machine Learning Toolbox. About 150,000 observations in total were employed in the ANOVA analysis. This includes the overall number of observations that came from the current and force signals acquired from 112 cutting tests. An average number of 350 samples per test for each acquired signal were analyzed for each processing operation. The f-values and p-values of the most significant features are presented in Tables 7-2, 7-3, 7-4 and 7-5 for the resultant force and resultant current signals acquired from the tools T16F2R00 and T12F2R00, respectively. These tables show the ANOVA test results after signal filtration, segmentation and normalization. They also show the flag values assigned to each feature according to its improvement in sensitivity to the tool condition after each processing operation, where an increase, no change and a decrease of the feature sensitivity to tool condition are represented by a flag value of 1, 0 and -1, respectively.

Table 7-2 N-way ANOVA test results for resultant force signals for tool T16F2R00

		E	min	rms	Mean	K	Var	P2rms	f_{mean}	Pw	f_{med}	BP	Pp
	TC	0.8	501.2	308.2	307.7	14.4	66.8	20.0	217.9	23.5	14.2	217.9	31.2
f-value filtration	*f*	0.8	91.0	54.5	54.4	2.1	6.0	0.1	41.6	1.1	30.9	41.6	0.2
	a_p	1.9	218.1	126.8	126.8	7.7	7.2	4.4	79.6	25.4	1.2	79.6	34.0
	TC	2.9	112.6	77.7	77.5	0.8	13.6	4.9	52.6	46.6	4.8	52.6	52.3
f-value segmentation (x10³)	*f*	0.5	19.8	13.6	13.6	0.1	1.1	0.0	9.9	8.8	0.0	9.9	9.9
	a_p	0.0	50.5	31.5	31.5	0.7	1.3	0.0	18.9	16.8	0.2	18.9	18.9
	TC	0.0	2.2	4.9	5.0	0.8	4.7	4.9	4.9	0.8	4.8	4.9	4.1
f-value normalization (x10³)	*f*	0.0	0.0	0.0	0.0	0.1	0.0	0.0	0.0	0.0	0.0	0.0	0.0
	a_p	1.8	1.1	0.0	0.0	0.7	0.3	0.0	0.0	0.0	0.2	0.0	0.0
	TC	432	0	0	0	19	1	11	0	8	20	0	5
p-value filtration (x10⁻³)	*f*	497	0	1	1	237	62	885	2	409	4	2	850
	a_p	238	0	0	0	50	55	103	1	7	334	1	4
	TC	0	0	0	0	0	0	0	0	0	0	0	0
p-value segmentation (x10⁻³)	*f*	0	0	0	0	0	0	505	0	0	23	0	0
	a_p	7	0	0	0	0	0	0	0	0	0	0	0
	TC	0	0	0	0	0	0	0	0	0	0	0	0
p-value normalization (x10⁻³)	*f*	0	0	427	424	0	17	505	388	834	23	388	450
	a_p	0	0	0	0	0	0	0	0	126	0	0	2
Segmentation Flag		1	1	1	1	1	1	1	1	1	1	1	1
Normalization Flag		-1	1	1	1	0	1	0	1	1	0	1	1

Table 7-3 N-way ANOVA test results for resultant force signals for tool T12F2R00

		E	min	rms	Mean	K	Var	P2rms	f_{mean}	Pw	f_{med}	BP	Pp
	TC	58.7	99.7	98.1	98.2	252.4	22.9	50.2	31.8	19.8	3.6	31.8	32.0
f-value filtration	*f*	13.1	34.0	29.5	29.6	0.0	2.3	0.2	11.4	0.6	55.7	11.4	0.2
	a_p	5.1	26.2	22.7	22.8	1.3	1.0	0.1	4.6	6.9	0.1	4.6	8.1
	TC	11.7	25.8	24.5	24.5	27.8	5.6	8.6	7.9	7.7	10.2	7.9	7.9
f-value segmentation (x10³)	*f*	0.5	8.8	7.3	7.3	0.0	0.5	0.0	2.8	2.8	0.1	2.8	2.8
	a_p	0.4	6.8	5.7	5.7	0.1	0.2	0.0	1.1	1.1	0.0	1.1	1.1
	TC	8.6	12.2	8.6	8.7	27.8	10.2	8.6	8.7	1.3	10.2	8.7	7.2
f-value normalization (x10³)	*f*	0.1	0.0	0.0	0.0	0.0	0.1	0.0	0.0	0.0	0.1	0.0	0.0
	a_p	0.1	0.0	0.0	0.0	0.1	0.0	0.0	0.0	0.0	0.0	0.0	0.0
	TC	2	1	1	1	0	9	2	5	11	129	5	5
p-value filtration (x10⁻³)	*f*	18	3	4	4	986	217	810	22	574	1	22	837
	a_p	88	7	9	9	320	373	821	99	58	750	99	47
	TC	0	0	0	0	0	0	0	0	0	0	0	0
p-value segmentation (x10⁻³)	*f*	0	0	0	0	200	0	0	0	0	0	0	0
	a_p	0	0	0	0	0	0	54	0	0	92	0	0
	TC	0	0	0	0	0	0	0	0	0	0	0	0
p-value normalization (x10⁻³)	*f*	0	0	0	0	200	0	0	0	259	0	0	0
	a_p	0	0	65	64	0	123	54	70	508	92	70	100
Segmentation Flag		1	1	1	1	1	1	1	1	1	1	1	1
Normalization Flag		1	1	1	1	0	1	0	1	1	0	1	1

Table 7-4 N-way ANOVA test results for current signals for tool T16F2R00

		E	min	rms	Mean	K	Var	P2rms	f_{mean}	Pw	f_{med}	BP	Pp
f-value filtration	TC	0.0	8.7	44.2	26.1	55.6	47.8	52.4	40.0	1.7	18.8	40.0	2.9
	f	8.0	0.1	44.9	57.6	2.1	7.8	1.9	41.6	0.5	26.9	41.6	4.1
	a_p	0.6	1.5	9.3	16.8	0.6	0.0	5.9	8.3	5.0	1.3	8.3	5.3
f-value segmentation	TC	30.1	1.0	57.1	29.7	58.8	253.8	275.6	75.7	36.5	204.3	75.7	40.2
	f	68.4	16.9	96.7	91.5	14.0	79.2	29.7	106.2	67.6	14.2	106.2	98.3
	a_p	4.8	84.2	28.7	34.1	9.9	2.3	7.0	27.9	21.2	4.3	27.9	33.2
f-value normalization	TC	23.4	69.9	268.7	284.8	58.8	22.2	275.6	260.8	183.9	204.3	260.8	273.1
	f	5.9	37.6	30.7	30.8	14.0	0.9	29.7	30.7	22.3	14.2	30.7	30.3
	a_p	43.9	17.1	8.9	4.7	9.9	26.1	7.0	9.8	4.9	4.3	9.8	5.3
p-value filtration (x10^{-3})	TC	929	42	3	7	2	2	2	3	260	12	3	164
	f	40	947	2	1	239	42	262	2	626	5	2	107
	a_p	489	290	38	15	478	993	73	45	88	311	45	82
p-value segmentation (x10^{-3})	TC	0	308	0	0	0	0	0	0	0	0	0	0
	f	0	0	0	0	0	0	0	0	0	0	0	0
	a_p	29	0	0	0	2	133	8	0	0	38	0	0
p-value normalization (x10^{-3})	TC	0	0	0	0	0	0	0	0	0	0	0	0
	f	3	0	0	0	0	423	0	0	0	0	0	0
	a_p	0	0	3	30	2	0	8	2	28	38	2	22
Segmentation Flag		-1	-1	-1	-1	1	1	1	-1	-1	1	-1	-1
Normalization Flag		-1	1	1	1	0	-1	0	1	1	0	1	1

Table 7-5 N-way ANOVA test results for current signals for tool T12F2R00

		E	min	rms	Mean	K	Var	P2rms	f_{mean}	Pw	f_{med}	BP	Pp
f-value filtration	TC	2.0	5.5	153.4	204.3	24.3	0.4	111.0	166.2	1.8	0.6	166.2	17.8
	f	12.2	0.4	2.5	9.7	4.1	20.2	66.9	2.9	4.6	45.1	2.9	41.2
	a_p	1.8	1.2	2.3	4.7	7.0	1.8	3.9	2.5	0.2	0.5	2.5	1.9
f-value segmentation	TC	8.4	176.1	317.6	405.2	93.7	1.1	270.0	337.8	270.3	280.0	337.8	431.5
	f	35.7	104.0	11.2	26.0	15.2	38.5	65.7	10.6	10.8	80.9	10.6	25.5
	a_p	6.8	21.0	2.9	5.7	28.0	4.3	6.9	2.7	2.0	14.9	2.7	5.5
f-value normalization	TC	1.5	139.2	271.7	305.8	93.7	104.2	270.0	269.7	180.3	280.0	269.7	306.4
	f	35.4	109.1	71.0	84.8	15.2	52.2	65.7	72.9	46.5	80.9	72.9	86.6
	a_p	8.6	18.1	6.4	8.8	28.0	7.8	6.9	6.1	3.9	14.9	6.1	8.3
p-value filtration (x10^{-3})	TC	226	79	0	0	8	576	0	0	246	476	0	14
	f	20	672	194	29	108	8	1	165	90	2	165	2
	a_p	246	335	204	97	57	255	121	188	695	537	188	244
p-value segmentation (x10^{-3})	TC	4	0	0	0	0	287	0	0	0	0	0	0
	f	0	0	0	0	0	0	0	0	0	0	0	0
	a_p	9	0	89	18	0	39	9	100	153	0	100	19
p-value normalization (x10^{-3})	TC	218	0	0	0	0	0	0	0	0	0	0	0
	f	0	0	0	0	0	0	0	0	0	0	0	0
	a_p	3	0	11	3	0	5	9	14	47	0	14	4
Segmentation Flag		-1	1	1	1	1	-1	1	1	1	1	1	1
Normalization Flag		-1	1	1	1	0	1	0	1	1	0	1	1

The tables are color mapped to easily visualize the results. For each feature, the highest *f*-value is shaded in dark blue, whereas the *p*-value is shaded and written in red if it exceeds the significance level (i.e., *p*-value > α). Finally, the flag value is colored in green, yellow and red for the flag values of 1, 0 and -1, respectively. The other tools showed equivalent results, and hence, they are not presented here.

7.3.1. Resultant Force Signal Results

As shown in Table 7-2 and Table 7-3, several features extracted from the filtered resultant force signals show high *f*-values corresponding to the tool condition while providing *p*-values less than α. This demonstrates that the variations in the force features, by nature, due to the tool condition are higher than the variation caused by the cutting conditions. Additionally, the processing approach improved feature sensitivity to the tool condition as follows.

- The segmentation process increased the feature sensitivity to the tool condition. This is evident by the decrease in the extracted feature *p*-values, while the f_{TC} values are at the maximum. This can also be noticed by the process flag values.
- The normalization process further decreased the signal sensitivity to the cutting conditions as seen by the decrease in the cutting condition *f*-values.

For example, in Table 7-2, in the filtration stage, features such as min, rms and f_{mean} were sensitive, without any further processing of signals, to the tool condition more than the cutting feed rate and the depth of cut just after filtering. Features such as Pw and Pp were, however, most sensitive to the depth of cut. Other features such as K and P2rms showed a relatively higher *p*-value than α, and hence, there was no correlation between their value and the tool condition regardless of the *f*-value. Just after segmentation per tool rotation and before extracting the tested features, all the features under investigation showed an almost zero p-value and relatively high *f*-value corresponding to the tool condition compared to the cutting conditions. This proved that the segmentation step increased the feature sensitivity to the tool condition. This sensitivity was increased further by the normalization stage as demonstrated by the increase in the *p*-value of some features corresponding to the cutting conditions (seen

in red) and the decrease in the cutting condition *f*-values of all the features to almost zero. Only the E feature, representing the area under the curve, showed inconsistent sensitivity to the tool condition after normalization. The plausibility and the strength of the effect of the stages of the processing approach on the tested feature sensitivity can be seen in the flag values for each stage. It is clearly shown that the segmentation has increased the sensitivity of all the features to the tool condition (flag value=1). In addition, the normalization step further increased this sensitivity for several features such as min, rms and Pw, whereas it did not significantly affect the K, P2rms and f_{med} sensitivity (flag value=0). The flag value shown in the last two rows of Table 7-2 confirms the importance of applying both processing stages to increase feature sensitivity to the tool condition. Such an output demonstrates the capability of the processing approach to mask the effect of the cutting conditions on the extracted features, while accentuating the tool condition effect. The same feature response to the processing approach was observed for other tools, as shown in Table 7-3 for example.

7.3.2. Resultant Current Signal Results

Contrary to the force signal, the current signal shows inconsistent output between the tools after the filtration and segmentation stages, as shown in Tables 7-4 and 7-5. This is expected as current signals generated by pulse width modulation techniques suffer from aliasing distortion [113]. The effect of this distortion was intensified by extracting the features per revolution, making the real representation of the cutting operation more difficult. However, the extracted features showed high sensitivity to the tool condition and high consistency after the normalization stage. This is demonstrated by the high f-value corresponding to the tool condition (shaded in dark blue), by the almost zero *p*-value and by the normalization flag value. This reveals the capability of the processing approach to mask the signal distortion and noise as well.

These results show the capability of the processing approach to depress the variations in the extracted features due to the cutting conditions, and hence, increase the impact of the tool condition variations. This can be observed through the features that are sensitive to the cutting conditions before processing and showed high

sensitivity to the tool condition and/or less sensitivity to the cutting conditions after the normalization operation, such as the rms, mean and *Pp* of the forces and current signals. Moreover, the reliability of the generalized, extracted features is demonstrated by the consistency of the ANOVA test results of these features for different cutting tools. However, it should be noted that the sensitivity of the kurtosis, peak to root mean square ratio, and the median frequency of the tool and cutting conditions was not improved after the normalization operation, as can be observed by their flag values. This action shows the independency of these specific features to the cutting conditions, which influence the peak values of the segments.

7.4. Feature Ranking Results

The ANOVA test results of the two tested cutting tools were employed for ranking the extracted features using Equation 6.1. Figure 7-3 shows the ranking scores of the features extracted from the resultant force and current signals. In the time domain, the peak to root mean square P2rms, mean and rms show high sensitivity to the tool condition in both resultant force and current signals, regardless of the tool geometry. For the same signals, the features f_{mean} and *BP* are, however, the highest ranked extracted features in the frequency domain. It is also worth noting that the feature *Pp* showed high sensitivity to the tool condition in the resultant current signals. This means that as the tool becomes worn, the distribution of the segmented current signal variance increases over its frequency range. Features such as *K* and min in the time domain show low ranking score, as they demonstrated sensitivity to the tool size in the ANOVA test. To demonstrate the processing approach effect on clustering the extracted features, Figure 7-4 shows the deviation in the mean values of selected generalized features extracted from the acquired signals before and after processing of all the cutting tests for tool T16F2R00 using fresh and worn tools. As shown in Figure 7-4 (b) and (d), the processing approach minimized the variations in the extracted features due to the cutting parameters and signal noise, and emphasized the effect of the tool condition, which confirmed the ANOVA test results. Hence, for both signals, the features can be clearly divided into two isolated clusters with respect to the tool condition.

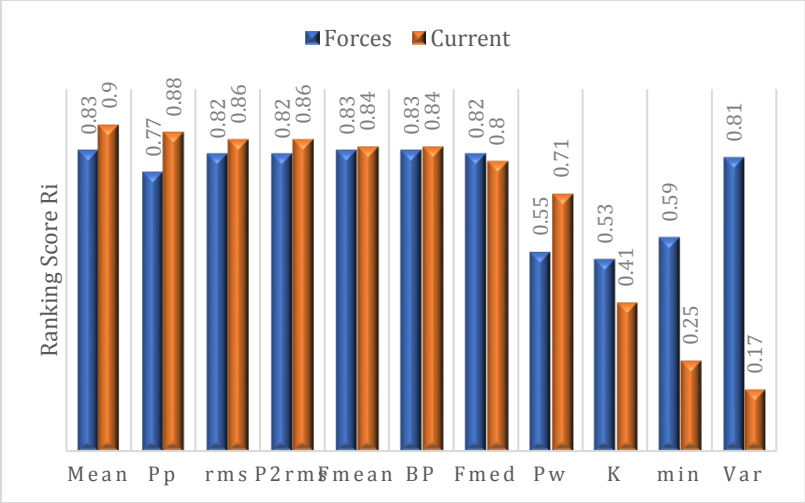

Figure 7-3 Ranking score of extracted features according to Equation 6.1

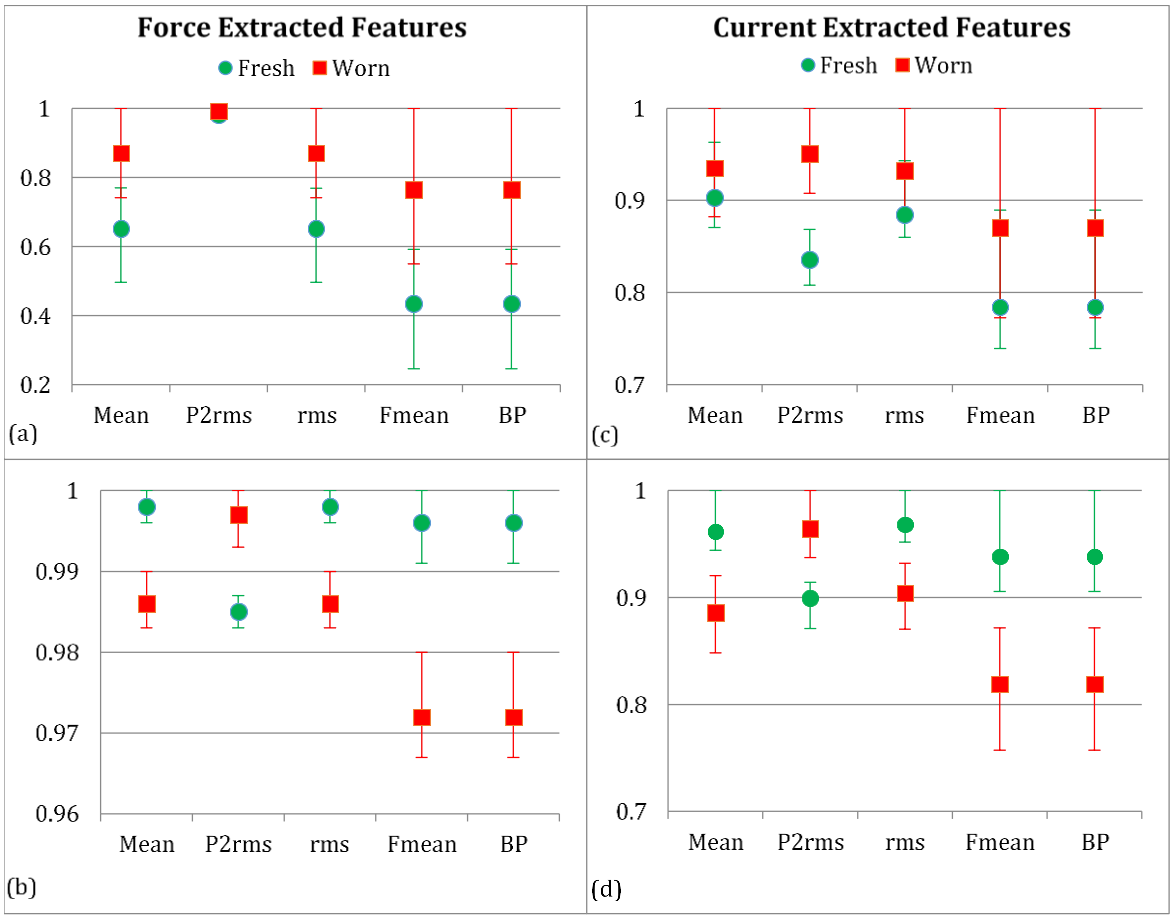

Figure 7-4 Features extracted from tool T1 of the resultant force signals (a) before processing and (b) after processing, and features extracted from the resultant current signals (c) before processing and (d) after processing

7.5. Results and Discussion of Benchmarking Pattern Recognition Methods

According to the benchmarking approach defined in Section 6.5, biased training data that consisted of only one cutting condition were used to train the classification models while the rest of the cutting conditions tests were used for validation. In this work, cuts with feed and axial depth of cut of 0.1 mm/rev/tooth and 5 mm respectively were randomly selected for training. In total, 14 cuts were used as a training database for the seven tested tools. The rest of the cutting tests (98 tests including one replicate of each set of cutting conditions) were used for testing the performance of the classification models.

7.5.1. Learning Effort and Accuracy

Figure 7-5 shows the maximum accuracy achieved by the six classification methods with respect to (a) the training dataset size and (b) the number of features used for training, respectively. In general, the LDA and SVM showed higher accuracy than the other methods. In addition, they were able to achieve an almost 90% accuracy using only 20% of the training data. This accuracy was more or less the same when five or more features were used regardless of the training dataset size. Hence, 20% of a training set consisting of the five top ranked features were enough to achieve high accuracy for both methods. The high performance of the LDA method was due to its assumption of training data normality and not adapting the data distribution. Therefore, the LDA prediction errors were due to the errors in estimating a representative mean and variance out of the training dataset whereas the SVM ability to minimize structural risk limited its classification errors to the difficulty of calculating global boundaries for the separation margin using the training data. In addition, the linear separation adopted by these two methods provided an underfit model, which is usually better for biased training data. However, the LDA showed higher accuracy compared to the SVM even when only one feature was used for training. Hence, the LDA classification method is recommended for applications with limited training data as in the TCM system learning process for machining operations. This was expected as the

LDA uses the training data mean and variance to enforce normal distribution on the classification model and does not adopt the distribution of training subset data as is. In addition, according to the central limit theorem [114], given a sufficiently large sample size from a population with a finite level of variance, the mean of all samples from the same population is approximately equal to the mean of the population. Furthermore, all the samples follow an approximate normal distribution pattern with all variances being approximately equal to the variance of the population divided by each sample's size. This is the case in a dynamic cutting application such as milling and due to the distortion in the acquired current signals from the PWM controller.

On the other hand, DT and KNN methods, which adopt the training set distribution, showed the lowest accuracy, with a maximum of 84.2% and 84.6% respectively, through all the training dataset sizes. The KNN method showed an increasing trend when the number of training samples increased. The NB and NN showed a steady accuracy of around 85% regardless of the number of features used. The NN had a decreasing trend by increasing the number of training samples. It also provided the highest accuracy when five features were used, which decreased afterwards. This performance illustrates the method's sensitivity to the training dataset size, which is in agreement with the results found in [76]. The decision tree models showed the same sensitivity. Such performance may not provide a generalized approach for TCM systems, and hence, the application of both classification methods should be limited.

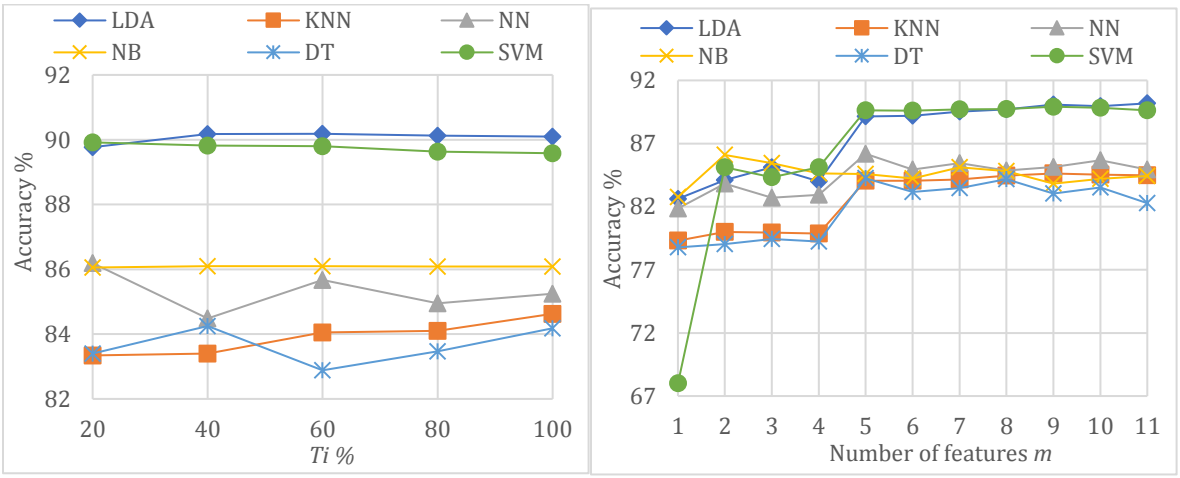

Figure 7-5 Classification method accuracy with respect to (a) the training dataset size T_i and (b) the number of features used for training

Figure 7-6 shows the safe and unsafe false alarm rates achieved by the classification methods at their highest accuracy levels. The LDA showed the lowest SFA and USFA rates with values of 6.2% and 3.6% respectively, followed by the SVM method. On the other hand, the DT, KNN and NN methods showed an USFA rate as high as 10%, while the NB method reached the highest SFA rate. From these results, a conclusion can be drawn that implementing the LDA and SVM methods in TCM systems should increase the systems accuracy and the machining process productivity.

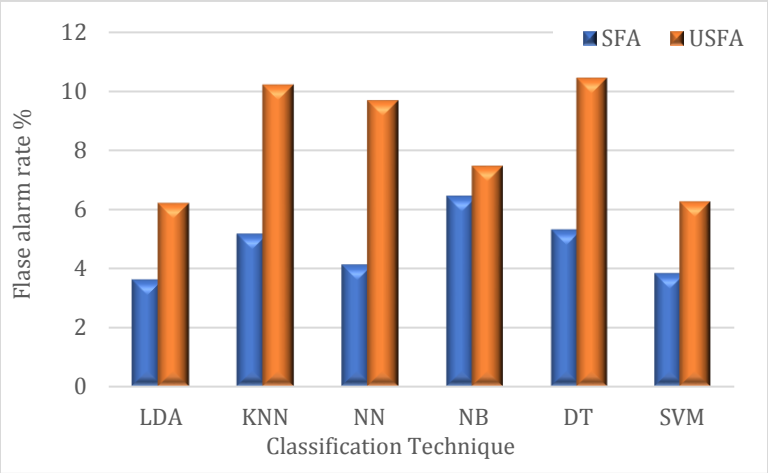

Figure 7-6 Safe and Unsafe false alarms at the highest accuracy values

It should be noted that, in this work, each model included five different tools. The results showed the capability of *fusing* the developed signal processing approach with pattern recognition methods to mask the effect of different tool diameters and corner radii while preserving a high accuracy level.

7.5.2. Computational Time

Early detection of tool wear minimizes the impact of a worn tool on the workpiece surface integrity. Hence, the time needed per one revolution was used as a reference for comparing the pattern recognition method classification time. In this work, a spindle speed of 14,000 rpm was applied. At this speed, 4.28 ms is required for one full tool rotation. Figure 7-7 shows the average time needed for each classification method to classify one segment. The time ranges were calculated for all the tested sample sizes Ti_m. The results show that the DT has the lowest classification time of 6.8 µs and the

lowest deviation as well, followed by the NB and LDA, respectively. As Figure 7-7 shows, the KNN showed the highest classification time of ~115 µs. Although these time ranges are low compared to the time needed for 1 revolution in high speed machining applications, it represents the relative computational effort and memory needed to classify the tool condition.

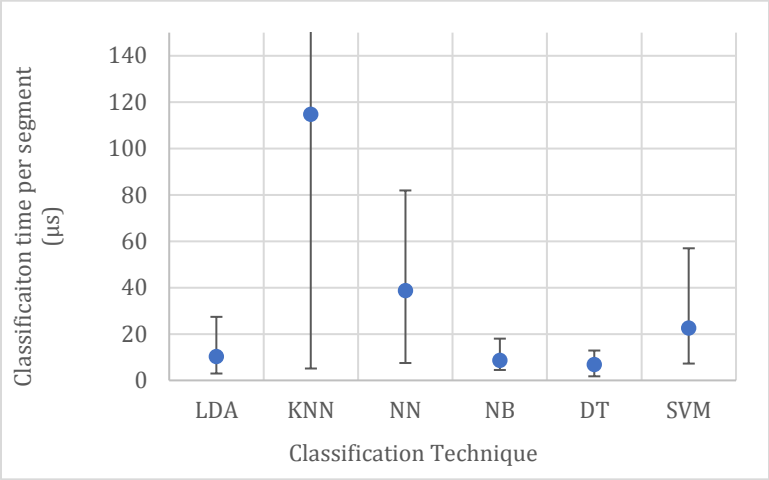

Figure 7-7 Classification time per segment

7.6. Results of Feature Selection and Optimization for Tool Wear Detection

7.6.1. Feature Correlation and Independency Results

Independency analysis was carried out on the top-ranked features extracted from the current signals of the seven tested tools. Table 7-6 shows the *r* value correlation matrix, which was calculated using the whole feature database. A threshold of 0.95 was applied to determine features with high dependency that have to be eliminated. The table has been color shaded to easily visualize the results with green, yellow and red colors representing low, medium and high correlation, respectively. As shown in this table, the Kurtosis K feature showed exceptionally low correlation with other features, ranging between -0.535 (with the Var feature) to 0.716 (with the min feature). This indicates the feature uniqueness and importance to describe the tool condition. The min and Var in the time domain and the Pw and f_{mean} in the frequency domain demonstrated below-threshold *r*-values as well. The f_{med} showed high correlation with the f_{mean}, and

hence, it was eliminated. Similarly, high correlation was found between the frequency domain features BP and Pp and the time domain features Mean, rms, and P2rms. These frequency domain features are costlier to compute, and hence, were eliminated. Among these time domain features, the Mean feature is the least costly to compute, and hence, was selected while eliminating the rms and P2rms features. Consequently, out of the 11 top-ranked features, only six features showed high independency. These features are the current Mean, f_{mean}, Pw, K, min and var.

Table 7-6 Correlation matrix for current features

	Mean	Pp	rms	P2rms	f_{mean}	BP	f_{med}	Pw	K	min	Var
Mean	1	0.997	0.981	-0.969	-0.809	0.981	-0.86	0.946	-0.25	0.8	-0.628
Pp		1	0.977	-0.958	-0.806	0.982	-0.851	0.948	-0.237	0.806	-0.637
rms			1	-0.993	-0.688	0.998	-0.746	0.944	-0.374	0.685	-0.465
P2rms				1	0.67	-0.984	0.738	-0.928	0.404	-0.658	0.432
f_{mean}					1	-0.692	0.968	-0.732	-0.193	-0.912	0.912
BP						1	-0.746	0.948	-0.357	0.694	-0.478
f_{med}							1	-0.766	-0.099	-0.923	0.904
Pw								1	-0.266	0.716	-0.535
K									1	0.036	-0.352
Min										1	-0.904
Var											1

The same independency analysis was carried out for the power and voltage signals as well. The analysis concluded that, out of the top-ranked features for power, only the K, f_{med}, min and Pw were highly sensitive and independent. Additionally, for the voltage signals, f_{mean}, f_{med}, SD and Var were selected.

7.6.2. Signal Fusion and Feature Optimization

In this section, the forward sequential feature selection SFS method was applied to train a linear discriminant analysis LDA model using the independent top-ranked features. The dataset collected from the current, voltage and power signals of the seven tested tools was used to develop one LDA model. Similar to the training method used in the comparison of the pattern recognition methods in Section 7.5, a training set consisting of the features collected from only one cutting condition was used to develop

the LDA model while the rest of the machining tests were used for testing model accuracy. The SFS selected 11 features in total from the power, current and voltage signals. These features are the K, f_{med} and min from the power signals, the f_{mean}, K, Mean, Var and min from the current signals, and the f_{mean}, f_{med} and SD from the voltage signals.

Again, for simplicity, the SFS iteration results of the features extracted from the current signals only are presented in Figure 7-8. The f_{mean} feature was the best individual feature, which generated the lowest misclassification error rate *MCE* of 17%. This error dropped significantly by adding the Kurtosis feature to the LDA model to only 8%. Such action indicates the significance of these two features on the classification process. This significance is due to the change in the geometry of the cutting edge owing to the developed wear and the resulting longer contact time between the worn tool and the workpiece. This alters the frequency spectrum and its mean value. In addition, the normalized segment of the worn tool showed a platykurtic shape (i.e., lower kurtosis value), as shown in Figure 6-3, compared to the fresh tool pattern.

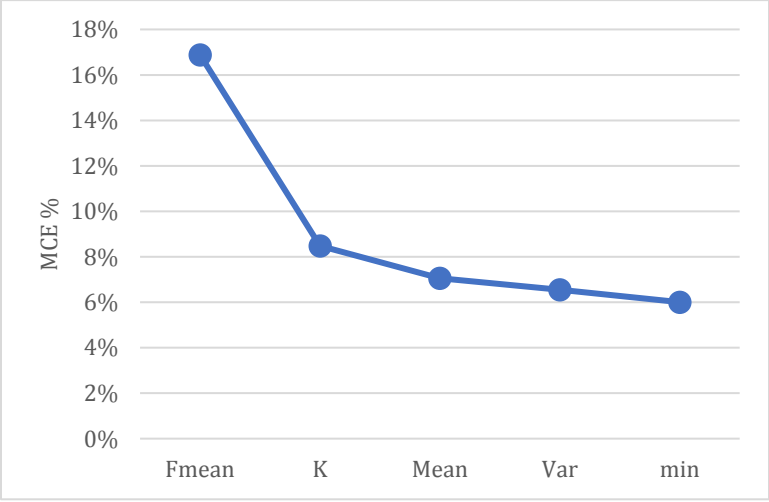

Figure 7-8 MCE% developed by adding features using the SFS method

The model prediction accuracy slightly increased when the Mean, Var and min features were added in sequence to reach a final total accuracy of 94% among all the tested tools. This is a 4% higher accuracy than what the LDA model achieved when it was trained by the first five features of the 11 top-ranked list, namely, Mean, Pp, rms, P2rms and f_{mean}. The SFS method ruled out the Pw, although it had a higher sensitivity

ranking score than both the min and Var. This is because adding more features overfits the model, which increases the classification error.

7.7. Correlation between Fresh and Worn Tools

In the LDA method, the mean and standard deviation of the training features, after assuming normal distribution among them, were used to generate a classification model. Hence, to find a correlation between the features extracted from the fresh and worn tools, a linear correlation was assumed between the features' mean, while the same standard deviation was assumed for both tool conditions. The dataset collected from the seven tested tools was used to develop the correlation vector between the mean values of the sequentially selected features of all the feedback signals of the spindle motor. The correlation vector of the features extracted from the current signals and their changing percentage are presented in Table 7-7. The f_{mean} feature shows a reduction of 13% when the tool is worn. This is the highest difference among all the features, which explains why it was selected as the best individual feature by the SFS method. This was followed by the Kurtosis and Mean features, where a reduction of 11% and 8% were reached, respectively. On the other hand, the Var and min show low difference percentage (<3%). However, when these features were fused in the LDA model, the classification accuracy was improved.

The obtained correlation vector was applied to the features extracted from only one cutting condition per each fresh tool to generate an LDA model similar to Section 7.5. The model showed similar accuracy to what was obtained when both fresh and worn tools were used. Such an output demonstrates the robustness and applicability of the usage of the correlation vector. The application of the correlation vector further reduced the learning effort by 50%. Hence, the total learning effort presented in this work was reduced by 87.5% compared to what is reported in the literature.

Table 7-7 Correlation vector between fresh and worn tool

Feature	f_{mean}	K	Mean	Var	min
Correlation value	0.87	0.89	0.92	1.02	0.97
Linear difference %	13	11	8	2	3

7.8. Online Implementation of the Tool Wear Monitoring System

The hardware and software described in Section 3.8 was used to implement the tool wear monitoring system in real-time. Tool wear is a lengthy progressive process. Hence, demonstrating the tool condition with high resolution (i.e., for each tool rotation) is not required. Therefore, for real-time implementation of the TCM system, the mode of the tool condition per segment for a period of 1 second of real cutting was used to define the final tool condition, while the classification accuracy per segment was referred to as the classification confidence level CL. The LDA classification model was generated offline using the feature correlation vector and the features extracted from one cutting condition using the fresh tool only. The model was subsequently integrated into the cRIO controller for real-time detection of tool wear. Current and voltage signals were acquired and segmented per one second of cutting in the FPGA while power generation, signal filtering, segmenting per revolution, processing and decision making were done by the real-time processor. The system was migrated from the MATLAB environment, which is the developing language, to LabView. The total needed time span starting from signal acquisition to decision making did not exceed 0.7 ms per revolution. The developed system is ultra-fast and can be applied for speeds up to 85,000 rpm.

The gradual nature of tool wear allows different types of decision making compared to only the need to stop as in sudden failure events such as chipping and breakage. These decisions could be, for example, to change the tool after finishing the tool path or finishing the part. Hence, in the case of tool wear detection, the system sends an alarm to the CNC machine HMI to declare tool wear. This communication can be done using the 2-way communication interface, as described in Section 3.8. In addition, an audible and visual alarm is sent to the operator to take suitable corrective action. This is done using a National Instruments simultaneous, ±10 voltage output module connected to an industrial warning tower and siren.

7.9. Validation Tests and Results

The performance of the generalized selected features and classification model for detecting tool wear was validated against a wide range of cutting parameters. These

parameters can be divided into two main categories, namely, (i) tool geometry, which includes the tool diameter, number of flutes and corner radius. (ii) tool/workpiece engagement, which includes the variations of the cutting radial depth of cut and multi-axis tool paths. Both categories were tested using a wide range of cutting conditions (i.e., speed, feed rate and axial depth of cut). The validation tests comprised 7 tools with different diameters and corner radii, 2 tool conditions VB, 2 speeds n, 6 feeds f, 4 axial depth of cut a_p and 12 radial depth of cut a_e.

7.9.1. Tool Geometry Validation Tests

Tests were performed to validate the developed system practicality and accuracy. Fresh and worn tools with 2, 3 and 4 flutes, different corner radii and diameters ranging from 20 to 50 mm where used in this test. In total, 96 slot cuts, including one repetition of each cutting condition, were performed. The cutting speed was 14,000 rpm while a feed of 0.1 and 0.14 mm/tooth/rev as well as a depth of cut of 3 and 5 mm were used. Table 7-8 shows the full factorial selection of the tools and cutting parameters used for linear slotting tests. The acquired current, voltage and power signals were processed to extract the sequentially selected features described in Section 7.6. Features extracted from the fresh tool tests with a feed of 0.14 mm/tooth/rev and 3 mm depth of cut were implemented along with the feature correlation vector, which was developed in Section 7.7, to generate a general LDA model. In total, features extracted from seven cutting tests out of 96 tests were used to train the LDA model, which represented 12.5% of the features dataset. The LDA classified tool condition and the classification confidence level percentage CL% of the fresh and worn tools are shown in Figure 7-9 (a) and (b) respectively. As seen in these figures, the generated TCM system accurately detected the tool condition in 96.5% of the validation tests with an average confidence level of 93%. Only two tests were misclassified as fresh whereas they were worn. In these two tests, the 50 mm tool was used at the maximum cutting condition. The cutting power required at these conditions was higher than 97% of the maximum spindle power of the machine tool. This increased the instability of the pulse width drive module, and hence, the generated feedback signals. Thus, the extracted features did not accurately

represent the tool condition. The LDA accuracy and confidence level demonstrated the generated TCM system capability to capture the tool condition under different tool geometries and cutting conditions.

Table 7-8 Full factorial of validation tests

Tool	VB (mm)	n (rpm)	f (mm/tooth/rev)	a_p (mm)	a_e (% of tool Diameter)	Repetitions	**Total number of cuts**
T20F2R40 T25F2R04 T25F2R40 T25F3R04 T25F3R33 T50F4R04 T50F4R40	0 - 0.07 0.25 - 0.3	14,000	0.1, 0.14	3, 5	100	2	112

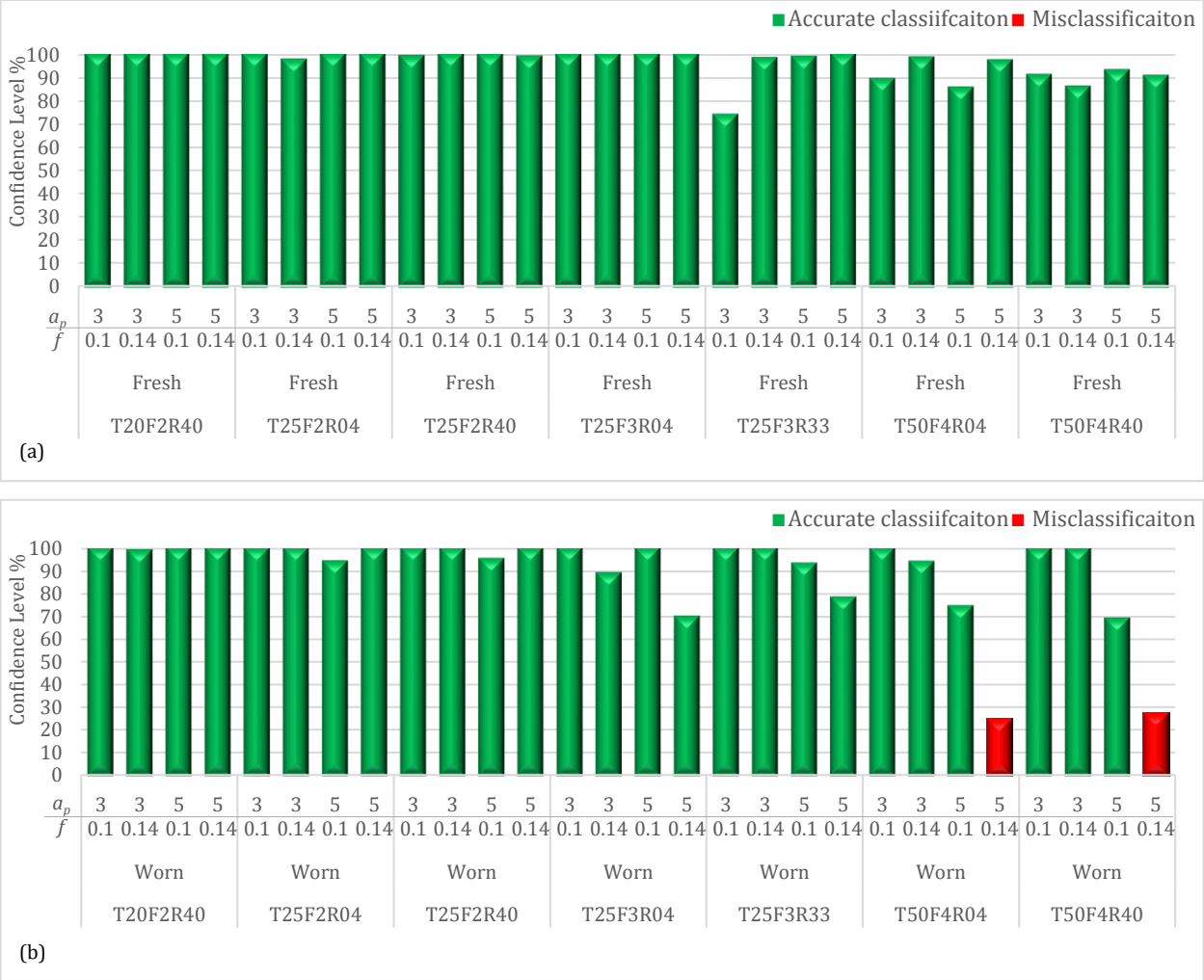

Figure 7-9 Classification accuracy of (a) fresh and (b) worn tools

7.9.2. Tool Path Validation Tests

The capability of the developed system to capture tool conditions in complex tool paths is demonstrated in this sub-section. A total of 128 partially immersed slotting cuts were performed to validate the TCM system accuracy. In addition, different complex features were machined including: 4-axis slanted surfaces (3), linear slots with variable depth of cut (4), curved slots (5), and straight (6) and inclined (7) pockets, as seen in Figure 7-10 (a). Each of these geometrical features was machined using fresh and worn tools. The different levels of axial and radial depth of cut of these features are shown in Figure 7-10 (b) while the cutting parameters are shown in Table 7-9. An *adaptive control system* with constraints (ACC) was used during the machining of the variable depth slots and inclined pockets. This system maintained a constant machine spindle power during cutting by continuously altering the feed rate. The system was programed to alter the feed rate within a range of 80 to 150% of the feed rate programmed in G-code to maintain a constant level of power equal to 90% of the machine maximum power.

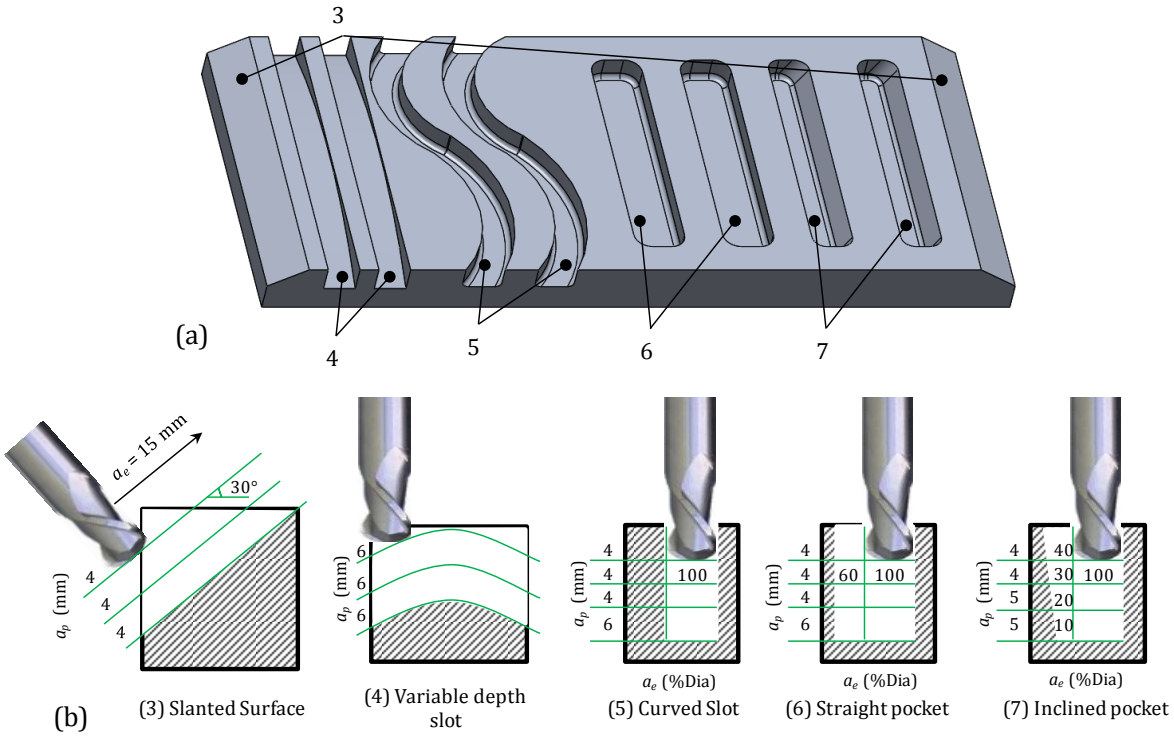

Figure 7-10 (a) Representative part (b) cutting radial and axial levels

Table 7-9 Geometrical and cutting parameters of tested tool paths

No.	Feature	Tool	VB (mm)	a_e (% Dia)	n (rpm)	f (mm/tooth /rev)	a_p (mm)	Total number of cuts
1	Partial immersion	T25F2R40	0 - 0.07 0.25 - 0.3	10, 20, …, 90	16,000	0.25, 0.3	4, 6	72
2	Partial immersion	T50F2R04		10, 20, …, 70	14,000	0.1, 0.125	3, 5	56
3	Slanted surfaces	T50F2R40		40	14000	0.1	0-4	2
4	Variable depth slots	T25F2R40		100	16000	0.14 - ACC	0-6	2
5	Curved slots	T25F2R40		100	14000	0.25	4,4,4,6	2
6	Straight pockets	T20F2R40		100 + 60	16000	0.25	4,4,5,5	2
7	Inclined pockets	T25F2R40		Variable	14000	0.22 - ACC	4,4,4,6	2
	Total number of tests							138

The general LDA model, described in Section 7.9.1, was used in this section to detect the tool condition in real-time. A static threshold was applied to the current signal to exclude air cuts from the collected signals before processing. Figure 7-11 (a) shows the TCM system accuracy level for the tests described in Table 7-9. The system successfully achieved nearly an accuracy of 91% for all the partial immersion tests conducted by two different tools (No. 1 and 2 in Table 7-9). It also attained a 100% accuracy for all full immersed slots regardless of the tool path (i.e., variable depth of cut (4) and curved slots (5)). Furthermore, accuracies of 93%, 95%, and 92% were reached when detecting the tool condition during the machining of slanted surfaces (3), straight pockets (6) and inclined pockets (7) respectively. Figure 7-11 (b) demonstrates the TCM system output during machining a straight pocket using a worn tool. As seen in this figure, the system can clearly define the tool as worn. The misclassification errors that occurred during this test were mainly taking place during the changing events of the tool path (i.e., at pocket corners). At these events, the CNC controller completely stopped the tool feed motion in one direction and started it in another one. This transient action reduced the load significantly on the cutting edge, which altered the extracted pattern features and led to this misclassification error. In general, the results demonstrated in this section proved the capability of the generated TCM system to

capture the tool condition under complex tool/workpiece engagements and different speeds with or without an adaptive control environment.

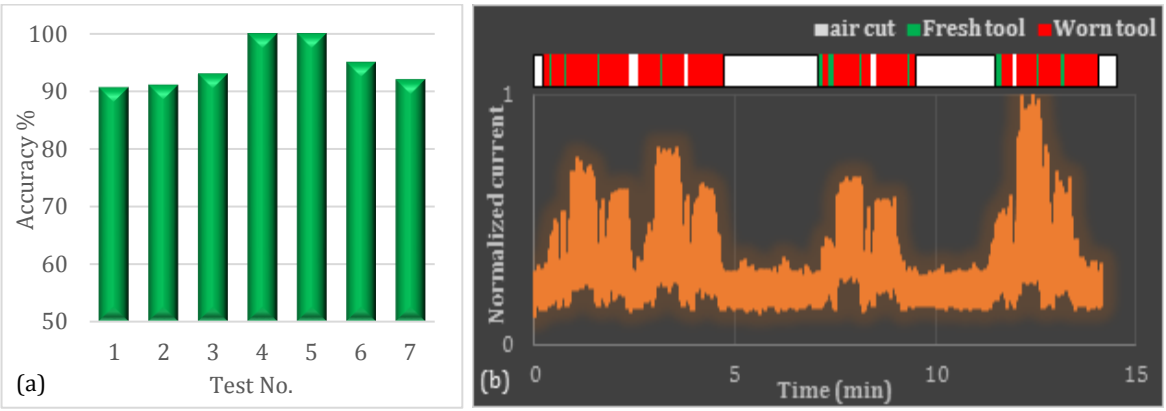

Figure 7-11 TCM system (a) accuracy for complex paths and (b) output for machining a straight pocket (6) using worn tool

7.10. Summary

Two levels of tool condition were adopted in this work, namely, a fresh tool (0 <VB<0.07) and a worn tool (0.25 < VB 0.3 mm). This level of tool wear was generated using severe, controlled cutting conditions prior to the experimental tests.

Features were extracted from the acquired force, voltage, current and power signals after processing them using the proposed approach. An N-way ANOVA test were conducted and showed the effectiveness of the proposed signal processing approach to depress the sensitivity of the extracted features to cutting conditions and accentuate the effect of the tool condition only. The resultant current signals showed a repetitive inconsistent pattern. However, the signal processing approach showed high capability to mask this effect as well on the extracted features.

Features were ranked depending on their sensitivity to the tool condition. The analysis revealed 11 top ranked features, out of 40 features, extracted from each signal. The results revealed the processing approach capability to separate the top-ranked features extracted from the spindle motor feedback signals into two mutually exclusive clusters according to their tool condition.

The practicality of applying different pattern recognition methods in TCM systems was benchmarked in this work. The following conclusions can be drawn from the conducted tests, analysis and comparison.

- The linear discriminant analysis, followed by the support vector machine, are the most recommended classification methods for TCM applications.
- The LDA showed the highest classification accuracy and lowest USFA rate using a limited learning effort with an applicable classification computational time. This shows the high performance and applicability of such method when the provided training data is limited as in the learning process of TCM systems.
- Decision trees and k-nearest neighbor classification methods provided the lowest accuracy and highest USFA rate. Hence, the application of these methods in TCM systems should be minimized.
- The neural network and naïve Bayes classification methods provided a steady accuracy regardless of the training size. However, the neural network method gave higher USFA rates.
- Fusing the adopted processing approach with pattern recognition methods can mask the effect of tool diameter and corner radius on the learning and classification process in TCM systems.

The independency analysis of the top ranked features reduced the computational effort by ~50%. Subsequently, the forward sequential feature selection method was applied to optimize the number of features using the misclassification error of a linear discriminant analysis model as the cost function. The outcome showed the significance of 11 features extracted from the power, current and voltage signals to capture the tool condition in a wide range of cutting parameters. A linear correlation vector was generated between the features extracted from seven fresh and worn tools to reduce the learning effort by 50%.

The same hardware and software described in Chapter 4 were used to implement the tool wear detection system in real-time applications. The total time span needed starting from signal acquisition to decision making did not exceed 0.7 ms per

revolution. The developed system is ultra-fast and can be applied for speeds up to 85,000 rpm.

Validation tests were conducted using untrained tools to authenticate the capability of the developed system to deal with different tool geometries and tool/workpiece engagement, including 4-axis milling operations and adaptive control environments. Using only the features extracted from one cutting condition combination of a fresh tool and the generated correlation vector, the system achieved an accuracy of 96.5% with respect to tool geometries and an accuracy ranging from 91% to 100% when the tool/workpiece engagement was tested.

CHAPTER 8
CONCLUSIONS AND RECOMMENDATIONS FOR FUTURE RESEARCH WORK

8.1. Conclusions

In this thesis, all the research objectives have been met. A new generalized sensor-fusion TCM system was developed for tool failure prediction and prevention during intermittent cutting processes. The developed system can predict tool chipping/breakage as well as detect tool wear in real-time. Using minimum learning effort, the system showed high sensitivity to the tool condition, regardless of cutting conditions, tool and workpiece materials, and cutting tool geometries. It was also insensitive to the dynamic tool-workpiece interaction during cutting. The developed system achieved an accuracy of 100% for tool prefailure detection and an accuracy ranging from 91% to 100% for tool wear detection, with a high confidence level. The developed system was integrated in real-time, high speed cutting applications and was able to take corrective action by stopping the cutting process before any damage to the machined part. No such system is currently available. The following conclusions are drawn from the experimental and analytical investigation that was performed in this research.

8.1.1. Conclusions from the Developed Tool Prefailure Detection and Failure Prevention System

- The AE_{rms} signals can represent the elastic waves associated with the generation of new surfaces during unstable crack propagation, which precedes tool chipping and/or fracture. Forces and vibrations are sensitive to the onset of fracture only whereas, in contrast to literature findings, the power signal cannot detect tool chipping.
- The AE_{rms} raw signal is insufficient by itself to be an indicator for tool prefailure detection. The main challenges for detecting the unstable crack

propagation phase, preceding tool chipping, using the AE_{rms} raw signal are: (i) the nonlinear relationship between the AE_{rms} response and the change in the crack area, (ii) the non-stationary nature of the stochastic unstable crack propagation process, which induces high frequency/amplitude bursts in the AE_{rms} signals, (iii) the contamination of the crack propagation bursts in the AE_{rms} signal by the bursts coming from the force variation during intermittent cutting, and (iv) the infinitesimal time spans of the high frequency bursts inherent in unstable crack propagation. This leaves a relatively short time (on millisecond-scale) for taking corrective action after detection.

- The AE_{rms} signals generated during the prefailure phase were found to have a relatively high frequency and high energy compared to the AE_{rms} signals during a normal cutting process.
- Based on the characterization study of the AE signals in the prefailure stage, this work introduced a two-stage novel signal processing approach that can deal with the aforementioned challenges of using the AE_{rms} raw signal for tool prefailure detection. In the first stage, the Hilbert-Huang Transform method is used to overcome challenges (i) and (ii) by representing the AE_{rms} in the time-frequency domain. In the second stage, the Teager–Kaiser Energy Operator is applied to highlight the prefailure phase and to suppress the bursts coming from the force variation and signal noise in the cutting process, overcoming challenge (iii). In addition, an algorithm was developed to optimize the implementation of this approach in a real-time application to provide an adequate time window to stop the machine before any damage to the machined part, thus dealing with challenge (iv).
- The developed two-stage signal processing approach analyzes the AE_{rms} signals to detect abrupt events with relatively high energy/frequency, which is a characteristic of the AE signals during unstable crack propagation. It can clearly identify the prefailure phase and depress any events with relatively low frequency and/or low energy.

- The approach successfully captured tool prefailure in all tested conditions and tools. It predicted tool failure earlier by a time window ranging from 4 to 6 tool/workpiece engagements, regardless of the cutting process (i.e., milling or intermittent turning), cutting parameters and tool path. Such results were supported by high speed imaging of the cutting process.
- An exponential relationship was identified between the prefailure detection indicator and the chipping area, regardless of the cutting conditions, tool path and workpiece material. The relationship can be used to define thresholds to tolerate acceptable chipping sizes or to prevent tool chipping during intermittent cutting operations.
- The developed real-time tool failure prediction and prevention system can control the machine tool in real-time to stop the feed motion of the cutting process before tool failure. This non-intrusive system was shown to safeguard the machined part from any damage in typical high-speed milling applications with speeds up to 18,000 rpm. No such system is currently available.

8.1.2. Conclusions from the Developed Tool Wear Detection System

- Neither the spindle motor power, current nor voltage signals can be used as a standalone signal to detect the tool condition. A feedback signal fusion is essential to develop a generalized TCM system that can define the tool condition under wide range of cutting conditions.
- The characterization of the acquired signals showed that tool wear increased the contact time between the tool and workpiece. Such a condition alters the physical and statistical features of the signal pattern per tool rotation.
- A novel generalized approach for real-time tool condition monitoring was developed. The processing approach can effectively mask the effects of the cutting conditions and signal noise on the extracted features, while emphasizing only the tool condition effect.

- The statistical analysis of the extracted features identified the features of high sensitivity to the tool condition, in both forces and current signals. Equivalent results were obtained for the power and voltage signals as well. These features were ranked according to their sensitivity to the tool condition, and then, used to benchmark six different pattern recognition methods. The analysis showed that linear discriminant analysis classification model outperforms other methods. It also proved that the highly ranked generalized features can be classified into two mutually exclusive clusters according to their tool condition. The developed model reduced the learning effort by 75%, compared to other models found in the literature.
- Feature optimization, based on independency analysis and the forward sequential feature selection method, decreased the computational effort by ~50%. Furthermore, the generation of a correlation vector between the features extracted from fresh and worn tools in the system development stage decreased the learning effort further by 50%. The correlation vector was shown to be effective for new tools that were not used to generate this correlation vector.
- A generalized signal-fusion based TCM system was developed to detect a tool wear condition in real-time. The system is able to deal with a wide range of cutting conditions, such as cutting speed, feed rate, axial and radial depth of cut, and tool geometries, such as tool diameter, number of flutes and corner radius. The system can also accurately detect the tool condition in an adaptive control environment and for 4-axis machining tool paths. The developed system reduced the learning effort by 87.5%, compared to those reported in the open literature. The system achieved an accuracy of 96.5% with respect to tool geometries, and an accuracy ranging from 91% to 100% for complex tool paths. The proposed system is robust with a total signal processing and decision-making time of 0.7 ms, which makes it applicable for high speed machining applications with a cutting speed up to 85,000 rpm. This non-intrusive system also effectively reduced the learning process and

provided high accuracy levels to achieve industrial requirements. Such a TCM system has never been previously developed.

8.2. Recommendations for Future Research Work

The following recommendations are proposed for future research work.

Future research work should be oriented toward developing an unmanned real-time intelligent TCM package, assisted by logical tools and methods, including self-learning and self-diagnostic algorithms, to increase the system accuracy, applicability and flexibility, and to minimize the inevitable intervention of the system developer and operator. Such aspects can be achieved, based on the presented work for tool wear and prefailure detection through:

1. Enhancing the tool prefailure detection capability by achieving the following:
    a. Testing the approach sensitivity to different interfering tool defect phenomena that can affect the generated AE signals such as, chip weldment, built-up edges and double cutting.
    b. Standardizing the learning process of the prefailure detection system to define a simple and rapid threshold function for different tool materials.
    c. Implementing embedded wireless sensors to monitor the tool condition in applications where using miniature sensors is not possible (e.g., micro-milling processes).
2. Developing a capability for online TCM self-learning and self-diagnostics based on AI algorithms. This includes automatic development of the system algorithm with minimal operator intervention as follows:
    a. Online feature extraction and selection,
    b. Online training and validating of pattern recognition models for TCM,
    c. Real-time adaptive update and tuning of the classification model during the cutting process.

REFERENCES

[1] 2014, "Invest in Canada - Aerospace Industries: Canada's compatitive advantages," No. 978-1-100-21999-8, Foreign Affairs, Trade and Development Canada.

[2] ISO8688-2, 1989, "Tool Life Testing in Milling – Part 2: End Milling," International Organization for Standardization, Geneva, Switzerland, International Standard, first edition.

[3] Zhou, Y., and Xue, W., 2018, "Review of tool condition monitoring methods in milling processes," The International Journal of Advanced Manufacturing Technology, pp. 1-15.

[4] Altintas, Y., 2012, Manufacturing automation: metal cutting mechanics, machine tool vibrations, and CNC design, Cambridge university press.

[5] Lei, X., 2006, "Typical phases of pre-failure damage in granitic rocks under differential compression," Geological Society, London, Special Publications, 261(1), pp. 11-29.

[6] Altintas, Y., 2014, "Adaptive Control," CIRP Encyclopedia of Production Engineering, L. Laperrière, and G. Reinhart, eds., Springer Berlin Heidelberg, pp. 17-19.

[7] Wang, L., and Gao, R. X., 2006, Condition monitoring and control for intelligent manufacturing, Springer.

[8] Groover, P., 1996, Fundamentals of modern manufacturing : materials, processes, and systems, Prentice Hall, Upper Saddle River, N.J.

[9] Kuttolamadom, M., 2012, "Prediction of the Wear & Evolution of Cutting Tools in a Carbide/Ti-6Al-4V Machining Tribosystem by Volumetric Tool Wear Characterization & Modeling."

[10] Zhang, D., 2011, "An adaptive procedure for tool life prediction in face milling," Proceedings of the Institution of Mechanical Engineers, Part J: Journal of Engineering Tribology, p. 1350650111414332.

[11] Chung, K. T., and Geddam, A., 2003, "A multi-sensor approach to the monitoring of end milling operations," Journal of materials processing technology, 139(1/3), pp. 15-20.

[12] Bassiuny, A., and Li, X., 2007, "Flute breakage detection during end milling using Hilbert–Huang transform and smoothed nonlinear energy operator," International Journal of Machine Tools and Manufacture, 47(6), pp. 1011-1020.

[13] Kim, T.-Y., Woo, J., Shin, D., and Kim, J., 1999, "Indirect cutting force measurement in multi-axis simultaneous NC milling processes," International Journal of Machine Tools and Manufacture, 39(11), pp. 1717-1731.

[14] Vallejo, A. J., Morales-Menéndez, R., and Alique, J., 2008, "On-line cutting tool condition monitoring in machining processes using artificial intelligence," Robotics Automation and Control, pp. 143-166.

[15] Haber, R. E., Jiménez, J. E., Peres, C. R., and Alique, J. R., 2004, "An investigation of tool-wear monitoring in a high-speed machining process," Sensors and Actuators A: Physical, 116(3), pp. 539-545.

[16] Dutta, S. D., A. Chakladar, N. D. Pal, S. K. Mukhopadhyay, S. Sen, R., 2012, "Detection of tool condition from the turned surface images using an accurate grey level co-occurrence technique," Precision Engineering, 36(3), pp. 458-466.

[17] Ghani, J. A., Rizal, M. Nuawi, M. Z. Ghazali, M. J. Haron, C. H. C., 2011, "Monitoring online cutting tool wear using low-cost technique and user-friendly GUI," International Conference on Wear of Materials, 271(9-10), pp. 2619-2624.

[18] Zhang, K.-f., Yuan, H.-q., and Nie, P., 2015, "A method for tool condition monitoring based on sensor fusion," Journal of Intelligent Manufacturing, pp. 1-16.

[19] Shaban, Y., Yacout, S., and Balazinski, M., 2015, "Tool wear monitoring and alarm system based on pattern recognition with Logical Analysis of Data," Journal of Manufacturing Science and Engineering.

[20] Maia, L. H. A., Abrao, A. M., Vasconcelos, W. L., Sales, W. F., and Machado, A. R., 2015, "A new approach for detection of wear mechanisms and determination of tool life in turning using acoustic emission," Tribology International, 92, pp. 519-532.

[21] Downey, J., O'Leary, P., and Raghavendra, R., 2014, "Comparison and analysis of audible sound energy emissions during single point machining of HSTS with PVD TiCN cutter insert across full tool life," Wear Wear, 313(1-2), pp. 53-62.

[22] Vallejo, A. J., Morales-Menendez, R., and Alique, J. R., "Intelligent monitoring and decision control system for peripheral milling process," Proc. Systems, Man and Cybernetics, 2008. SMC 2008. IEEE International Conference on, IEEE, pp. 1620-1625.
[23] Nouri, M., Fussell, B. K., Ziniti, B. L., and Linder, E., 2015, "Real-time tool wear monitoring in milling using a cutting condition independent method," International Journal of Machine Tools and Manufacture, 89(0), pp. 1-13.
[24] Ostasevicius, V., Jurenas, V., Augutis, V., Gaidys, R., Cesnavicius, R., Kizauskiene, L., and Dundulis, R., 2017, "Monitoring the condition of the cutting tool using self-powering wireless sensor technologies," The International Journal of Advanced Manufacturing Technology, 88(9-12), pp. 2803-2817.
[25] Shao, H., Wang, H. L., and Zhao, X. M., 2004, "A cutting power model for tool wear monitoring in milling," International Journal of Machine Tools and Manufacture, 44(14), pp. 1503-1509.
[26] Kalvoda, T., and Y, H., 2010, "A cutter tool monitoring in machining process using HilbertHuang transform," International Journal of Machine Tools and Manufacture International Journal of Machine Tools and Manufacture, 50(5), pp. 495-501.
[27] Prickett, P. W., and Grosvenor, R. I., 2007, "A Microcontroller-Based Milling Process Monitoring and Management System," Proceedings of the Institution of Mechanical Engineers, Part B: Journal of Engineering Manufacture, 221(2), pp. 357-362.
[28] Hsueh, Y.-W., and Yang, C.-Y., 2008, "Prediction of tool breakage in face milling using support vector machine," The International Journal of Advanced Manufacturing Technology, 37(9-10), pp. 872-880.
[29] Cao, H., Chen, X., Zi, Y., Ding, F., Chen, H., Tan, J., and He, Z., 2008, "End milling tool breakage detection using lifting scheme and Mahalanobis distance," International Journal of Machine Tools and Manufacture, 48(2), pp. 141-151.
[30] Wang, S.-M., Ho, C.-D., Tsai, P.-C., and Yen, C., 2014, "Study of an efficient real-time monitoring and control system for BUE and cutter breakage for CNC machine tools," International Journal of Precision Engineering and Manufacturing, 15(6), pp. 1109-1115.

[31] Vallejo, A. J., and Morales-Menendez, R., 2010, "Cost-effective supervisory control system in peripheral milling using HSM," Annual Reviews in Control Annual Reviews in Control, 34(1), pp. 155-162.
[32] Coker, S. A., Oh, S. J., and Shin, Y. C., 1998, "In-Process Monitoring of Surface Roughness Utilizing Ultrasound," Journal of Manufacturing Science and Engineering, 120(1), pp. 197-200.
[33] Kondo, E., and Shimana, K., 2012, "Monitoring of prefailure phase and detection of tool breakage in micro-drilling operations," Procedia CIRP, 1(0), pp. 581-586.
[34] Ravindra, H. V., Srinivasa, Y. G., and Krishnamurthy, R., 1997, "Acoustic emission for tool condition monitoring in metal cutting," Wear, 212(1), pp. 78-84.
[35] Liu, C., Wu, J.-q., Liu, H.-l., Li, G.-h., and Tan, G.-y., 2015, "Geometry features of breakage section and variation of cutting force for end mills after brittle breakage," The International Journal of Advanced Manufacturing Technology, pp. 1-14.
[36] Chinchanikar, S., and Choudhury, S. K., 2014, "Characteristic of Wear, Force and their Inter-relationship: In-process Monitoring of Tool within Different Phases of the Tool Life," Procedia Materials Science, 5, pp. 1424-1433.
[37] Tipping, M. E., 2001, "Sparse Bayesian learning and the relevance vector machine," Journal of machine learning research, 1(Jun), pp. 211-244.
[38] Zheng, D. N., Wang, J. X., and Zhao, Y. N., 2006, "Training sparse MS-SVR with an expectation-maximization algorithm," Neurocomputing, 69(13), pp. 1659-1664.
[39] Collins, M., 1997, "The EM algorithm," fulfillment of Written Preliminary Exam II requirement.
[40] Satpute, D. R., Mhaske, M. S., and Belkar, S., 2014, "Vibration Analysis of Multiple Cracked Shaft," International Journal of modern rngineering research.
[41] Marinescu, I., and Axinte, D. A., 2008, "A critical analysis of effectiveness of acoustic emission signals to detect tool and workpiece malfunctions in milling operations," International Journal of Machine Tools and Manufacture, 48(10), pp. 1148-1160.
[42] Tlusty, J., and Andrews, G. C., 1983, "A Critical Review of Sensors for Unmanned Machining," CIRP Annals, 32(2), pp. 563-572.
[43] Dornfeld, D., and Lee, D.-E., 2008, Machine design for precision manufacturing, Springer.

[44] Kannatey-Asibu, E., and Dornfeld, D. A., 1981, "Quantitative relationships for acoustic emission from orthogonal metal cutting," Journal of Manufacturing Science and Engineering, 103(3), pp. 330-340.
[45] Abellan-Nebot, J., and Romero Subirón, F., 2010, "A review of machining monitoring systems based on artificial intelligence process models," The International Journal of Advanced Manufacturing Technology, 47(1-4), pp. 237-257.
[46] Liang, S. Y., Hecker, R. L., and Landers , R. G., "Machining process monitoring and control: The state–of–the–art," Proc. IMECE2002, ASME International Mechanical Engineering Congress & Exposition.
[47] Bahr, B., Motavalli, S., and Arfi, T., 1997, "Sensor fusion for monitoring machine tool conditions," International Journal of Computer Integrated Manufacturing, 10(5), pp. 314-323.
[48] Coker, S. A., and Shin, Y. C., 1996, "In-process control of surface roughness due to tool wear using a new ultrasonic system," International Journal of Machine Tools and Manufacture, 36(3), pp. 411-422.
[49] Aliustaoglu, C., Ertunc, H. M., and Ocak, H., 2009, "Tool wear condition monitoring using a sensor fusion model based on fuzzy inference system," Mechanical Systems and Signal Processing, 23(2), pp. 539-546.
[50] Amer, W., Grosvenor, R. I., and Prickett, P. W., 2006, "Sweeping filters and tooth rotation energy estimation (TREE) techniques for machine tool condition monitoring," International Journal of Machine Tools and Manufacture, 46(9), pp. 1045-1052.
[51] Vallejo, A. J., Morales-Menéndez, R., Rodriguez, C. A., and Sucar, L. E., "Diagnosis of a cutting tool in a machining center," Proc. Neural Networks, 2006. IJCNN'06. International Joint Conference on, IEEE, pp. 3706-3713.
[52] Michalski, R. S., Carbonell, J. G., and Mitchell, T. M., 2013, Machine learning: An artificial intelligence approach, Springer Science & Business Media.
[53] Charest, M., Finn, R., and Dubay, R., "Integration of artificial intelligence in an injection molding process for on-line process parameter adjustment," Proc. Systems Conference (SysCon), 2018 Annual IEEE International, IEEE, pp. 1-6.
[54] Chandrasekaran, M., Muralidhar, M., Krishna, C. M., and Dixit, U. S., 2010, "Application of soft computing techniques in machining performance prediction and

optimization: a literature review," The International Journal of Advanced Manufacturing Technology, 46(5-8), pp. 445-464.
[55] Hanchuan, P., Fuhui, L., and Ding, C., 2005, "Feature selection based on mutual information criteria of max-dependency, max-relevance, and min-redundancy," IEEE Transactions on Pattern Analysis and Machine Intelligence, 27(8), pp. 1226-1238.
[56] Aha, D. W., and Bankert, R. L., 1996, "A comparative evaluation of sequential feature selection algorithms," Learning from data, Springer, pp. 199-206.
[57] Imiya, A., and Perner, P., 2005, Machine Learning and Data Mining in Pattern Recognition, Springer.
[58] Zhang, C., and Zhang, H., 2015, "Modelling and prediction of tool wear using LS-SVM in milling operation," International Journal of Computer Integrated Manufacturing(ahead-of-print), pp. 1-16.
[59] Lamraoui, M., El Badaoui, M., and Guillet, F., 2015, "Chatter Detection in CNC Milling Processes Based on Wiener-SVM Approach and Using Only Motor Current Signals," Vibration Engineering and Technology of Machinery, Springer, pp. 567-578.
[60] Xu, T., and Feng, Z., "Tool wear identifying based on EMD and SVM with AE sensor," Proc. Electronic Measurement & Instruments, 2009. ICEMI '09. 9th International Conference on, pp. 2-948-942-952.
[61] Widodo, A., and Yang, B.-S., 2007, "Support vector machine in machine condition monitoring and fault diagnosis," Mechanical Systems and Signal Processing, 21(6), pp. 2560-2574.
[62] Zhu, K., Wong, Y. S., and Hong, G. S., 2009, "Wavelet analysis of sensor signals for tool condition monitoring: A review and some new results," International Journal of Machine Tools and Manufacture, 49(7–8), pp. 537-553.
[63] Bhuiyan, M., and Choudhury, I., 2014, "13.22-Review of Sensor Applications in Tool Condition Monitoring in Machining," Comprehensive Materials Processing, 13, pp. 539-569.
[64] Castejon, M., Alegre, E., Barreiro, J., and Hernández, L., 2007, "On-line tool wear monitoring using geometric descriptors from digital images," International Journal of Machine Tools and Manufacture, 47(12-13), pp. 1847-1853.

[65] Barreiro, J., Castejón, M., Alegre, E., and Hernández, L., 2008, "Use of descriptors based on moments from digital images for tool wear monitoring," International Journal of Machine Tools and Manufacture, 48(9), pp. 1005-1013.
[66] Du, R., Elbestawi, M., and Wu, S., 1995, "Automated monitoring of manufacturing processes, part 1: Monitoring methods," Journal of Engineering for Industry, 117(2), pp. 121-132.
[67] Hassan, M., Sadek, A., Damir, A., Attia, H., and Thomson, V., 2017, "Real-time Tool Breakage Detection Using K-Nearest Neighbor Method in Milling Operations," Canadian Aeronautics and Space Institute – CASI 63rd Aeronautics conference AERO17.
[68] Rajesh, V., and Namboothiri, V. N., 2010, "Flank wear detection of cutting tool inserts in turning operation: application of nonlinear time series analysis," Soft Computing, 14(9), pp. 913-919.
[69] Burke, L. I., 1993, "An unsupervised neural network approach to tool wear identification," IIE transactions, 25(1), pp. 16-25.
[70] Sick, B., 2002, "On-Line And Indirect Tool Wear Monitoring In Turning With Artificial Neural Networks: A Review Of More Than A Decade Of Research," Mechanical Systems and Signal Processing, 16(4), pp. 487-546.
[71] Liu, T.-I., and Jolley, B., 2015, "Tool condition monitoring (TCM) using neural networks," The International Journal of Advanced Manufacturing Technology, pp. 1-9.
[72] Elangovan, M., Devasenapati, S. B., Sakthivel, N. R., and Ramachandran, K. I., 2011, "Evaluation of expert system for condition monitoring of a single point cutting tool using principle component analysis and decision tree algorithm," Expert Systems with Applications, 38(4), pp. 4450-4459.
[73] Elangovan, M., Ramachandran, K., and Sugumaran, V., 2010, "Studies on Bayes classifier for condition monitoring of single point carbide tipped tool based on statistical and histogram features," Expert Systems with Applications, 37(3), pp. 2059-2065.
[74] Karandikar, J., McLeay, T., Turner, S., and Schmitz, T., 2015, "Tool wear monitoring using naive Bayes classifiers," The International Journal of Advanced Manufacturing Technology, 77(9-12), pp. 1613-1626.

[75] Devendiran, S., and Manivannan, K., 2013, "Condition monitoring on grinding wheel wear using wavelet analysis and decision tree C4. 5 algorithm," International Journal of Engineering and Technology, 5(5), pp. 4010-4024.

[76] Wu, D., Jennings, C., Terpenny, J., Gao, R. X., and Kumara, S., 2017, "A Comparative Study on Machine Learning Algorithms for Smart Manufacturing: Tool Wear Prediction Using Random Forests," Journal of Manufacturing Science and Engineering, 139(7), pp. 071018-071018-071019.

[77] Jiaa, C. L., and Dornfeld, D. A., 1998, "A self-organizing approach to the prediction and detection of tool wear," ISA Transactions, 37(4), pp. 239-255.

[78] Benardos, P., and Vosniakos, G.-C., 2003, "Predicting surface roughness in machining: a review," International Journal of Machine Tools and Manufacture, 43(8), pp. 833-844.

[79] Snr, D. D., 2001, "Correlation of cutting force features with tool wear in a metal turning operation," Proceedings of the Institution of Mechanical Engineers, Part B: Journal of Engineering Manufacture, 215(3), pp. 435-440.

[80] Li, H., Zeng, H., and Chen, X., 2006, "An experimental study of tool wear and cutting force variation in the end milling of Inconel 718 with coated carbide inserts," JOURNAL OF MATERIALS PROCESSING TECHNOLOGY, 180(1), pp. 296-304.

[81] Ertekin, Y. M., Kwon, Y., and Tseng, T.-L. B., 2003, "Identification of common sensory features for the control of CNC milling operations under varying cutting conditions," International Journal of Machine Tools and Manufacture, 43(9), pp. 897-904.

[82] Ghosh, N., Ravi, Y., Patra, A., Mukhopadhyay, S., Paul, S., Mohanty, A., and Chattopadhyay, A., 2007, "Estimation of tool wear during CNC milling using neural network-based sensor fusion," Mechanical Systems and Signal Processing, 21(1), pp. 466-479.

[83] Dong, J., Subrahmanyam, K., San Wong, Y., Hong, G. S., and Mohanty, A., 2006, "Bayesian-inference-based neural networks for tool wear estimation," The International Journal of Advanced Manufacturing Technology, 30(9-10), pp. 797-807.

[84] Kim, H.-Y., and Ahn, J.-H., 2002, "Chip disposal state monitoring in drilling using neural network based spindle motor power sensing," International Journal of Machine Tools and Manufacture, 42(10), pp. 1113-1119.
[85] Behjat, V., Mahvi, M., and Rahimpour, E., 2016, "New statistical approach to interpret power transformer frequency response analysis: non-parametric statistical methods," IET Science, Measurement & Technology, 10(4), pp. 364-369.
[86] Lee, J., Choi, D., Kim, J., and Chu, C., 1995, "Real-time tool breakage monitoring for NC milling process," CIRP Annals-Manufacturing Technology, 44(1), pp. 59-62.
[87] Lahdelma, S., and Juuso, E., 2011, "Signal processing and feature extraction by using real order derivatives and generalised norms. Part 1: Methodology," International Journal of Condition Monitoring, 1(2), pp. 46-53.
[88] Wang, G. F., Yang, Y. W., Zhang, Y. C., and Xie, Q. L., 2014, "Vibration sensor based tool condition monitoring using ν support vector machine and locality preserving projection," Sensors and Actuators A: Physical, 209, pp. 24-32.
[89] Huang, C. Y., Lee, R. M., and Yang, S. K., "Implement of low cost MEMS accelerometers for vibration monitoring of milling process," Proc. 2016 International Conference on Applied System Innovation (ICASI), pp. 1-4.
[90] Wang, C., Cheng, K., Chen, X., Minton, T., Rakowski, R., 2014, "Design of an instrumented smart cutting tool and its implementation and application perspectives," Smart Mater Struct Smart Materials and Structures, 23(3).
[91] Siddiqui, R. A., Amer, W., Ahsan, Q., Grosvenor, R. I., and Prickett, P. W., 2007, "Multi-band infinite impulse response filtering using microcontrollers for e-Monitoring applications," Microprocessors and Microsystems, 31(6), pp. 370-380.
[92] Hase, A., Wada, M., Koga, T., and Mishina, H., 2014, "The relationship between acoustic emission signals and cutting phenomena in turning process," The International Journal of Advanced Manufacturing Technology, 70(5-8), pp. 947-955.
[93] Diei, E. N., and Dornfeld, D. A., 1987, "A Model of Tool Fracture Generated Acoustic Emission During Machining," Journal of Engineering for Industry, 109(3), pp. 227-233.
[94] Huang, N. E., and Shen, S. S., 2005, Hilbert-Huang Transform and Its Applications, World Scientific Publishing Co., River Edge, NJ, USA.

[95] Mukhopadhyay, S., and Ray, G., 1998, "A new interpretation of nonlinear energy operator and its efficacy in spike detection," Biomedical Engineering, IEEE Transactions on, 45(2), pp. 180-187.
[96] 2016, "SIMATIC S7-1500, ET 200SP, ET 200pro Cycle and resposne times," No. A5E03461504-AC, SIEMENS AG.

[97] Cuppini, D., D'errico, G., and Rutelli, G., 1990, "Tool wear monitoring based on cutting power measurement," Wear, 139(2), pp. 303-311.
[98] Altintaş, Y., and Budak, E., 1995, "Analytical Prediction of Stability Lobes in Milling," CIRP Annals, 44(1), pp. 357-362.
[99] Elbestawi, M., Papazafiriou, T., and Du, R., 1991, "In-process monitoring of tool wear in milling using cutting force signature," International Journal of Machine Tools and Manufacture, 31(1), pp. 55-73.
[100] Wang, G., Yang, Y., and Li, Z., 2014, "Force Sensor Based Tool Condition Monitoring Using a Heterogeneous Ensemble Learning Model," Sensors, 14(11), pp. 21588-21602.
[101] Scheffer, C., Kratz, H., Heyns, P. S., and Klocke, F., 2003, "Development of a tool wear-monitoring system for hard turning," International Journal of Machine Tools and Manufacture, 43(10), pp. 973-985.
[102] Jonak, J., and Gajewski, J., 2008, "Identification of ripping tool types with the use of characteristic statistical parameters of time graphs," Tunnelling and Underground Space Technology, 23(1), pp. 18-24.
[103] Choi, Y. J., Park, M. S., and Chu, C. N., 2008, "Prediction of drill failure using features extraction in time and frequency domains of feed motor current," International Journal of Machine Tools and Manufacture, 48(1), pp. 29-39.
[104] Mannan, M. A., Broms, S., and Lindström, B., 1989, "Monitoring and Adaptive Control of Cutting Process by Means of Motor Power and Current Measurements," CIRP Annals - Manufacturing Technology, 38(1), pp. 347-350.
[105] Shi, D., and Gindy, N. N., 2007, "Tool wear predictive model based on least squares support vector machines," Mechanical Systems and Signal Processing, 21(4), pp. 1799-1814.

[106] McLachlan, G., 2004, Discriminant analysis and statistical pattern recognition, John Wiley & Sons.
[107] Peterson, L. E., 2009, "K-nearest neighbor," Scholarpedia, 4(2), p. 1883.
[108] Bose, N. K., and Liang, P., 1996, "Neural Network Fundamentals with Graphs, Algorithms and Applications, McGraw-Hill Series in Electrical and Computer Engineering."
[109] Hagan, M. T., and Menhaj, M. B., 1994, "Training feedforward networks with the Marquardt algorithm," IEEE transactions on Neural Networks, 5(6), pp. 989-993.
[110] Murphy, K. P., 2006, "Naive bayes classifiers," University of British Columbia.
[111] Myles, A. J., Feudale, R. N., Liu, Y., Woody, N. A., and Brown, S. D., 2004, "An introduction to decision tree modeling," Journal of Chemometrics, 18(6), pp. 275-285.
[112] Duch, A. E. V. W., Masulli, P. É. F., and Palm, G., "Artificial Neural Networks and Machine Learning–ICANN 2012."
[113] Hausmair, K., Chi, S., Singerl, P., and Vogel, C., 2013, "Aliasing-free digital pulse-width modulation for burst-mode RF transmitters," IEEE Transactions on Circuits and Systems I: Regular Papers, 60(2), pp. 415-427.
[114] Bhattacharya, R. N., and Rao, R. R., 1986, Normal approximation and asymptotic expansions, SIAM.